PhD Thesis

Structure and Dynamics of Biopolymer Networks

A thesis presented in partial fulfillment of the requirements for the degree of

Doctor of Philosophy
in
Physics

at Massey University, Manawatu,
New Zealand.

Author: Bradley William Mansel
Supervisor: Prof. Bill Williams
Co-supervisor: A. Prof. Yacine Hemar

November 2015

Abstract

The aim of this work was to further understand the structural and dynamical properties of pectin-based biopolymer networks. This is pertinent to furthering our understanding of the plant cell wall and has further implications for the food and pharmaceutical industries where biopolymer networks play a fundamental role in thickening and stabilizing food products and controlling the rate of drug release.

Firstly, microrheological studies on an acid-induced pectin network revealed previously unseen slow motions of the network at times longer than one second. This "slow mode" is reminiscent of so-called alpha processes that are predicted with mode coupling theory in colloidal glasses. Such slow motions present in the networks are a signature of an out-of-equilibrium system and lead to further work on studying slow relaxation processes in pectin networks.

Secondly, structural and rheological measurements were performed on the acid-formed pectin networks. It was found using small-angle x-ray scattering that the network was composed of flexible cylindrical entities with a radius of 7 Å. At larger length scales these entities were arranged in a clustered confirmation that upon heating increased in density, indicating the importance of kinetic trapping for the initial network formation.

Finally, multi-speckle dynamic light scattering experiments were performed on three different ionotropic pectin gels formed with calcium to study the dependence of the slow dynamics on the junction length (and binding energy) between pectin chains. It was found that increasing the junction length slows the dynamics until a point where the internal stress becomes so large that the dynamics increase again. Spatially resolved photon correlation spectroscopy measurements revealed previously unmeasured millimetre sized heterogeneity in the networks. Angle-resolved multi-speckle photon correlation spectroscopy showed conclusively that the dynamics are driven by internal stresses and further more allowed the temporal heterogeneity to be measured.

Acknowledgements

Many people have given me help and support throughout the last few years, I appreciate this very much. First of all I would like to thank my supervisor Bill Williams, words are not enough to describe how much he has given me over the past few years, from crazy adventures to worldly advice and perfectly timed encouragement. You have taught me so much and I will be forever indebted to your supervision. Yacine, thanks for having me in your group in Auckland, the help with the rheology and being a great co-supervisor. The Biophysics and soft matter group have provided me a lot of support, I thank all of you! Leif Lunden, Andrew Leis from CSIRO, thank you both for yo ur hospitality and excellent input to our collaborative work. Dr. Che-Yi Chu and Professor Chen from National Tsing-Huia University, my time in Taiwan would not of been possible without you both. Thank you for sharing your time, knowledge and beamtime. I learnt a lot from you both. To my friends and family, thank you all for the support and encouragement, especially my parents (I haven't added any names encase I forget someone). Steve Keen and Jess Costall thank you for having me to stay "temporarily" for the last 4 months, I appreciate your kindness. This project would not of been possible without funding from: The MacDiarmid Institute, The Royal Society of New Zealand and Massey University.

Daphne, I would like to thank you for your support and commitment over the last few years! You have put up with a lot!

Contents

List of Figures

List of Tables

List of Publications

[1] R R Vincent, B W Mansel, A Kramer, K Kroy, and M A K Williams. Microrheological behaviour and nonlinear rheology of networks assembled from polysaccharides from the plant cell wall. *New Journal of Physics* **15(3)** March 2013. ISSN 1367-2630. doi: 10.1088/1367-2630/15/3/035002.

[2] B W Mansel, C-Y Chu, A Leis, Y Hemar, H-L Chen, M A K Williams. Zooming In: Structural Investigations of Rheologically Characterized Hydrogen-Bonded Polysaccharide Networks, submitted to *Biomacromolecules*

[3] B W Mansel, M A K Williams, Internal Stress drives slow glassy dynamics and quake-like behaviour in ionotropic pectin gels, submitted to *Soft Matter*

[4] Y F lim, R G Lentle, P W M Janssen, M A K Williams B W Mansel, P Chambers. Determination of Villous Rigidity in the Distal Ileum of the Possum (Trichosurus vulpecula). *PLoS ONE* **19(6)** June 2014. ISSN 1932-6203 doi: 10.1371/journal.pone.0100140.

[5] Y F Lim, M A K Williams, R G Lentle, P W M Janssen, B W Mansel, S A J Keen, P Chambers. An exploration of the microrheological environment around the distal ileal villi and proximal colonic mucosa of the possum (Trichosurus vulpecula). *Journal of The Royal Society Interface* **81(10)** Feb 2013. ISSN 1742-5689. doi: 10.1098/rsif.2012.1008.

1. Background

1.1 Introduction

Soft matter is a benign name for a group of materials with complex mechanical properties that range from flowing like fluids, to supporting their own weight [1]. While having a diverse range of mechanical properties the materials share a common trait for which they are named; they can be deformed by stresses on the order of room temperature thermal force [2]. Commonly, these materials are called emulsions, foams, gels and pastes which occupy a position on the continuum from liquids to solids and also display differing mechanical properties depending on the time scale over which one observes the material. A common example of a material that has differing mechanical properties depending on the time scale for which one observes it is pitch, or tar as it is commonly referred to in New Zealand. A famous example is the pitch drop experiment, the longest running experiment in the world, and possibly one of the most simple [3]. The pitch drop experiment is simply a funnel filled with pitch that over many years forms a drop that approximately every 8 years drips into a beaker under the funnel, see figure 1.1. On the time scales that we observe pitch, that is on the order of minutes or less for the not so patient, it is classed as a strong solid that can be shattered by hitting it with a hammer, although on very long time scales it behaves as a viscous liquid that flows like honey. A more formal name for a disordered solid, such as pitch, is a glass. These are currently some of the least understood and most fascinating materials [4–6].

Recently, many frustrated, or out-of-equilibrium materials have been shown to display glassy dynamics [7–12]. Gels are one such material that have been shown to display these complex dynamics. They are a solid material, although primarily composed of a low viscosity material, the continuous phase. The remaining mass is an interconnected

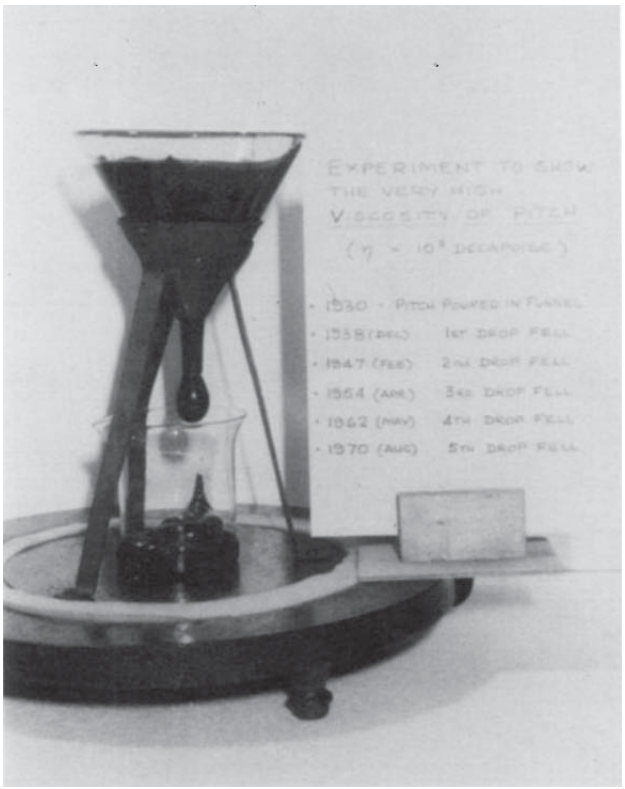

FIGURE 1.1: The pitch drop experiment sometime between 1970 and 1979 at the University of Queensland where it is on display. Picture from ref. [3].

dispersed phase that is suspended in the continuous phase [13–18]. The dispersed phase can be a range of different micron sized entities, although is typically polymers, proteins or colloidal spheres, and the continuous phase can be a liquid or gas. The dispersed, solid phase, is typically only a few percent of the overall volume of the material, and this gives gels interesting properties that are highly desirable for many applications. For gels with a gas as the continuous phase, known as an aerogel, they are incredibly light, porous, thermally insulating and have a very large surface area [19]. Gels with a liquid as the continuous phase are known as hydrogels if the liquid is water or organogels if the liquid is an organic liquid [20]. Much interest lies in hydrogels due to their applicability to the medical, pharmaceutical and food industries. Part of this interest is due to the ease with which it is possible to make biocompatible materials and also the ease with which one can make materials that have designed properties.

Biopolymers, the building blocks of life, form much of nature. They are present in many different forms, polysaccharides, nucleic acids and proteins, that have differing properties depending on the functional role of the specific biopolymer. An important area of research in the soft matter field is trying to understand the properties of the monomeric

building block that form the gel, and how these self-assemble and manifest the mechanical properties of the gel. This so called "bottom-up" approach leads to significant insights into not only the material properties of these solids but also how nature designs the biopolymers to self assemble and form structural entities that form part of living systems [21]. It is a beautiful example of something that on its own is simply a molecule but a group of such molecules self assemble into a solid material with highly specific material properties for their function in a biological setting. Polysaccharides, molecules formed of many sugar residues, are a particularly important group of biopolymers that have not received the same level of interest as protein based biopolymers such as actin. Actin is a ubiquitous structural biopolymer in mammalian cells [22], while polysaccharides on the other hand play little structural role in animals, except in the extracellular matrix, although, are arguably equally important due to their ubiquity in the plant cell wall [23]. The cell wall is one of the most important structures in nature and is currently not well understood. There are a vast array of structural polysaccharides in the cell wall of terrestrial plants, although there are 3 common groups, cellulose, hemicelluloses, and pectins [24]; herein we focus on pectin.

1.2 Pectin

Pectin is a heteropolysaccharide composed primarily of a homogalacturonan backbone which is connected through alpha 1-4 linkages [25]. Pectin has considerable value as a thickener in the food industry and can be sourced from waste originating from the fruit juice industry, which can reduce costs compared with other biopolymer thickeners and stabilizers[26]. It is also widely used as a dietary supplement due to its long held reputation as a healthy part of the diet and furthermore recent research suggests that it may have anti-cancer properties [27, 28]. Pectin, when eaten, can only be digested in the large intestine by microbial action. This fact is exploited by the pharmaceutical industry for targeted drug delivery where a substance can be encapsulated and the capsule only digested upon entry to the large intestine [29]. An important property of pectin is the degree of esterification (DE), with characterizes the average percentage of de-esterified groups that reside at the C6 position of the galacturonan rings in an average chain [30]. It has a significant effect on both the solution conformations of the chain and their self-assembly into gelled materials. The gelling properties of pectin

have been known for centuries as pectin rich fruit has long been utilized to produce fruit jam [31]. The gelation process of pectin in jam, which contains high amounts of sugar, typically up to 60%, exploits hydrogen bonding and hydrophobic interactions[32]. While pectin can form a gel in the absence of sugar and in acidic conditions, as is employed in chapters 2 [33] and 3, such polymers need to have a highly block-wise distribution of the de-esterified residues which makes this method under-utilized compared to the more common calcium pectin gels [34–37]. At pH values above the pK_a de-protonated carboxyl groups on the C6 position will chelate divalent ions and if the degree of methyl-esterification is low enough and the polymer concentration greater than the over lap concentration, $c^* \approx 0.5$ wt%, a gel will form. Typically the divalent ions are calcium, which is a mechanism of bonding in the plant cell wall [38], although other ions can take the place of calcium [39]. It is thought that pectin may be able to remove some undesirable metal ions from the body through this type of interaction [40].

1.2.1 Pectin structure

The polymeric structure of pectin must be resolved at many different length scales to understand the structural properties that make it an important primary component of the plant cell wall and also to understand properties relevant for thickening or stabilizing soft systems. At the smallest length scale the structure of the individual monomers has been well established for a significant period of time [41], although the exact layout of the monomers is sill a matter of debate [42]. At a slightly larger length scale there has been much interest in the conformations of monomers along the chain, which depending on the ions present and the solvation state have been shown to be either in a 3_1 or 2_1 helical structure, although most commonly a 2_1 helix has been measured unless in highly acidic conditions [43, 44]. Some of the first measurements to elucidate the conformations of single chains and junction zones were performed using x-ray fibre diffraction (XFD) which tried to resolve, at atomic scales, structural information from fibres, although the sample was typically not crystalline enough to resolve the exact atomic positions in all cases [45, 46]. Extended x-ray absorption fine structure (EXAFES) measurements have shown that dried pectin, as was used in XRD or XFD studies, has a different structure to that present in pectin-calcium junction zones. This was interpreted as a 3_1, when dried, or 2_1 when in a gel or solution state, helical conformations respectively [47]. A similar difference in the helical structure has been observed in pectin's sister polysaccharide

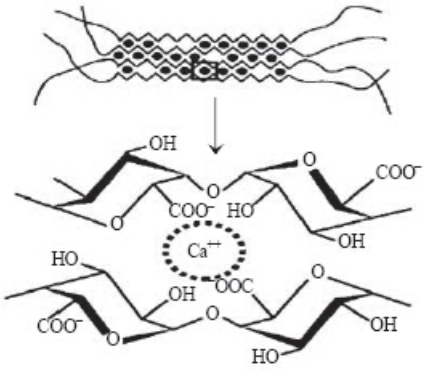

FIGURE 1.2: The egg box model as it appears in ref. [49] for guluronate.

alginate when using XRD to study the gelled or dried state [48]. Currently, molecular dynamics calculations appear to provide the most realistic method for determining the structure of pectin junction zones in solution due to the experimental difficulties related to obtaining atomic scale structural information from an amorphous material, and the structural changes induced upon drying.

Much interest lies in understanding how pectin binds ions to form a junction zone. The understanding of junction zones is important in further understanding the plant cell wall. A commonly referenced binding mechanism between pectin and calcium is known as the egg box model where four galacturonic acid residues form a structure that resembles a rhombus with a calcium ion in the centre, see figure 1.2 [50]. However, recent calculations using molecular modelling suggest that the egg-box model is not the correct model for pectin, at least with calcium, although it may be a somewhat better model for alginate [49]. A more recently calculated model is shown in figure 1.3 [51]. An interesting result of these recent calculations, that also fits well with our results in chapter 4, is that multimeric entities larger than a dimer are predicted to be less likely to occur than as predicted with the egg-box model [49]. This is due to single chain association being highly specific and much stronger than dimer-dimer associations which are non-specific.

One of the most important structural properties of a polymer is its flexibility. This measurement can be performed using a variety of different methods and pectin has generally been shown to be a semi-flexible polymer[52–54]. The common parameter used to describe the flexibility of a polymeric molecule is a length scale known as the persistence length. The persistence length describes the curvature of a polymer

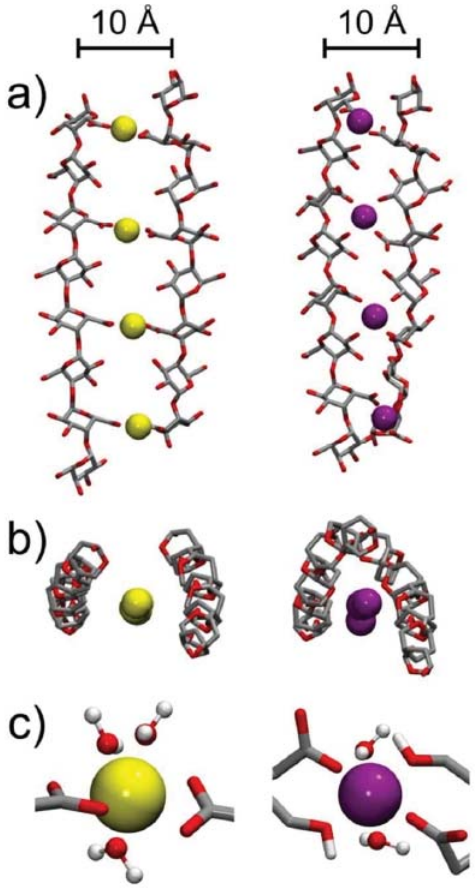

FIGURE 1.3: Model of pectin binding calcium (left) and zinc (right) as calculated in ref. [51]

chain through a series of straight segments of length l_p [55, 56]. For pectin the exact measurement of the persistence length has not been well established. This is due to the effects from charged residues, called polyelectrolyte effects. Polyelectrolyte effects are highly complex and significantly affect the polymer conformation in unexpected ways. The ionic conditions have a significant effect on the large scale conformation of the chain, as do the degree of esterification and possibly the chemical techniques used during the extraction from plant material [57]. A commonly referenced paper that measures the persistence length using small-angle neutron scattering and viscometry [58], has measured lengths that differ by approximately a factor of 2 for the two different techniques. These discrepancies could be due to tenuous aggregation of the pectin chains, as has often been reported [59], and in the experience of the author, are very difficult to remove. While this potentially makes obtaining an exact agreement on the measured persistence length impossible, it is generally accepted that the persistence length of individual pectin chains is between 6.7 and 9 nm [60, 61].

The larger scale structure of pectin and pectin gels can be investigated using x-rays or neutrons scattered at small-angles to resolve structural information on length scales of 1-1000nm [62–64]. One recent study reports on the bundle size of pectin calcium gels which are assembled through two different mechanisms, one of which is the common control release method [65] and the other an in-situ enzymatic de-esterification and subsequent association of the chains [66]. It is clearly shown by modelling the small-angle scattering data of the junction zones using Guinier's expression that gels formed using an enzymatic method produces dimeric assemblies of polymer chains while the control release method produced some additional larger assemblies, although still a high percentage of dimers [67]. The bundle size of the control release method reported therein agrees well with the work carried out in this thesis. Few other studies have produced any meaningful data describing the structure of pectin networks. While one paper has presented some data, the samples were made with a ratio of calcium ions to junction binding sites of one and higher which means that much of the added calcium cannot be in junction zones [68]. Most recently SANS measurements have been performed on pectin in the absence and presence of calcium and zinc ions [51]. A persistence length of between 50 and 70 Angstrom is found for the individual chains, which compares well with other measurements, while the radius of the entities forming the gel could not be calculated due to weak scattering and large uncertainties in the high q data.

1.3 Glassy materials and slow dynamics

Many systems such as glasses, spin-glasses, and granular soft matter have long been known to display dynamics characteristic of out-of-equilibrium systems. The characteristic dynamics typically show distinct motions at two different time scales, the first, on shorter time scales is often described as caged motion where the cage represents particles jamming the system and causing the motion to be constricted [69]. For colloidal systems the particles cause the jamming while for other systems the particles can be atoms or molecules for glasses, and polymers for polymeric systems. The motion at longer times can be described as cage hopping where if one waits for a long enough time there is some chance that a gap will arise that is large enough for one of the particles to make a large jump and occupy that space. In-between these two timescales of increased motion a plateau exists. A model based on these dynamics can be used to describe

the glass transition. It is thought that at temperatures close to the glass transition the second slower motion will transition to occurring at longer times, and once the system is deep into the glass transition the time when the second slow mode occurs is thought to be at an infinity large time. Although, much work on these glassy systems is still being undertaken. Mode couple theory is a popular mathematical framework to describe and predict the motion of these jammed out-of-equilibrium systems [70], and while it appears to predict the general motion of the elements in the systems it is still unclear if the theory truly predicts the motions close to the glass transition.

Here some mathematics are introduced, as presented in ref. [71] that will serve as a prelude to introducing scattering formalisms that are introduced in chapter 2.

The density of particles in a liquid can be described by:

$$\rho(\mathbf{r},t) = \sum_i \delta(\mathbf{r} - \mathbf{r}_i(t)) \tag{1.1}$$

where $\mathbf{r}$ is a vector which describes the length scale over which the sum of the number of particles is performed and δ is the Dirac delta function. To reproduce data that can be compared to scattering that is measured in reciprocal space($L \sim 2\pi/k$) the Fourier transform is taken:

$$\begin{aligned}\rho_{\mathbf{k}}(t) &= \sum_i \int d\mathbf{r} e^{i\mathbf{k}\cdot\mathbf{r}} \delta(\mathbf{r} - \mathbf{r}_i(t)) \\ &= \sum_i e^{i\mathbf{k}\cdot\mathbf{r}_i(t)}\end{aligned} \tag{1.2}$$

A time and $\mathbf{k}$ dependent correlation function of the density can then be taken, which is essentially what is performed in a scattering experiment:

$$F(k,t) = \frac{1}{N}\langle \rho_{-\mathbf{k}}(0)\rho_{\mathbf{k}}(t)\rangle = \frac{1}{N}\sum_{ij}\left\langle e^{-i\mathbf{k}\cdot\mathbf{r}_i(0)} e^{i\mathbf{k}\cdot\mathbf{r}_j(t)}\right\rangle \tag{1.3}$$

The intermediate scattering function $F(k,t)$ is measured experimentally. If no time dependence is measured and only the density as a function of $k = |\mathbf{k}|$ obtained, $F(k, t = 0)$ is called the static structure factor and is typically measured with static scattering techniques. For liquids, glasses or other particulate systems it resolves inter-particle density fluctuations and is related to the k dependent particle density by(see fig. 1.4):

$$F(k, t = 0) = \frac{1}{N}\langle \rho_{-\mathbf{k}}(0)\rho_{\mathbf{k}}(0)\rangle \equiv S(k) \tag{1.4}$$

The radial distribution function $g(r)$ is proportional to the probability that a particle is a distance r away from a particle at the origin, see fig. 1.4. Although not used during this thesis, $g(r)$ is included here for completeness and to go back to a function that describes real space complementary to $S(k)$

$$S(k) = 1 + \rho \int d\mathbf{r} e^{-\mathbf{ik}\cdot\mathbf{r}} g(\mathbf{r}) \tag{1.5}$$

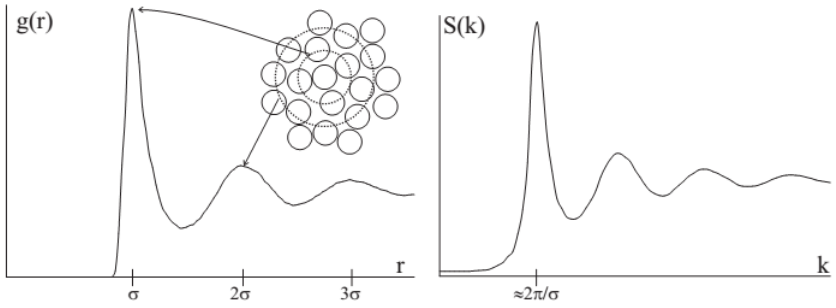

FIGURE 1.4: The figure on the left is the radial distribution frunction that is proportional to the probability of finding a particle at a distance from the particle at the origin. On the right is the static structure factor that is essentially the reciprocal space version of the radial distribution function and is used extensively in scattering measurements. Obtained from ref. [71]

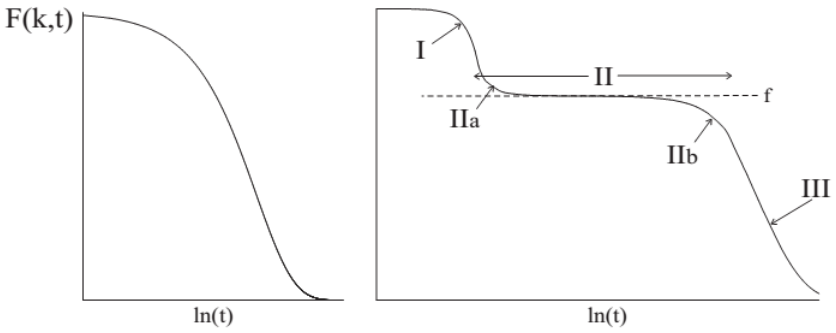

FIGURE 1.5: Here $F(k,t)$ is plotted for two different systems, on the left a simple liquid which displays a simple exponential decay $F(k,t) \propto e^{-t/\tau_f}$ and on the right a glassy system, such as a supercooled liquid, that has three different regimes. Regime I is the fast rattling in a cage type motion, regime II is the plateau related to the confinement of the cage and, regime III is cage jumping motion at long times. Obtained from ref. [71]

For many types of condensed matter one can study the dynamics of glassy materials using inelastic neutron or x-ray scattering to probe the dynamics. Typically these occur on very short time and length scales which require highly specialized beamlines. Furthermore acquisition times are generally on the order of hours or days, which makes these measurements even more unfeasible for many researchers. To circumvent these issues colloidal gels are commonly utilized as model systems to investigate materials in

a glassy state. They display similar interesting phenomena as glass forming solids but can be studied using less technically demanding techniques such as light scattering or light microscopy. It is possible to create a range of interesting phenomena by changing different properties of colloidal systems, such as packing fraction, charge density, and ionic conditions. While colloidal systems have been the traditional materials used to study glassy systems, recently it has been found that many other soft systems also display slow dynamical processes. This has led to a new area of research that is focussing on characterising dynamical phenomena occurring over long times. Much of this work has been spurred on by theoretical work which sought new ways of interpreting the rheological properties of soft matter as the dynamics are often slow and cross the glass transition. Early models such as reptation with constraint release, for example, were used to describe the dynamics of a polymer melt, where each polymer is enclosed by a tube formed by surrounding polymers that restrict its motion [72]. The model is based around the idea that at short times the motion of the polymer is restricted by the tube enclosing it and then at some longer time this constraint is released and the polymer can make a large displacement. Another body of work called the soft glassy rheology model, proposed by Cates, describes soft glasses where energy wells constrain the motion of the subunits forming the material. An effective noise temperature modifies the behaviour between a glassy state and that of more usual rheological models such as a Maxwellian fluid [73]. This model is not limited to polymer like systems and has been well accepted by the soft matter community. A more recent model proposed by Kroy, known as the glassy wormlike chain model, is developed from the regular worm-like chain model with extra parameters that describe the depth of the energy wells which constrain large scale motion in the system together with a characteristic interaction length [74]. The model has not been as well accepted as the soft glassy rheology model by the soft matter community. From the authors experience, see chapter 2, the model has a large amount of freedom in the parameters, meaning that data may be fitted with a range of parameters and produce the same outcome. The model may still be an interesting way to think of soft glassy polymeric systems, although it is based on similar ideas to other models which describe soft glasses, such as the trap model [75].

2. Methods

2.1 Introduction

Nearly everything we know about the universe has been observed from the interaction of radiation with matter and some of the most beautiful phenomena we can observe in nature, such as rainbows, sunsets, and aurora are due to scattered radiation producing beautiful colours. By measuring how radiation interacts with matter one can extract information on the structure, composition, motion and even magnetic properties of matter on length scales down to Angstrom resolution. To demonstrate different scattering techniques experiments and simulations were performed by the author throughout this section.

FIGURE 2.1: Aurora Australis viewed from the International Space Station on September 26th 2011. From: www.nasa.gov

2.1.1 Static scattering

Static scattering is typically performed using light, x-rays or neutrons to study the structure of the material of interest. Different types of radiation interact differently with materials and access different length scales. For this thesis light and x-rays were

used and will be the focus of this section. X-rays and light interact with a materials electron cloud, while neutrons the nucleus, which makes them far more penetrating. Scattering, for x-rays and light, is produced when the radiation hits a material with different dielectric properties. X-rays have many benefits over light, the smaller wavelength means that far larger scattering vectors can be accessed, and they can be used for materials that are not optically transparent or highly turbid. Additionally, multiple scattering is rarely a problem.

For this section we follow the scattering formalisms as in ref. [76, 77] with a beam of monochromatic light, a plane wave, represented by:

$$E_I(\mathbf{r},t) \equiv E_0 \exp[i(\mathbf{k}_I \cdot \mathbf{r} - \omega t)] \tag{2.1}$$

E_0 is the electric field vector polarized perpendicular to the scattering plane, $\mathbf{k}_I$ is the propagation vector of the incident light and ω is the angular frequency. When this beam of radiation hits a non-magnetic, non-conducting, non-absorbing medium with an average dielectric constant ϵ_0, where the refractive index, n, that is related by $n = \sqrt{\epsilon_0}$. Then the electric field of the component scattered from the medium at a large distance (in the far field) is given by:

$$E_s(\mathbf{R},t) = -\frac{k^2 E_0}{4\pi} \frac{\exp[i(kR - \omega t)]}{R} \int_V \left[\frac{\epsilon(\mathbf{r},t) - \epsilon_0}{\epsilon_0}\right] \exp(-i\mathbf{q}\cdot\mathbf{r}) d^3r \tag{2.2}$$

where $\mathbf{R}$ is the position of the detector in the far field, $k_I \equiv |\mathbf{k}_I| = k = 2\pi/\lambda$, λ is the wavelength of the light in the medium , V is the scattering volume, $\mathbf{q}$ is the scattering vector where:

$$\mathbf{q} \equiv \mathbf{k}_s - \mathbf{k}_I; \qquad q \equiv |\mathbf{q}| = \frac{4\pi}{\lambda} \sin\frac{\theta}{2} \tag{2.3}$$

and θ is the angle between incident and scattered radiation.

Equation 2.2 can be rewritten as the sum of amplitudes of the fields $\mathrm{d}E_s(\mathbf{R},t)$ scattered by volume elements $\{\mathrm{d}V \equiv \mathrm{d}^3r\}$ at positions $\{\mathbf{r}\}$

$$E_s(\mathbf{R},t) = \int_V \mathrm{d}E_s(\mathbf{R},t), \tag{2.4}$$

where

$$\mathrm{d}E_s(\mathbf{R},t) = -\frac{k^2 E_0}{4\pi}\frac{\exp[i(kR-\omega t)]}{R}\left[\frac{\epsilon(\mathbf{r},t)-\epsilon_o}{\epsilon_o}\right]dV\exp(-i\mathbf{q}\cdot\mathbf{r}) \tag{2.5}$$

This equation describes radiation resulting from an oscillating dipole.

For N discrete scatterers in the scattering volume V, with their centres of mass described by position vectors $\{\mathbf{R}_j(t)\}$ at time t, equation 2.2 can then be written as volume elements in each particle j by $dV_j(=d^3r_j)$, relative to its centre of mass:

$$E_s(\mathbf{R},t) = -E_0\frac{\exp[i(kR-\omega t)]}{R}\times\sum_j\left[\int_{V_i}\Delta\rho(\mathbf{r}_j,t)\exp(-i\mathbf{q}\cdot\mathbf{r}_j)\right]\exp(-i\mathbf{q}\cdot\mathbf{R}_j(t)) \tag{2.6}$$

Here V_j is the volume of particle j and $\Delta\rho(\mathbf{r}_j,t)$ is defined by:

$$\Delta\rho(\mathbf{r}_j,t) = \frac{k^2}{4\pi}\left[\frac{\epsilon_P(\mathbf{r},t)-\epsilon_L}{\epsilon_o}\right] \tag{2.7}$$

where $\epsilon_P(\mathbf{r},t)$ is the local dielectric constant in particle j at position $\mathbf{r}_j$, ϵ_L is the average dielectric constant of the surrounding medium and ϵ_0 is the average dielectric constant of the whole suspension.

Commonly equation 2.6 is written as follows, and can be used to describe neutrons, x-rays or light.

$$E_s(\mathbf{R},t) = -E_0\frac{\exp[i(kR-\omega t)]}{R}\sum_{j=1}^{N}b_j(\mathbf{q},t)\exp[-i\mathbf{q}\cdot\mathbf{R}_j(t)] \tag{2.8}$$

The scattering length for the jth particle is described by:

$$b_j(\mathbf{q},t) = \int_{V_j}\Delta\rho(\mathbf{r}_j,t)\exp(-i\mathbf{q}\cdot\mathbf{r}_j)\mathrm{d}^3r_j \tag{2.9}$$

The measured scattered intensity is related to the electric field by: $I(\mathbf{q},t) = |E(\mathbf{q},t)|^2$

Finally, the instantaneous scattered intensity can then be calculated:

$$I_s(\mathbf{q},t) = \frac{E_0^2}{R^2}\sum_{j=1}^{N}\sum_{k=1}^{N}b_j(\mathbf{q},t)b_k^*(\mathbf{q},t)\exp\{-i\mathbf{q}\cdot[\mathbf{R}_j(t)-\mathbf{R}_k(t)]\} \tag{2.10}$$

In an experiment the scattering is from an ensemble of scatterers and for an ergodic sample the time average is equal to the ensemble average and one gets:

$$\langle I_s(\mathbf{q},t)\rangle = \left\langle \frac{E_0^2}{R^2}\sum_{j=1}^{N}\sum_{k=1}^{N} b_j(\mathbf{q},t)b_k^*(\mathbf{q},t)\exp\{-i\mathbf{q}\cdot[\mathbf{R}_j(t)-\mathbf{R}_k(t)]\}\right\rangle \tag{2.11}$$

For dilute systems, that by definition have no inter-particle interactions, we can write the intensity as:

$$\begin{aligned}\langle I_s(q)\rangle &= \sum_{j=1}^{N}\langle|b_j(\mathbf{q})|^2\rangle + \sum_{j=1}^{N}\sum_{k=1}^{N}\langle b_j(\mathbf{q})\exp(-i\mathbf{q}\cdot\mathbf{R}_j)\rangle\langle b_k^*(\mathbf{q})\exp(i\mathbf{q}\cdot\mathbf{R}_k)\rangle \\ &= \sum_{j=1}^{N}\langle|b_j(\mathbf{q})|^2\rangle\end{aligned} \tag{2.12}$$

with the second part of equation 2.12 equal to zero due to the particle describing a random walk. This results in the particle position distribution being a Gaussian centred on zero and the mean of such a function is zero.

Formalisms for static scattering techniques have been developed and the function that describes the shape of the scatterer is known as the form factor: $P(q)$. For identical particles in the dilute regime the intensity of the scattering is proportional to a sum over the number of particles and is related to the form factor by:

$$\langle I_s(q)\rangle = N\langle|b(0)|^2\rangle P(q) \tag{2.13}$$

with $P(q) = \langle|b(\mathbf{q})|^2\rangle/\langle|b(\mathbf{0})|^2\rangle$

For concentrated systems of identical particles $b_j(\mathbf{q}) = b(q)$ and with inter-particle correlations equation 2.13 becomes:

$$\langle I_s(q)\rangle = b^2(q)\sum_{j=1}^{N}\sum_{k=1}^{N}\langle\exp[-i\mathbf{q}\cdot(\mathbf{R}_j-\mathbf{R}_k)]\rangle = nb^2(0)P(q)S(q) \tag{2.14}$$

with the static structure factor $S(q)$ is defined by:

$$S(q) \equiv \frac{1}{N}\sum_{j=1}^{N}\sum_{k=1}^{N}\langle\exp[-i\mathbf{q}\cdot(\mathbf{R}_j-\mathbf{R}_k)]\rangle \tag{2.15}$$

2.1.1.1 Form factor

The form factors of many shapes have been calculated and are commonly used to analyse small angle scattering data. The simplest shape to calculate is a sphere: see fig. 2.2, showing the form factor of a sphere of radius R [78]:

$$P(q) = \left[\frac{3}{(qR)^3}(\sin(qR) - qR\cos(qR)\right]^2 \tag{2.16}$$

The form factor of a cylinder has been calculated to be [78]:

$$P(q) = \int_0^{\pi/2} \left[2\frac{\sin(qL\cos(\alpha)/2)}{(qL\cos(\alpha)/2)}\frac{J_1(qR\sin(\alpha))}{(qR\sin(\alpha))}\right]^2 \sin\alpha d\alpha \tag{2.17}$$

where L is the length, R is the radius and α is the angle between the axis of the cylinder and the momentum transfer vector, see fig. 2.2.

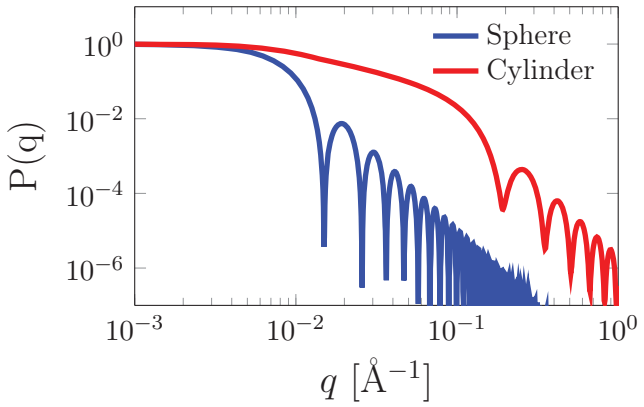

FIGURE 2.2: Plot of form factors for a cylinder of radius of $R = 20$Å, and length of $L = 500$Å and sphere of $R = 300$Å

In order to thoroughly acquaint myself with scattering theory, I calculated and subsequently measured: a) The x-ray scattering pattern from $R = 25$ nm latex spheres (figure 2.3) b) The light scattering pattern from $2R = 500nm$ latex spheres (figure 2.8)

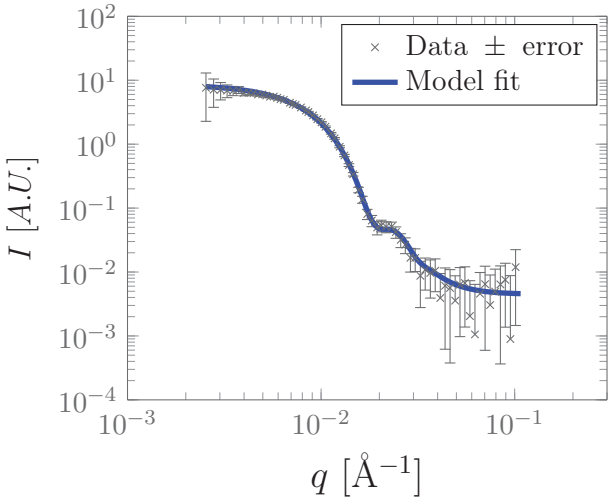

FIGURE 2.3: SAXS data of $a = 25$ nm latex spheres suspended in water, model data in the form of a spherical form factor model with polydispersity described by a Schulz distribution of 0.15 (S.D / mean), and radius of $R = 22.5$ nm

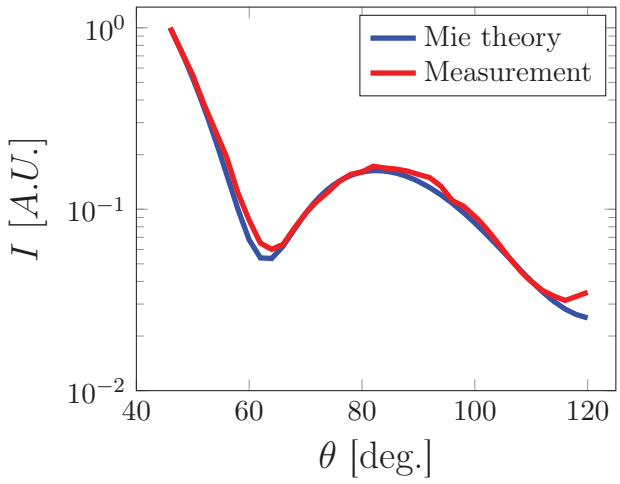

FIGURE 2.4: Static light scattering data of $2R = 500$ nm latex spheres suspended in water with data calculated from Mie theory for this system with a polydispersity of 0.05 and a radius of $a = 495$ nm

2.1.1.2 Structure factor

While the calculation for the form factor of common shapes is not overly difficult, the structure factor, relevant in all but the dilutest of systems, is typically significantly more challenging. To calculate a structure factor one typically starts with the Ornstein-Zernike equation to describe correlation in the system. The radial distribution function, $g(r)$ is related to the inter-particle interaction potential, $U(r)$ through [79–82]:

$$g(r) = \exp[-U(r)/k_B T] \tag{2.18}$$

where $U(r)$ is the potential of mean-force and contains contributions from many-body interactions:

$$U(r) = \sum_{i,j} w_{i,j}(r) + \sum_{i,j,k} w_{i,j,k}(r) + \cdots \tag{2.19}$$

$w_{i,j}(r)$ is the contribution from binary interactions and $w_{i,j,k}(r)$ is the tertiary interactions. There are also more higher order interactions which have been omitted. The Ornstein-Zernike equation relates the direct correlation function $c(r)$ and the total correlation function $h(r)$:

$$h(\vec{r}) = c(\vec{r}) + \bar{N} \int d\vec{r}' c(\vec{r} - \vec{r}') h(\vec{r}) \tag{2.20}$$

where $\bar{N} = N/V$ is the particle number density.

In Fourier space the equation is written as:

$$H(q) = C(q) + \bar{N} C(q) H(q) \tag{2.21}$$

and the inter-particle structure factor is defined as:

$$S_I(q) = \frac{1}{1 - \bar{N} C(q)} \tag{2.22}$$

This equation cannot be solved, unless another closure equation is used. The hard sphere interaction can be simply defined by a binary potential where the inter-particle potential is 0 at distances greater than one radius and infinite less than a particle radius. A plot of the hard sphere interaction using the Perkus-Yevick approximation is shown in fig. 2.5.

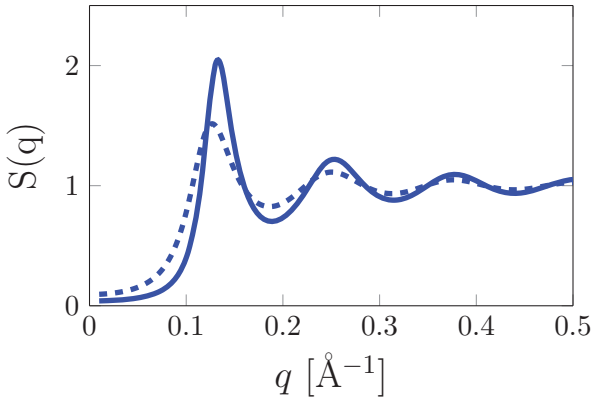

FIGURE 2.5: The hard sphere structure factor using the Perkus-Yevick approximation for $a = 25$Å and volume fractions of 0.3 (dashed lines) and 0.4 (solid line).

2.1.1.3 Fractal analysis

A fractal object is an object that is self similar on many different length scales. Such objects are ubiquitous in nature and are also commonly observed in synthetic materials such as in polymer conformations and the geometry of colloid aggregates, such as flocculated emulsion drops[83, 84]. A fractal object is often characterized by its fractal dimension D, for three dimensional space $d = 3$ and D can take the following values: $0 < D \leqslant 3$[83]. For small-angle scattering the distribution of mass in space is related to the intensity of the scattered radiation and for objects that are self similar the intensity of the scattered radiation is related to a power law, with exponent α[85]:

$$I(q) = I_0 q^{-\alpha} \tag{2.23}$$

For experiments using small-angle scattering there are two different fractal regimes: mass fractals and surface fractals[86]. The surface fractal regime occurs from the interaction of radiation with a surface and describes the fractal dimension of the surface, while the mass fractal is the interaction of radiation at length scales greater than the cross-section of the scatterer and describes how the mass is distributed in space. The mass fractal of a scatterer can take a value of between one for a thin cylinder and three for a spherical object, while the surface fractal can take a value ranging from two for a smooth surface to a limit of 3 for a very rough surface[86]. At values of $q > \frac{2\pi}{R_c}$, where R_c is the cross sectional radius of gyration, the scattering is from a surface and the measured exponent is related to the surface fractal by:

$$\alpha = 2d - D_{surf} \tag{2.24}$$

and if $q < \frac{2\pi}{R_c}$, then the power law is directly related to the mass fractal:

$$\alpha = D_{mass} \tag{2.25}$$

For a polymeric system the fractal dimension gives information about how the polymer fills space, if $\alpha = 2$ then the polymer randomly fills space, if $\alpha = 5/3$ the polymer is swollen, or self avoiding, and for $2 < \alpha \leqslant 3$ the polymer is clustered. To analyse data with power law scaling a fractal structure factor can be used to describe the scattering in the low q region [85, 87]. The fractal structure factor is described by a high q plateau,

TABLE 2.1: Fractal dimensions for different scatterers reproduced from ref. [86]

Scatterer	D_{mass}	D_{surf}
Mass fractal	D	D
Surface fractal	3	D
Extended scatterer	3	2
Thin platelet	2	2
Thin filament	1	1

then starting at r_0, which corresponds to the length scale where the scattering becomes self similar, there is a power-law region. It is described by an exponent related to the fractal dimension of the scatterer and finally a large scale cut-off, ξ, that is described by a Guinier type behaviour, see figure 2.6. These parameters are related by [85, 87]:

$$\begin{aligned} S(q) &= 1 + \frac{D}{r_0^D} \int_0^\infty r^{D-1} \exp(-r/\xi) \frac{\sin(qr)}{qr} \\ &= 1 + \frac{1}{(Qr_0)^D} \frac{D\Gamma(D-1)}{1 + 1/(q^2\xi^2)^{(d-1)/2}} \times \sin[(D-1)\tan^{-1}(q\xi)] \end{aligned} \tag{2.26}$$

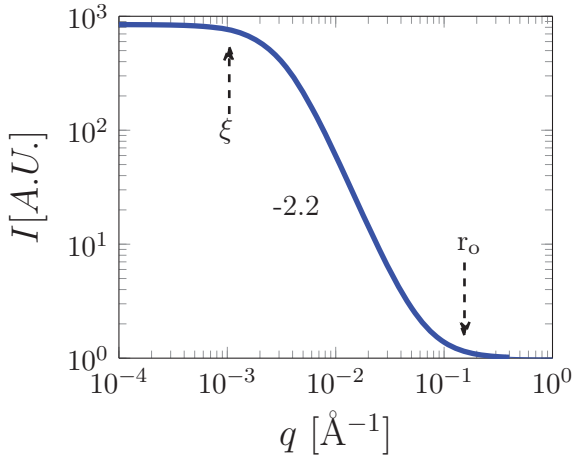

FIGURE 2.6: Fractal structure factor for $D = 2.2$, $r_0 = 30$Å, and $\xi = 300$Å

As an example of scattering from a polymeric system a simulation was performed, see figure 2.7. For this simulation the mass is distributed in space using a biased random walk and the mass distribution was then transformed into Fourier space using a fast Fourier transform. For a random walk that is biased to turn back on itself, as is shown in figure 2.7 part (a) a low spatial-frequency power law exponent of greater than two is found. A non-biased random walk shows a low spatial-frequency power law exponent

of 2 and finally a simulation where the walk is biased to create a sparse network shows a low spatial-frequency power law exponent is less than 2.

2.1.2 Quasi-elastic light scattering techniques

Quasi-elastic light scattering techniques cover a range of techniques. One such technique called dynamic light scattering (DLS) is commonly used as a particle sizing technique. It is utilized in many different labs that are interested in measuring the hydrodynamic radius of colloids, proteins or nano-particles. Photon correlation spectroscopy (PCS) is essentially the same as DLS although a pragmatic distinction between the two can be made, in that PCS is performed on a material of interest and a dynamic structure factor extracted that describes over what time scales motion is present. For a DLS experiment, on the other hand, a material typically contains either colloids of a known size in order to extract viscoelastic properties of the medium or colloids of an unknown size in a material of known viscosity in a sizing study. DLS and PCS are performed by correlating the intensity of coherent radiation scattered at one spatial position as a function of time and scattering vector [77]. Incident coherent and monochromatic radiation is used to irradiate a sample, which is typically laser light, to produce a speckle pattern (see figure 2.10 for an example of a speckle pattern). The sample, in the most simple case, consists of a suspension of dilute spherical particles. As light travels through the sample it is scattered isotropically for particles smaller than the wavelength of the incident radiation. Light is scattered from each scatterer in the scattering volume, which is defined as the region in the sample illuminated by the light source. At a point in the far field, say a position on the laboratory wall, the sum of the fields from each individual particle could sum to give a maximum, near to this maxima a minima in intensity would be observed where the fields cancel. As one observes the intensity fluctuations on the laboratory wall it would be observed that the pattern is moving, or if one only observes one position on the wall the intensity fluctuates with time. The rate at which the intensity fluctuates is related to the motion of the scatterers in the sample. This rather beautiful, so called speckle pattern (see fig. 2.10), is used to record the average motion of scatterers in a sample.

Traditionally DLS is used as a technique to size particles, an example of this is shown in figure 2.8 where the viscosity of the solvent is known and the Stokes-Einstein relation is

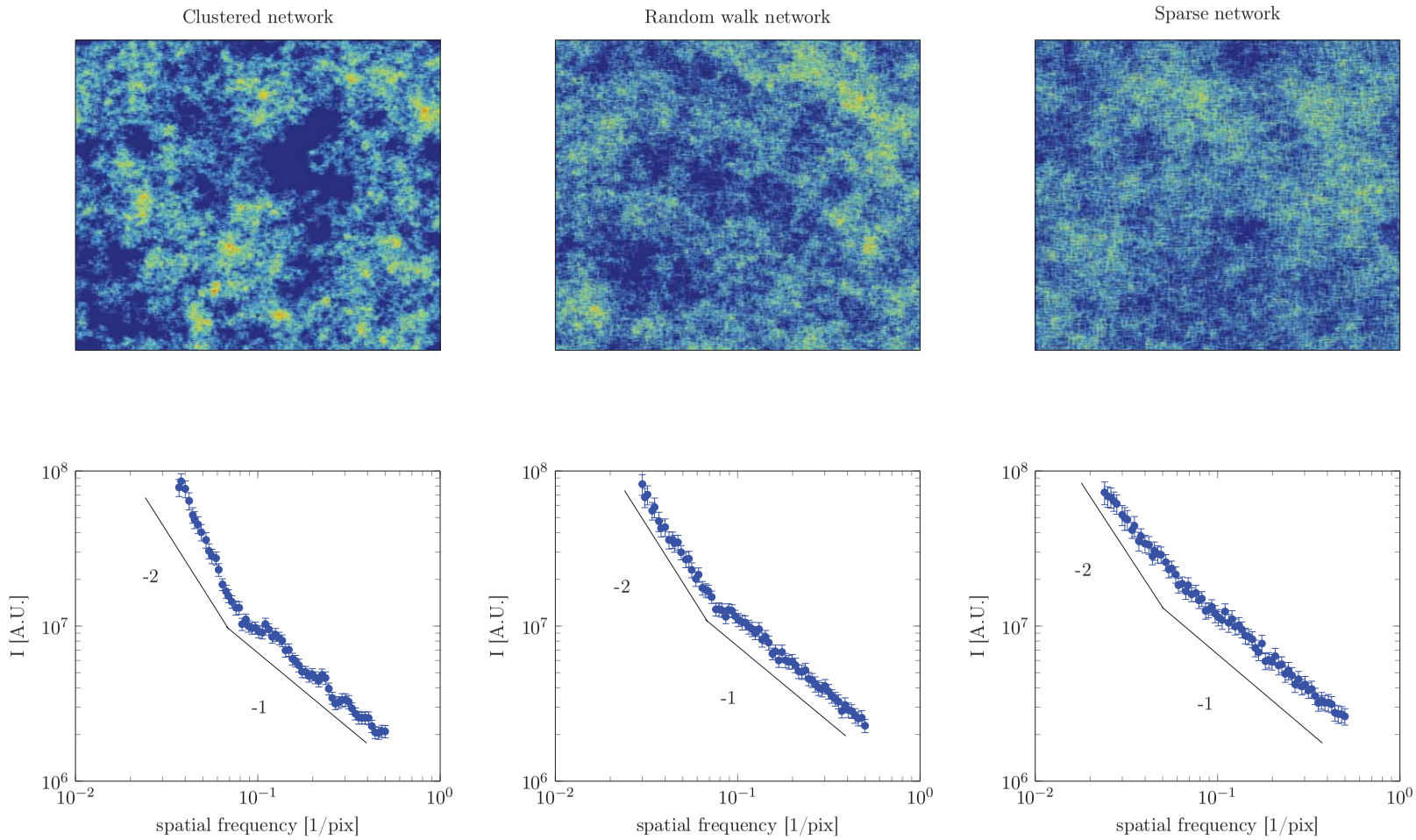

FIGURE 2.7: Simulated scattering data from networks with different architectures. The top figures are the network architectures, and the lower plots the calculated corresponding small angle scattering. In the low q regime the difference in the amount of clustering is visible as a change in slope on the log-log plots. It follows the predicted trend of a random walk having a slope of 2, a clustered network a slope greater than 2 and a self-avoiding chain a slope less than 2.

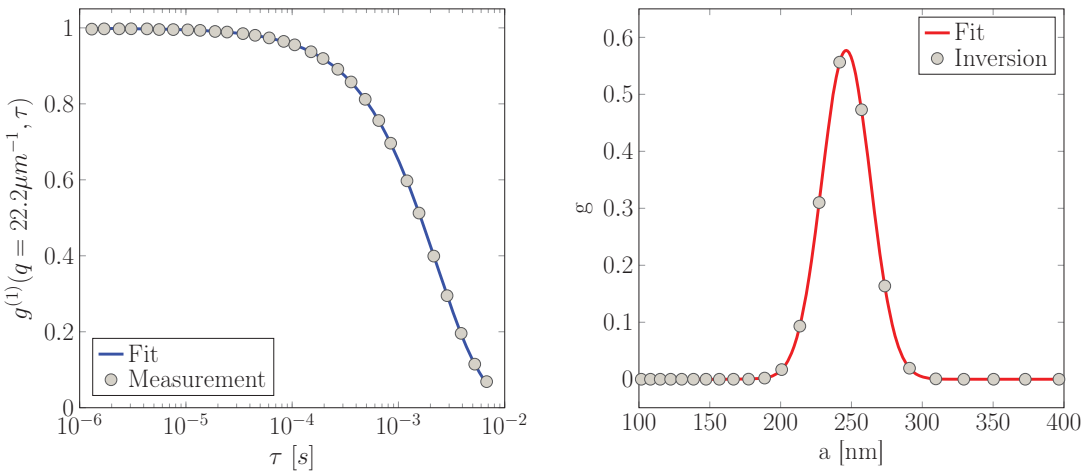

FIGURE 2.8: Dynamic light scattering from $2a = 505$ nanometre latex spheres, and size information extracted using an inverse Laplace transform. The red data on the right is a fit to a Gaussian function with $\mu = 246.3 \pm 0.7$ nm and $\sigma = 24 \pm 1$ nm.

used to extract the particle size [88]. A more recent use of dynamic light scattering is to extract the viscoelastic properties of the medium that particles of a known size diffuse through and is known as passive microrheology [89]. Another common use of dynamic light scattering is sizing of molecules, such as polymers and proteins in solution. Often these large molecules in solution can self assemble and have unpredictable hydrodynamic radii, such as in micelle formation. In figure 2.9 a plot of the PCS of a dilute pectin solution is shown. It can be seen that even in a dilute solution, pectin does not reside as a single entity but as tenuous aggregates.

During an experiment the normalized time correlation function of the scattered light is typicality calculated by measuring the intensity at some initial time, $I(\mathbf{q}, 0)$, and some time later, $I(\mathbf{q}, \tau)$, with the following correlation calculation:

$$g^{(2)}(q, \tau) \equiv \frac{\langle I(\mathbf{q}, 0) I(\mathbf{q}, \tau) \rangle}{\langle I(\mathbf{q}) \rangle^2} \tag{2.27}$$

performed in hardware. The dynamics measured are related to the scattering angle through the difference in path length of light scattered from different positions within the sample. Light collected at smaller angles means that the scatterers must travel a larger distance to produce a phase difference change of 2π. Once the phase is changed by a factor of 2π the light can be said to be completely uncorrelated.

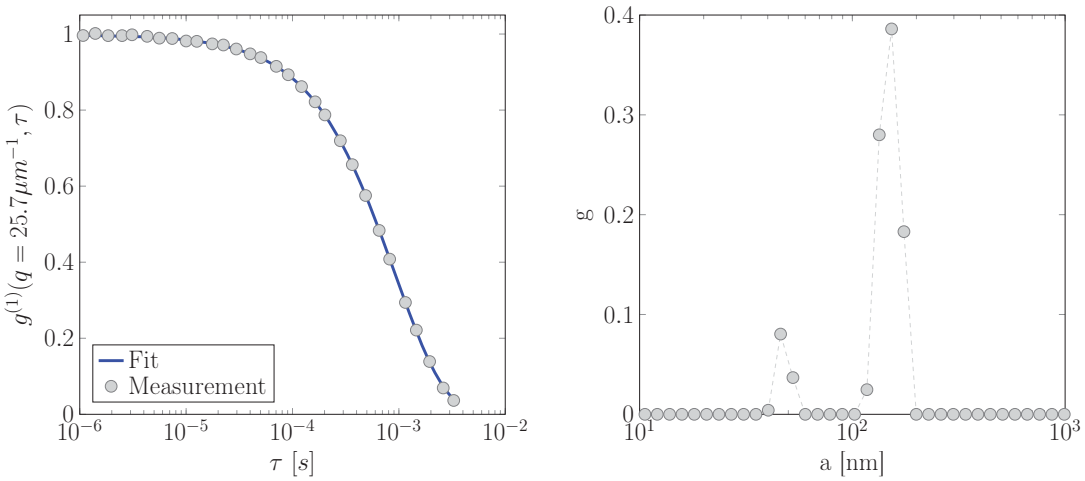

FIGURE 2.9: DLS data for a dilute solution of B76 pectin at pH 4.5. It can be seen that there is a bimodal distribution of the particle size.

To extract information on the particle size the field correlation, $g^{(1)}$ is calculated using the Siegert relation [90, 91]:

$$g^{(2)}(q,\tau) = 1 + \beta|g^{(1)}(q,\tau)|^2 \tag{2.28}$$

where β is a parameter related to the efficiency of the detection optics, and for a well aligned system should be close to unity.

For particle size measurements the field correlation is related to the particle radius, a, through:

$$g^{(1)} = \exp(-q^2 D_0 \tau) \tag{2.29}$$

where D_0 is the diffusion constant given by the Stokes-Einstein equation:

$$D_0 = \frac{k_B T}{6\pi\eta a} \tag{2.30}$$

For a system with polydisperse particle radii it has been shown that the field correlation function is a sum of exponentials:

$$g^{(1)}(q,t) = \int \mathrm{d}D P(D_0) \exp(-D_0 q^2 \tau) \tag{2.31}$$

where $P(D_0)$ is the normalized intensity-weighted distribution of the diffusion constants. $g^{(1)}$ is the inverse Laplace transform of $P(D_0)$ with respect to D_0, and therefore by applying the inverse Laplace transform on the field correlation function one can extract

a distribution of particle sizes [77], see figures 2.8 and 2.9. The inverse Laplace transform is a highly ill-posed problem, so great care must be taken to iteratively increase the accuracy of the inversion to avoid producing erroneous results.

Traditional DLS measurements are limited in that measurements cannot be performed in materials with very slow dynamics, multiple scattering and / or that are non-ergodic (where the time and spatial averages are not equal) [92]. To perform measurements in highly multiple scattering media one must use a formalism called diffusing wave spectroscopy. Non-ergodic or materials with very slow dynamics can be measured using many different techniques, although one of the smplest and most robust is called multiple-speckle light scattering. It consists of a detector that collects and averages over multiple speckles, rather than performing the averaging in time.

2.1.2.1 Diffusing Wave Spectroscopy

Diffusing wave spectroscopy (DWS) is an extension of DLS that is undertaken in the highly multiple scattering regime [93, 94]. A sample prepared for DWS has a turbidity similar to that of milk and as light passes through the sample it is scattered multiple times so that the light itself takes a random walk as it passes through the sample. Due to the light being scattered many times each particle position only needs to change by a very small amount for a significant change in the correlation function to be observed, which makes the technique very sensitive. Unlike DLS / PCS where the scattering vector determines the length scale of the dynamics, the length scale is governed by the number of times that light is scattered in the sample and as a result DWS measures dynamics on smaller length scales. The parameter l^*, which describes the distance light must travel before it's direction is completely randomized, also describes the sensitivity, and a smaller l^* means the sample scatterers light more often as it passes through the sample. At the detector the intensity is related to the superposition of all fields from light of all paths through the sample to the detector, which is related to the field correlation by a sum of exponentials [93]:

$$g^{(1)}(t) = \int_0^\infty P(s) e^{-(2k_0^2 < \Delta r^2(t) > /6) s/l^*} ds \tag{2.32}$$

where s is the path length, $k_0 = 2\pi/\lambda$ and $P(s)$ represents the distributions of path lengths through the sample. For the work carried out in this thesis the entire side of the

cuvette was illuminated and transmitted light collected. For this geometry a solution to the Laplace transform exists (commonly used to describe the transfer of heat in a solid) and the field correlation can be related to the mean-square displacement of particles in the media by [93]:

$$g^{(1)}(\tau) = \frac{\left[\frac{L/l^*+4/3}{z_0/l^*+2/3}\right]\left[\sinh\left(\frac{z_0}{l^*}\sqrt{k_0^2\langle\Delta r^2(\tau)\rangle}\right) + \frac{2}{3}\sqrt{k_0^2\langle\Delta r^2(\tau)\rangle}\cosh\left(\sqrt{k_0^2\langle\Delta r^2(\tau)\rangle}\right)\right]}{\left[1+\frac{8t}{3\tau}\right]\left[\sinh\left(\frac{L}{l^*}\sqrt{k_0^2\langle\Delta r^2(\tau)\rangle}\right) + \frac{4}{3}\sqrt{k_0^2\langle\Delta r^2(\tau)\rangle}\cosh\left(\sqrt{k_0^2\langle\Delta r^2(\tau)\rangle}\right)\right]} \tag{2.33}$$

here L is the thickness and z_0 is the penetration depth, which is typically set equal to l^*. To extract the mean square displacement (MSD), $\langle\Delta r^2\rangle$, first an experiment is performed with a known phase volume of probe particles in water (a medium of known viscosity) to extract the l^* of this standard, l^*_{std}. The l^* of the sample, l^*_{smp}, can then be calculated by measuring its transmitted intensity relative to the standard which is related to l^*_{std} by:

$$\begin{aligned} T_{std} &\propto \frac{l^*_{std}/L}{1+4l^*_{std}/3L} \\ T_{smp} &\propto \frac{l^*_{smp}/L}{1+4l^*_{smp}/3L} \end{aligned} \tag{2.34}$$

Thus by measuring the ratio of the transmitted intensities of the two samples the l^*_{smp} of the unknown sample can be calculated when l^*_{std} is known. Finally an inversion on equation 2.33 can be performed to extract the MSD.

2.1.2.2 Scattering from non-ergodic media

A major challenge in measuring the dynamics of media where the scatterers are confined, such as in a glass or gel, is that the scatterers cannot occupy all of phase space [92]. The typical method to perform a photon correlation spectroscopy measurement uses time averaging to obtain better statistics and one assumes that the time average is equal to the ensemble average. If the particles are confined this method is not valid. A number of techniques exist to obtain the dynamics of non-ergodic materials. The techniques rely on spatially averaging over many speckles. One of the first techniques, which used the same detector and optics as a regular PCS measurement, was slowly rotating the sample [95]. For DWS a second cell with an ergodic sample can be used to decorrelate the light while still obtaining the part of the correlation where the dynamics are faster than those of the second, ergodic sample [96]. A rotating diffusing disk [97] or an angled

plate [98] can be used to obtain the fast dynamics but at the expense of the long-time information, which is truncated to ensure a proper inversion of the field correlation function. The most simple and robust technique to access the slower dynamics is using a 2 dimensional CCD or CMOS detector to average over many speckles (see figure 2.10 for an example of the speckle pattern) and remove the need to perform a temporal average [99]. This technique is known as multi-speckle light scattering (MSLS) and has many advantages over the other techniques. The biggest disadvantage with this technique is the frequency that data can be recorded is many orders of magnitude less than using a photo multiplying tube or avalanche photo diode, which are the most common detectors for single speckle light scattering techniques.

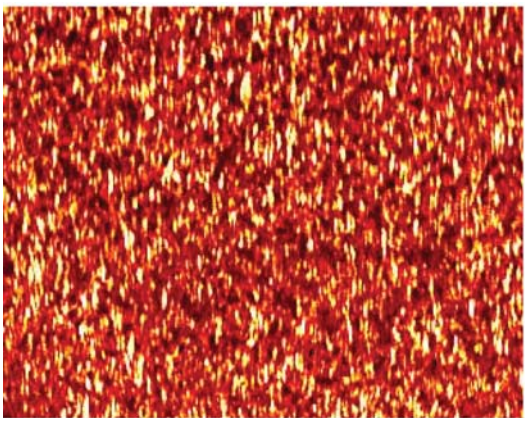

FIGURE 2.10: False color portion of the speckle pattern from a carrageenan network formed in potassium chloride, measured by the author.

2.1.2.3 Photon Correlation Imaging

Photon correlation imaging is a recently developed extension to MSLS: see figure 2.11 for a schematic of the technique. It is similar to MSDLS, although it also measures coarse grained spatial information about the dynamics by using a lens with an aperture that serves as a spatial filter [100]. The recorded speckle images are averaged over in 10x10 pixel areas and a map of the dynamics in space is produced. For the apparatus used during this work the resolution over which the dynamics could be measured was approximately 50 micron sections of the sample.

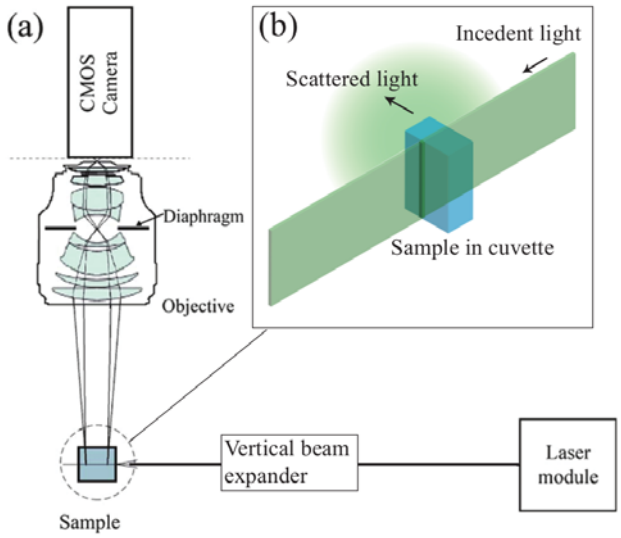

FIGURE 2.11: Schematic of PCI setup used in this work. Figure modified from ref. [16]. (a) shows an overview of the optical layout and (b) the colimation of the laser at the sample and the sample cell.

2.1.3 Rheology

Rheology is a field devoted to the study of the flow and deformation of matter and it is the "gold standard" method used to characterise the mechanical properties of matter. A rotational rheometer applies either a rotational stress σ or strain γ to a material held in a known geometry and measures the response. For a purely elastic material, in the small deformation limit, Hooke's law applies: $\sigma \propto \gamma$, and a shear modulus, G is defined for different materials to give [101]:

$$\sigma = G \times \gamma \tag{2.35}$$

which only applies to materials that are elastic, that store the energy exerted on deforming them. For materials which only dissipate the energy applied to deform them, the stress is proportional to how fast you deform them, $\dot{\gamma}$ and the constant that defines the ease with which one can deform them is the viscosity η:

$$\sigma = \eta \times \dot{\gamma} \tag{2.36}$$

For a sinusoidal strain:

$$\gamma(t) = \gamma_0 \sin(\omega t) \tag{2.37}$$

with an amplitude γ_0 and angular frequency ω. It can be seen that for a liquid where $\sigma \propto \dot{\gamma}$ the frequency dependence of a sinusoidal stress are now out of phase by 90 degrees. So for a material that displays both a liquid-like and solid-like behaviour the frequency dependent response of an oscillatory stress can be written as:

$$\sigma(t) = \gamma_0[G'(\omega)\sin(\omega t) + G''(\omega)\cos(\omega t)] \tag{2.38}$$

where G' defines the storage modulus and G'' the loss modulus.

2.2 Aims of the thesis

This project aims to apply experimental techniques to further characterise the structure, dynamics and mechanical properties of pectin networks. A general soft-matter physics approach is utilized to further understand the properties of the constituents, the mechanism of self-assembly, their self assembled architecture, and finally the mechanical properties of the resulting material. Furthermore, we extend knowledge of the dynamical processes in pectin networks into the low dynamical regime which describes the non-equilibrium state of the systems. The relationship between the structure, dynamics and mechanical properties of pectin based materials are not well understood, and while pectin is an important part of the plant cell wall, it has been left in the shadows of other more well-studied carbohydrates such as alginate. Previous studies on the structure and dynamics of gelled pectin networks have focus on the high frequency dynamics [66, 102] and the bundle size of junction zones [67] respectively. The

current work reveals previously unseen slow dynamics in pectin gels and focusses on characterising this slow motion and the structure over a broad range of length scales.

The thesis can be divided into three main experimental chapters. Firstly we performed dynamical and rheological measurements on an acid-induced pectin gel at a range of temperatures. A slow dynamical process was measured, this slow motion has not been observed before in pectin gels and initiated the focus on slow dynamics. A phenomenological model, called the glassy wormlike chain model, was employed to further interpret the results. This will be elaborated on in chapter 2. We then further structurally and mechanically characterise pectin acid gels and solutions. We started by measuring the evolution of the gelled structure using time resolved small-angle x-ray scattering. A worm-like chain model was fitted to characterise the structure over length-scales from the radius of dimeric structures and the fractal dimension of the network extracted. Rheological studies were then utilized to monitor the mechanical properties as the gelation process evolved and compared to the evolution of the large-scale structural properties of the network. This work formed chapter three. Finally, we sought understanding of the mechanism behind the slow dynamics that were observed in chapter two. To understand this slow motion we designed gels that we predicted to have different structures, which would result in modifying the slow dynamics. We measured the structure using small-angle x-ray scattering and carried out novel light scattering techniques to measure the dynamics over the period of minutes to hours, which formed chapter 4. Further results on the structure of dilute pectin pectin solutions and pectin gels are reported on in the Annexes.

3. Micro-Rheological and Nonlinear Rheology Studies Reveal the Glassy Nature of Acid-Induced Pectin Networks

As published in:

R R Vincent, B W Mansel, A Kramer, K Kroy, and M A K Williams. Micro- rheological behaviour and nonlinear rheology of networks assembled from polysaccharides from the plant cell wall. *New Journal of Physics*, 15(3):035002, March 2013. ISSN 1367-2630. doi: 10.1088/1367-2630/15/3/035002.

Abstract

The same fundamental questions that have driven enquiry into cytoskeletal mechanics can be asked of the considerably less-studied, yet arguably just as important, biopolymer matrix in the plant cell wall. In this case, it is well-known that polysaccharides, rather than filamentous and tubular protein assemblies, play a major role in satisfying the mechanical requirements of a successful cell wall, but developing a clear structurefunction understanding has been exacerbated by the familiar issue of biological complexity. Herein, in the spirit of the mesoscopic approaches that have proved so illuminating in the study of cytoskeletal networks, the linear microrheological and strain-stiffening responses of biopolymeric networks reconstituted from pectin, a crucial cell wall polysaccharide, are examined. These are found to be well-captured by the glassy worm-like

chain (GWLC) model of self-assembled semi-flexible filaments. Strikingly, the nonlinear mechanical response of these pectin networks is found to be much more sensitive to temperature changes than their linear response, a property that is also observed in F-actin networks, and is well reproduced by the GWLC model. Additionally, microrheological measurements suggest that over long timescales (>10 s) internal stresses continue to redistribute facilitating low frequency motions of tracer particles.

3.1 Introduction

3.1.1 Mesoscopic models

Much progress has been made recently in the study of the mechanical properties of solutions and networks of semi-flexible protein filaments, driven largely by the desire to understand the functionality of the cytoskeleton [21, 103–107]. Indeed, the results gleaned from the study of such biologically relevant structures as F-actin have been exploited by soft-matter physicists interested in modelling the behaviour of all manner of semi-flexible filaments [102, 108–110]. In particular the worm-like chain (WLC) model of polymer physics [55, 74] has found considerable utility in describing the dynamics and the force-extension behaviour both of single biopolymer chains, and of higher-order semi-flexible assemblies such as multimeric filaments, ribbons, tubes and worm-like micelles. Generally speaking the malleable mechanics and slow dynamics characteristic of soft and biological matter arises from the thermo-reversible assembly of low-dimensional manifolds into (transient) meso-structures.

In order to understand the time and length-scale dependent rheological properties of such systems, the central task is to understand how the interactions interfere with the dynamics of the individual constituents. Inspired by the underlying similarity of constraint release in these systems and the thermally-activated jumping between local traps in soft glasses [73, 111], the glassy worm-like chain (GWLC) model [112–114] addresses this problem by exponentially stretching the relaxation spectrum for single-chain motions involving wavelengths beyond a characteristic backbone length, Λ. While the exponential form of the stretching is not microscopically derived, the model builds on the known mesostructure of the polymer network, and introduces a single stickiness parameter that intuitively corresponds to the characteristic depth of the potential

well that a cross-linked chain section must escape in order to dissociate. Despite its simplicity, the model has been successfully used to parameterize the frequency- dependent linear rheology of such systems, their nonlinear strain-stiffening behaviour, and additionally, by considering the stress dependence of the number of cross-links, their eventual softening [115].

The GWLC theory has not however been previously applied to the analysis of polysaccharide systems, despite the fact that they too play a significant role in controlling the mechanical properties of tissues, ranging from mammalian connective tissues to the ubiquitous plant cell wall. Herein, pectin gels have been studied to test the utility of existing models in describing the rheological properties of networks of this important class of carbohydrate biopolymers. Specifically the acid-gel system was selected where the stickiness of the interaction between network strands originates from hydrogen bonding between extended patches on different chains. Microrheological studies were undertaken using (i) diffusing wave spectroscopy (DWS), which maximizes the accessible frequency range and (ii) multiple-particle tracking (MPT), which allows the homogeneity of the system to be probed. In addition measurements of the stressstrain behaviour following the application of varying pre-stresses were carried out. Results are discussed within the framework of models of semi-flexible networks and slow, glassy network relaxation.

3.2 Materials and methods

3.2.1 Pectin structure

Pectin is a complex polysaccharide of the plant cell wall that is thought to be a crucial player in the control of its mechanical functionality [26]. Indeed, recent reappraisal of cell wall mechanics and growth control suggests not only that pectin is crucial in this regard in Charophycean algae, the closest relatives of land plants, but that primitive pectin-based control mechanism may still be functional in terrestrial plants. In this context, it has been proposed to be operating in parallel to more recently evolved and more widely-studied mechanisms involving cellulose, xyloglucans and expansins [116]. While the detailed structure of pectin is still a matter of debate to some extent [42] the preponderance of homogalacturonan (HG) regions within the macromolecular chains is well established. These regions consist of the order of 100 sugar residues connected

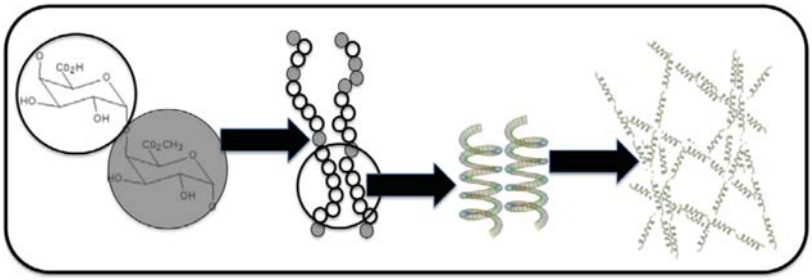

FIGURE 3.1: Molecular to Mesoscopic: a schematic diagram showing the molecular structure of the pectin used herein, its proposed assembly mechanism in conditions of low pH, and larger-scale formation of a network.

together by axial 14 linkages and are essentially co-polymers of two types of sugar ring: galacturonic acid and its methylesterified counterpart (figure 1). Depending upon the pH-controlled protonation state of the bare galacturonic acid group, and the enzymatically controlled pattern of the uncharged but hydrophobic methylester substituents this yields chain sections that have varying local charge densities and differing propensities to associate through polyelectrolytic, specific ion, hydrophobic or hydrogen bonding effects. These HG regions are primarily responsible for the associations between chains, and from a physical point of view, offer the exciting possibility of tuning the interaction potentials by various mechanisms.

3.2.1.1 Pectin assembly

In vivo, one mechanism employed in network building is the establishment of cross-linking of the chains by employing calcium ions to bridge runs of contiguous charged sugar residues on HG components of different polymeric backbones. The importance of the pectin methylesterase (PME) enzymes in controlling the amount and distribution of uncharged methylester groups is highlighted by the fact that around 10 consecutive charged residues on each HG are required to form stable calcium-mediated junctions at room temperature [117–119, 119]. Such ionotropic pectin gels have been considered as a simple model of the middle lamellar of primary plant cell walls and a reasonable description of the pollen tube [120] and indeed recent work has focused on utilizing plant-cell-wall enzymes to release the ion-binding galacturonic-acid-sequences in an attempt to model biomimetic processes of network formation [66, 121–123]. The study of more traditional calcium-set gels where the ions are either introduced into hot pectin solutions

that are then cooled or are released slowly from the dissolution of sparingly soluble salts under ambient conditions has a long history [26], owing primarily to the industrial relevance of such systems in food processing.

By contrast, it was only relatively recently that it was demonstrated that highly concentrated solutions ($\sim$10 c^*) of pectins containing limited amounts of the methylesterified version of the sugar rings (low degree of methylesterification (DM)) could also form networks in the absence of ions at low pH [34]. Subsequently it was shown that pectic polymers displaying more extreme contiguous intramolecular arrangements of the unmethylesterified galacturonic acid groups could in fact form acid-induced networks at much lower polymer concentrations, similar to those familiar in the more traditional calcium-mediated systems [36]. There is good experimental evidence from chiroptical methods, calorimetry, potentiometry and NMR to suggest that, as the pH is lowered in these systems and the charged residues are progressively protonated, the preferred polysaccharide conformation about which the solution-state structure fluctuates changes from being a 2-fold extended helix to a more compact 3-fold structure [124–126]. In its turn this conformational change favors the lateral aggregation of chains between antiparallel 3-fold helical stretches via hydrogen bonding [45, 46]. This hydrogen bonding, that is ultimately responsible for the association of the chains into a stress-bearing network, involves interactions between protonated or charged carboxyl moieties and thus clarifies the detrimental effect of methylesterification in these systems. The presence of methylester groups reduces the pH sensitivity of the intramolecular conformational changes and hinders the zipping together of intermolecular junction zones that require concerted runs of hydrogen bonds in order to form relatively thermally stable connections. The propensity of the polymers to form such zipped junction-zones is similarly maximized in samples in which the methylester content has been reduced using plant derived PME enzymes that are known to produce extreme contiguous sequences of bare galacturonic acid residues. While the relevance of these acid-induced gels, assembled primarily from hydrogen-bonded associations, is unclear at present for the native plant cell wall compared to their calcium-assembled cousins, these systems are considerably more thermoreversible than their ionotropic counterparts and as such are convenient model systems for experiments on semi-flexible networks.(Fig.3.1)

3.2.1.2 Pectin

Pectin (Mw 30-100 kDa), extracted from apple pomace, was purchased from Fluka Biochemika (Sigma Aldrich, Switzerland) as a starting material. The sample average DM and the degree of blockiness [36] of this sample, and that produced by modification as described below, were determined using capillary zone electrophoresis as previously described [127, 128].

3.2.1.3 Pectinmethylesterase

Pectinmethylesterase (EC 3.1.1.11) was purchased from Sigma Aldrich (P5400) in order to remove methylester groups from the starting pectin in a contiguous manner. Stock solutions of the enzyme were prepared by dissolving 0.01 g of dried PME in 20 ml in Milli-Q water, and were stored at -20 °C in Eppendorf tubes. Aliquots were thawed prior to conducting experiments and used immediately.

3.2.1.4 Polygalacturonase

Polygalacturonase (EC 3.2.1.15) was used to digest the polymeric substrates in order to verify a contiguous intramolecular distribution of the unmethylesterified (acidic) groups. The enzyme was kindly provided by Jacques Benen from the University of Wageningen. It is a pure endo-PG II isoform from Aspergillus niger and has an absolute requirement for the sugar residues in the active site to be unesterified in order for the chain to be severed, which yields the degradation pattern methylester-sequence dependent. A 1 ml solution of substrate at a concentration of 0.5 wt % and pH 4.2 (acetate buffer 50 mM) was incubated with 20 μl of enzyme solution (0.094 mg ml^{-1} protein). At the end of the reaction, the enzyme was denatured at 90 °C for 3 min and the oligosaccharides liberated by the digestion were quantified using capillary electrophoresis as previously described [129–131].

3.2.1.5 Polystyrene

Polystyrene tracer particles, either with a diameter of 505 nm or fluorescently-labelled with a diameter of 546 nm were purchased from Polyscience Inc. (Warrington, PA) (2.62% solid stock solutions) for use as microrheological probes.

3.2.1.6 Pectin fine structure engineering

Pectin solutions of 1% w/w were made by dissolving pectin powder in a 50 mM 4-(2-hydroxyethyl)-1 piperazineethanesulfonic acid (HEPES) buffer, adjusted to pH 7.5 with NaOH. 0.5 ml of enzyme solution was then mixed into 30 ml of solution, and the solutions were left at 20 ° C for a chosen time, depending on the final DM decrease required and on the rate of the de-methylesterification processes. Assuming the enzyme reaction followed a simple Michaelis-Menton law and were in the linear section of the product production curve (which was monitored independently using NMR to follow the liberation of methanol [132]), preliminary experiments were used to determine the rate of DM decrease as 4% per hour for the plant PME de-methylesterification used. Thus, the PME action could be stopped after a pre-requisite time in order to achieve a desired final DM. This was carried out by decreasing the pH and subsequently heating the solution to 80 ° C for 5 min to denature the enzyme. The modified polymers were extracted by dialysing twice against Milli-Q water. The dialysed solutions were freeze-dried and the engineered polymers recovered and stored dry. The recovered pectin samples had their fine structures analysed by capillary electrophoresis, which characterized the sample-average DM of the pectin, and provided evidence of the distribution of the acidic residues by analysing the endo-PG II-digest products. The result of this measurement was crucial as it confirmed our ability to prepare a polymer with the propensity to form long contiguous runs of hydrogen bonded sugar rings, unhindered by the presence of methylester substituents.

3.2.1.7 Acid induced gels

The acid-induced gels studied herein were obtained by gradually decreasing the pH of solutions of a pectin of DM (42 ± 4)%, (designated DM42) that had been obtained by PME modification of a more highly methylesterifed starting pectin as described

above. This polymer was confirmed (by the dominance of unmethylesterified oligomers present in its endo-PG II digest pattern) to have a highly blockwise distribution of its unmethylesterified, bare galacturonic residues. The acidification of the polymer solution was performed slowly over a few hours, initiated by the addition of glucono delta-lactone (GDL) to the polymer solutions, which slowly hydrolyses releasing protons (figure 3.2, inset). While low DM pectins are known to be capable of forming gelling systems under simple acidification [123], polymers with blocky fine structures as engineered herein have been found to have a greater propensity to assemble under these conditions than those with the same DM but a random distribution thereof [36]. Indeed, at 1% polymer concentration preliminary experiments (data not shown) on various low-DM pectin solutions found that upon acidification (i) a DM 35% pectin with a random distribution of its acidic residues showed no discernible change in its materials properties, (ii) a DM of 37% sample with a medium blockiness simply viscosified slightly and (iii) the more blockwise 42% sample studied in depth here formed a respectable gel network. This indicates that long contiguous blocks of acidic residues (longer than those required to chelate calcium into a stable cross-link for example) are indeed necessary to form stable junction zones under these conditions, consistent with the idea of weak but concerted hydrogen bonded junctions being formed when the pH is decreased.

To form the gels the required amount of a pectin stock solution of 2 wt% adjusted to pH 7, bead solution (for DWS experiments and MPT), Milli-Q water and GDL were mixed in order to achieve a polymer concentration of 1% w/w and an initial GDL concentration of 8% w/w. The solution was quickly loaded into the appropriate sample cell and left to set for 24 h. The final pH of the gels studied was around 2, below the approximate pKa of the galacturonic acid groups (3.5-4.5), and well within in the acid-gel forming domain found previously [31].

3.2.2 Microrheology

The aim of microrheology is to extract the rheological properties of soft materials from the motion of probe particles immersed in the material [109, 133, 134]. It is a non-destructive technique and recovers the linear response of the material. The essential quantity that passive microrheology experiments set out to measure is the mean square

displacement (MSD) of tracer particles, which can be acquired to high frequencies using DWS or in a spatially resolved fashion with MPT.

3.2.2.1 Diffusing Wave Spectroscopy

The DWS apparatus used in this study is based on a system that has been fully described previously [135]. The samples were contained in polystyrene cells of width 10 mm, height 50 mm and path length L of 4 mm, and were illuminated with a 35 mW HeNe Melles-Griot laser operating at 633 nm. The laser beam was expanded to approximately 8 mm on the surface of the cell. The transmitted scattered light was detected using a graded-index (GRIN) lens and a single-mode optical fibre (P1-3224-PC-5, Thorlabs Inc., Germany), which was typically split by a fibre optic beam splitter and sent to two Hamamatsu HC120-08 PMT photomultiplier-tube modules. The correlation function was then calculated using a cross-correlation method in software on a standard personal computer. Using cross-correlation helped circumvent dead-time in the electronics as well as eliminating after-pulsing effects. Tests were run for between 10 and 100 min to minimize noise. The temperature was controlled using a TLC 50 temperature-controlled cuvette holder purchased from Quantum Northwest (www.qnw.com), which uses a thermoelectric device. For heat removal, a small flow of water passes through a heat exchanger and a calibrated TC 125 temperature controller was used with a thermistor to control the temperature to within 0.1 ° C. For an expanded beam mode, the field autocorrelation function is obtained from the measured intensity autocorrelation function using the Siegert equation. In the transmission geometry, the field correlation function has been given by Weitz and Pine [94] and once the light mean free path is determined, the MSD can be obtained from the experimental correlation functions by inverting them with a zero-crossing routine.

3.2.2.2 Multiple Particle Tracking

An inverted microscope (Nikon Eclipse TE2000-U) on an air damped table (photon control) equipped with a mercury lamp (X-cite Series 120PC EXFO) and a 60x 1.2 NA (Nikon, Plan Apo VC 60x WI) water immersion objective lens was used for MPT experiments. Samples were gelled in welled microscope slides and sealed with a cover slip. A CCD camera (Foculus FO124SC) was used to record image series taken for

up to 100 s; at 43 frames per second. Typically around 40 individual particles were tracked in any one experiment. xy coordinate data was extracted from the movies using a homebuilt program written using algorithms obtained from: http://physics.georgetown.edu/matlab/. In-house programs to calculate the MSD and Van Hove correlation function were used in combination with a program to de-drift the data obtained from: http://people.umass.edu/kilfoil/downloads.html.

3.2.2.3 Pre-Stress experiments

A stress controlled ARG2 rheometer from TA Instruments (Delaware, US) was used with a cone and plate geometry of 40 mm diameter and a cone angle of 4 °. The linear complex modulus was determined by applying small amplitude strain oscillations (0.1 %) at 1 Hz, and the normal force was also recorded at every time step. Pre-stress experiments were performed by superimposing small-amplitude stress-oscillations, dσ, on top of a constant pre-stress σ_0 [136]. The differential stiffness was then computed for different pre-stresses according to:

$$K = \frac{d\sigma}{d\gamma} \tag{3.1}$$

with dγ being the measured small-amplitude strain oscillation. The temperature was controlled using a Peltier system to within 0.1°C.

3.2.3 Theoretical description of the GWLC

3.2.3.1 Differential shear modulus

In the GWLC model, the microscopic susceptibility is given by

$$\alpha_f(\omega) = \frac{L^4}{k_B T \pi^4 l_p^2} \sum_{n=1}^{\infty} \frac{1}{(n^4 + n^2 f/f_L)(1 + i\omega\tilde{\tau}_n/2)}, \tag{3.2}$$

where L is the polymer length, l_p the persistence length, f an optional backbone tension, and $f_L = \kappa\pi^2/L^2$ the Euler buckling force of a rod with bending rigidity κ [74]. The

mode relaxation time $\tilde{\tau}_n$ is given by

$$\tilde{\tau}_n = \begin{cases} \tau_n & (\lambda_n < \Lambda) \\ \tau_n \exp[\mathcal{E}(\lambda_n/\Lambda - 1)] & (\lambda_n \geq \Lambda), \end{cases} \tag{3.3}$$

where

$$\tau_n = \frac{\tau_L}{n^4 + n^2 f/f_L} \qquad \text{with} \qquad \tau_L = \frac{\zeta_\perp L^4}{\kappa \pi^4} \tag{3.4}$$

is the mode relaxation time of the WLC. For wavelengths $\lambda_n \equiv L/n$ longer than the typical contour length Λ between neighboring bonds, the relaxation is stretched by an Arrhenius factor, where the stretching parameter $\mathcal{E}$ controls the slowing down of the dynamics, which is understood to be caused by the interactions of the test polymer with the surrounding polymer network.

The stretching parameter $\mathcal{E}$ is interpreted as the height of a characteristic barrier in units of $k_B T$. It may be either enhanced or lowered by external or internal stresses, which are therefore coupled into the Arrhenius factor in Eq. 3.3 as follows:

$$\mathcal{E} \to \mathcal{E} \pm f/f_T \qquad \text{with} \qquad f_T \equiv k_B T/\Delta, \tag{3.5}$$

where, f_T represents the scale of the thermal equilibrium tension present in a force-free sample, and Δ the characteristic width of the free energy barrier. For the fits in the following, we invariably assume that the negative sign holds in Eq. 3.5. Within this scheme, the shear modulus of the prestressed sample is equivalent to the nonlinear differential shear modulus:

$$K^*(\omega) = \frac{c}{15} \frac{c_p \Lambda}{\alpha_f(\omega)} - i\omega\eta, \tag{3.6}$$

where c_p is the polymer concentration, η the solvent viscosity and c a fitting parameter [137].

Experimental data can be fitted to the model by inserting the microscopic susceptibility $\alpha_f(\omega)$ from Eq. 3.2 into Eq. 3.6 and evaluating it numerically for $\omega = \omega_\Lambda = 2\pi/\tau_\Lambda$. Assuming strong entanglement, $L \gg \Lambda$, and with the substitution $n \to z = n\ (\Lambda/L)$,

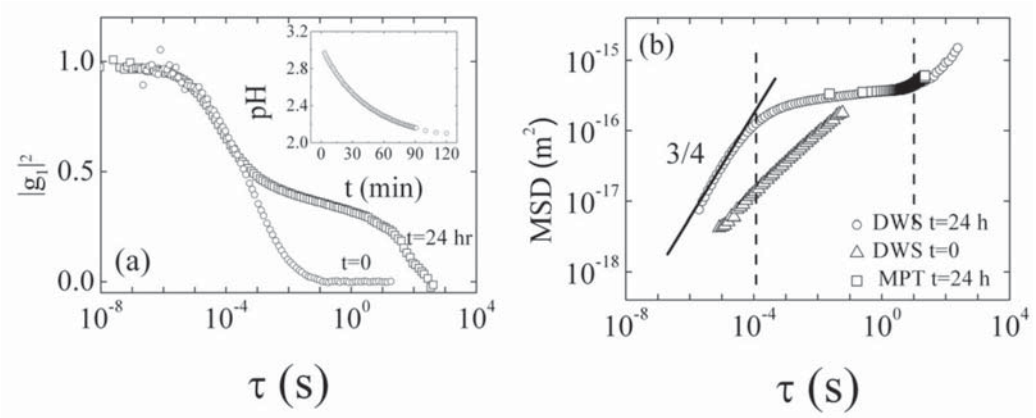

FIGURE 3.2: (a) De-correlation of scattered laser light induced by the movement microspheres within a sample of the engineered DM42 blocky-pectin recorded immediately, and 24 hours after, the introduction of GDL at 25°C. The inset shows the rate of the pH decrease induced by the hydrolysis of the GDL. (b) The corresponding mean square displacement of the probe particles.

the sum can be approximated by the following intergrals:

$$\alpha_f(\omega) \approx \frac{\Lambda^4}{k_B T \pi^4 l_p^2} \left\{ \int_1^\infty \mathrm{d}z \frac{1}{z^4 + z^2 f/f_\Lambda + i\omega\tau_\Lambda} + \int_0^1 \mathrm{d}z \frac{1}{z^4 + z^2 f/f_\Lambda + i\omega\tau_\Lambda \exp[\mathcal{E}(1/z - 1)]} \right\}. \tag{3.7}$$

The prestress σ is related to the tension f via $\sigma = f/(5\xi^2)$, where the mesh size ξ is given by $\xi \equiv (3/c_p L)^{1/2}$.

3.2.3.2 Mean-Square Displacement

The transverse mean-square displacement (MSD) of the polymer backbone, which we assume to be proportional to the MSD of the embedded microspheres, is given by:

$$\delta r_\perp^2(t) = \frac{4L^3}{l_p \pi^4} \sum_n \frac{1 - \exp(-t/\tilde{\tau}_n)}{n^4 + n^2 f/f_L}, \tag{3.8}$$

Analogous to the procedure for the susceptibility in the preceding section the sum can be approximated by the following integrals:

$$\delta t_{\perp}^{2}(t) \approx \frac{4\Lambda^{3}}{l_{p}\pi^{4}} \left\{ \int_{1}^{\infty} \mathrm{d}z \frac{1-\exp[-t/\tau_{\Lambda}(z^{4}+z^{2}f/f_{\Lambda})]}{z^{4}+z^{2}f/f_{\Lambda}} + \int_{0}^{1} \mathrm{d}z \frac{1-\exp[-t/\tau_{\Lambda}(z^{4}+z^{2}f/f_{\Lambda})\mathrm{e}^{-\mathcal{E}(1/z-1)}]}{z^{4}+z^{2}f/f_{\Lambda}} \right\}. \tag{3.9}$$

3.3 Results and discussion

3.3.1 Diffusing Wave Spectroscopy

(Fig.3.2) (a) shows the de-correlation of scattered laser light induced by the movement of microspheres within a 1% solution of the engineered DM42 blocky pectin, recorded both immediately and 24 hours after the introduction of GDL at 25°C. The inset shows the rate of the pH decrease induced by the hydrolysis of the GDL. In particular it is noteworthy that the pH was stable within uncertainties at around (2.1±0.1) when the measurements were taken in the gelled state. There is a clear change in the form of the correlation function as the acidification induces interactions between the chains and a network is formed. While generally reminiscent of the behaviour of glasses and the qualitative form predicted by mode-coupling theory [138] the correlation function of the gel does ultimately show ergodic behavior and (Fig.3.2) (b) shows the derived MSD of the tracer particles corresponding to the recorded correlation function.

3.3.1.1 Short times: $\tau < 0.1$ ms:

The high-frequency (short-time) data reveals that the MSD of the tracer particles scales with lag time according to a power law with an exponent close to 0.75 of (0.76±0.01). This behaviour has also been seen in previous experiments carried out on calcium-induced pectin gels, where it was assumed to arise from the fact that the persistence length of the network strands was an appreciable fraction of the mesh size so that the bending of semi-flexible entities dominates the resistance to small displacements of the tracer particles. Indeed, many hierarchically assembled biopolymer networks have been found to behave as semi-flexible networks [102–110, 139, 140], as exemplified by F-actin. In previous work on calcium-induced pectin gels, the proposal that the 3/4

power law scaling found at short times was a strong signature of the bending undulations of individual semi-flexible polymers was supported by TEM and SAXS data [67], and carrying out such studies of the current acid gel systems forms part of ongoing work.

3.3.1.2 Intermediate times: 0.1 ms $<\tau<$ 10 s:

While the short-time behaviour exhibited by the tracer particles embedded in the acid-induced gels studied herein echoes that observed in the previously studied calcium-induced networks, the longer time behaviour is strikingly different. Whereas a largely time-independent elastic plateau is observed for calcium-induced gels (as expected for long-lived cross-links), the acid-induced gels clearly show some time dependency in this regime (Fig.3.2) (b). Such behaviour has been demonstrated for F-actin networks [114] and living cells [141] and is thought to arise from the thermally activated release of cross-links permitting the sliding of network chains. Its observation in our measurements could indicate that the binding energies of the putative hydrogen bonded cross-links are less than those associated with the ionic bonding in the previously studied systems, as might be expected. In order to pursue the molecular nature of the associations, the experiment was repeated in the presence of urea, a recognized hydrogen-bond breaker. (Fig.3.3) (a) shows these results along with fits to the GWLC model. It can be seen that i) the GWLC model provides an excellent description of the microrheological data exhibited by these systems over some six orders of magnitude in time; ii) that the insensitivity of the 3/4 scaling region to the presence of urea confirms its origin in the mechanics of single filament deformations; and iii) that the increased mobility of tracer particles upon increasing the urea concentration supports the hypothesis that hydrogen bonds are largely responsible for the formation of the cross-links.

The experiments were repeated for a number of polymer concentrations. Despite the fact that a plateau in the MSD data at the lower frequencies was not strictly observed, the value of the MSD in this slowly varying intermediate region (at 0.1 s) was recorded and is plotted in (Fig.3.3) (b). It can be seen that the concentration dependence of this quasi-plateau value is close to a power law scaling with an exponent of 1.4; as was found in previous work on calcium mediated pectin networks and indeed as predicted for lightly cross-linked semi-flexible networks [102, 108]. Thus, the microrheological

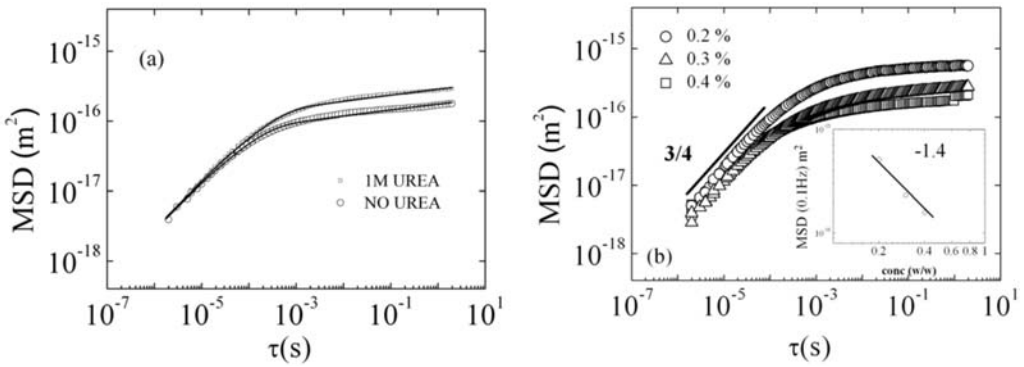

FIGURE 3.3: (a) MSD of tracer particles as obtained by DWS measurements: 0.4 % wt DM42 acid induced gel, and the same gel formed in the presence of 1 M urea (Only every third data-point is shown for clarity). The lines are the best fits from the GWLC model, with Λ=0.1215 μm (lower curve), Λ=0.146 μm (upper curve), $\zeta_\perp$=0.223 pNs/μ m^2, $\mathcal{E} = 26$ and L, l_p, ξ as for the fits in the temperature dependent data discussed in due course. (b) The value of the MSD in the slowly varying intermediate region for a set of experiments performed at low concentrations (at 0.1 s). It can be seen that the concentration dependence of this quasi-plateau value is close to a power law scaling with an exponent of 1.4.

properties of acid pectin gels over the frequency range from $1-10^6$ Hertz are well captured by a model of self-assembled semi-flexible filaments, with weak hydrogen-bonded connections permitting slippage at longer timescales.

3.3.1.3 Long times: $\tau >$ 10 s:

However, over longer timescales still another processes is observed that completely decorrelates the scattered light and manifests as the MSD increasing as a power law with a sub-diffusive exponent that is substantially greater than that found at intermediate times. Multiple particle tracking (MPT) experiments were subsequently undertaken in this regime in order to validate the observed phenomena and investigate the possibility that it arises from dynamical heterogeneities or the "pore-hopping" behavior of a subpopulation of beads. While the latter process has previously been observed in F-actin networks when the size of the tracer particles approached that of the mesh [142], in this system a uniform mesh size is estimated to be an order of magnitude smaller than the probes.

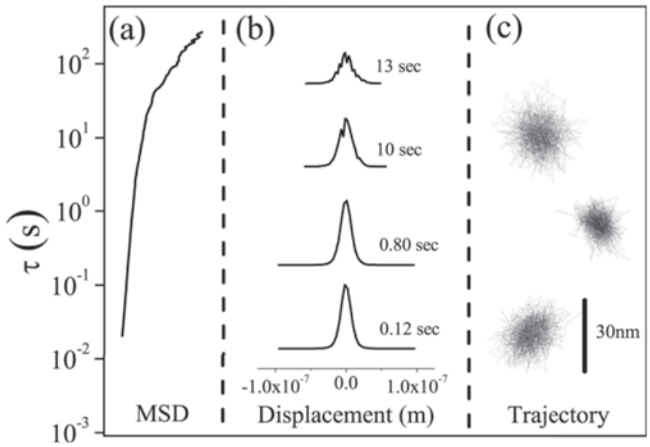

FIGURE 3.4: (a) The ensemble-averaged MSD obtained from the MPT experiments carried out on a gelled sample of the the engineered DM42 blocky-pectin recorded 24 hours after the introduction of GDL at 25°C. (b) and (c) show Van Hove plots of the probe particles displacements and a selection of individual particle trajectories respectively, calculated for a variety of times lags within the short, intermediate and long-time regimes.

3.3.2 Multiple Particle Tracking

(Fig.3.2)(b) includes the ensemble-averaged MSD from the MPT experiments compared with that obtained from DWS. The MPT result has been scaled to three dimensions and additionally by a factor to account for slight differences in probe size between the two experiments. It can be seen that there is reasonable agreement between the results of the two independent experiments suggesting that indeed the long-time behavior observed is physically meaningful. (Fig.3.4)(a) shows the ensemble-averaged MSD, while (Fig.3.4)(b) and (c) show Van Hove plots of the probe particles displacements and a selection of individual particle trajectories respectively, calculated for several time lags within the intermediate and long-time regimes. Van-Hove plots calculated for times less than 1 s could all be very clearly described by Gaussian distributions, suggesting a unambiguously dynamically homogeneous system over these timescales. For sampling displacements over the scarcer longer time intervals the statistics become substantially worse, and while there are no clear indications in the Van-Hove plots of sub-populations of probe particles moving in different micromechanical environments (Fig.3.4) it is difficult to eliminate such a possibility completely. All individual trajectories appear similar by eye, as illustrated in the figure, with typical dimensions on the order of less than one tenth of the beads size.

3.3.3 Nonlinear Rheology: stress-stiffening experiments

Nonlinear rheological measurements provide a further critical test to assess how far the similarity between our pectin gels and cytoskeletal and extra-cellular networks extends. They also allow for a more thorough investigation of the utility of the GWLC model in capturing the essential behavior of the acid-induced pectin networks. Stress-stiffening experiments were performed on the microrheologically-interrogated systems as described in the experimental section. Fig.3.5 shows the scaled normalized differential shear modulus of pectin plotted against the scaled prestress, where three regimes can be distinguished. At low stress, it is approximately constant, meaning that the stress-strain relation is linear. Above a certain stress, one observes a stiffening with increasing prestress, until it drops sharply.

3.3.3.1 Temperature dependence of Nonlinear Rheology

Of particular interest to us is the dependence of the stress-stiffening response on temperature. The data in Fig.3.5 reveal a characteristic reduction in the stiffening response of the differential shear modulus as the temperature increases by a few degrees. The measurements were performed at four different temperatures, 10, 20, 30 and 40°C. Temperature enters the model via different pathways. The solvent viscosity decreases with temperature and is estimated using the empirical Vogel–Fulcher relation

$$\eta(T) = \eta_\infty \exp\left(\frac{A}{T - T_{VF}}\right) \tag{3.10}$$

with the parameters for H_2O, $\eta_\infty = 0.02984$ mPas, $A = 496.9$ K and $T_{VF} = 152.0$ K. This affects the transverse friction coefficient which is proportional to η. In the nonlinear regime, the effect of the temperature dependence of the viscosity on the differential shear modulus is negligibly small, but it cannot be neglected for linear measurements, as we will see in the following section for the mean-square displacement. Besides the viscosity, the bending rigidity $\kappa = k_B T l_p$ and the dimensionless effective barrier height, $\mathcal{E}$, depend on temperature. The precise functional for the experimental system is unknown. While any relation of the form $\kappa, \mathcal{E}^{-1} \propto T^x$ with $0 \leq x \leq 1$ seems physically plausible, the precise value of the exponent x only affects the predictions of the model relatively mildly. In contrast the model predictions turn out to be more sensitive to the structural

properties encoded in the crossover scale Λ and the bond length Δ, for which even a weak temperature dependence matters. For the fits in Fig. 3.5, a linear increase of Δ with temperature is assumed, as shown in Fig. 3.6 (a).

Furthermore, there seems to be a small signature of the fact that the pectin sample was prepared at room temperature and then heated up or cooled down to the temperature of study, as seen from the slight but significant deviations of the best-fitting values for Λ from the average (Fig. 3.6 (b)). While such temperature-history dependent effects can be seen to be minor in these thermoreversible gels, it is possible that trapping and annealing effects might be detectable. The slight increase of Λ for temperatures of 10°C and 20°C might be interpreted as an indication that the fraction of closed bonds is slightly reduced when the sample is cooled instead of heated. This is in accordance with the results of several stiffness measurements for pectin [34], but also for other polysaccharides, such as κ-carrageenan [143] or agarose [144]. In these experiments, it has been observed that the stiffness of the polysaccharide networks was higher when the sample is heated up to a certain temperature compared to the case when it is cooled down to it. Attributing a lower stiffness to a lower fraction of closed bonds, and thus a larger distance Λ between neighboring bonds for the cooling process, our data seem consistent with these studies.

Indeed, these experiments show the clear stress-stiffening and eventual softening as is predicted by the same GWLC model that described the microrheological response so well [74, 114] and the sensitive dependence of its strength on various parameters such as temperature and polymer concentration that has previously been observed in many biopolymer networks (F-actin [74]; intermediate filaments [145, 146]; microtubule-actin mixtures [147]; and collagen [148]).

3.3.4 Temperature dependence of Microrheological experiments

Inspired by ability of the GWLC to capture the temperature dependence of the non-linear behaviour, the microrheological study was revisited and the DWS experiments were repeated as a function of temperature (fig.3.7). After the gel had formed experiments were carried out as a function of temperature between 20 and 40°C. It was noted that any differences in the pH caused by the temperature changes were minimal (<0.2). Samples were left to equilibrate for 30 minutes at each temperature before the

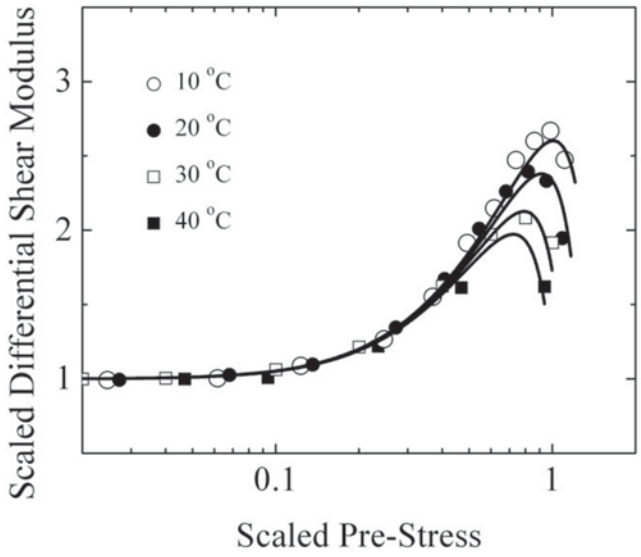

FIGURE 3.5: Differential modulus plotted against the pre-stress, scaled by the zero-pre-stress differential modulus, for a 1 %w/w pectin solution (DM42) acidified to pH 2 by GDL, at four different temperatures. Fitted with the assumptions described in the text and the following parameters: $L = 0.5\mu m$, $l_p = 0.3\mu m$, $\xi = 0.011\mu m$, $\mathcal{E}/k_BT = 32$ for $T = 30°$C, $\zeta_\perp$=62.17η, c=0.121. The barrier width Δ and the distance Λ between closed bonds as a function of temperature are plotted in Fig. 3.6.

measurements were made. On revisiting previous temperatures minimal hysteresis was observed. Interestingly, while the behaviour on short and intermediate times did not significantly change over the relatively small temperature range that could be practically investigated at present, the anomalous longer time-scale de-correlation of the scattered light described previously, showed a clear evolution with temperature. On increasing the temperature such behaviour can be observed at shortened timescales and with an increasing terminal relaxation rate (fig.3.7). Neglecting these long timescale processes then it could be said that whereas in the nonlinear regime the stiffness of the pectin gels investigated decreases noticeably with increasing temperature, in the linear regime the effect of temperature is small.

The predictions of the GWLC model, given by the result of the numerical evaluation of equation 8 for vanishing prestress and with the *same* parameters used in the preceding section in order to successfully fit the non-linear behaviour, are shown by the black curves in Fig.3.7. The slight increase of the MSD with temperature at short times is mainly due to the decreasing solvent viscosity according to the Vogel-Fulcher relation, Eq. 3.10; while at intermediate times, temperature enters mainly via the barrier height $\mathcal{E}$, and the data are consistent with the presumed standard Arrhenius behaviour

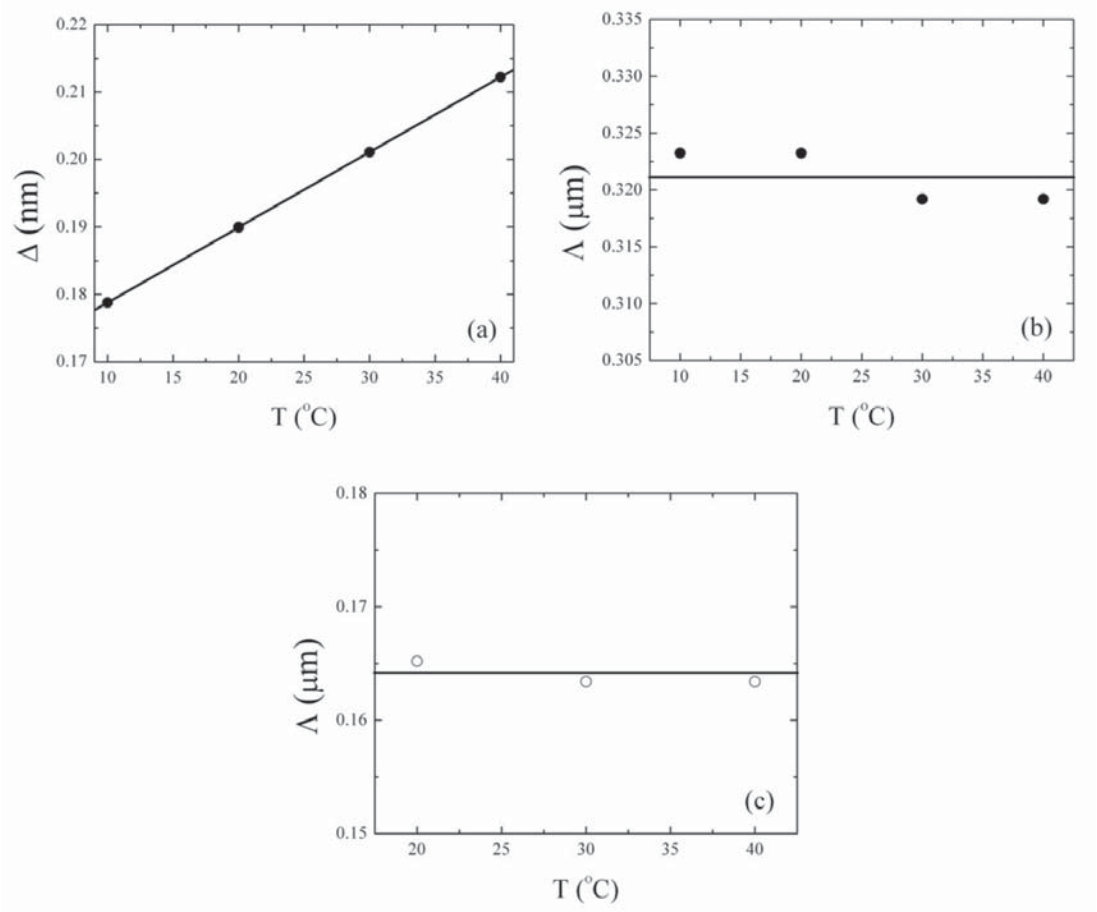

FIGURE 3.6: Barrier width Δ and distance Λ between closed bonds as a function of temperature used for the fits in Fig. 3.5

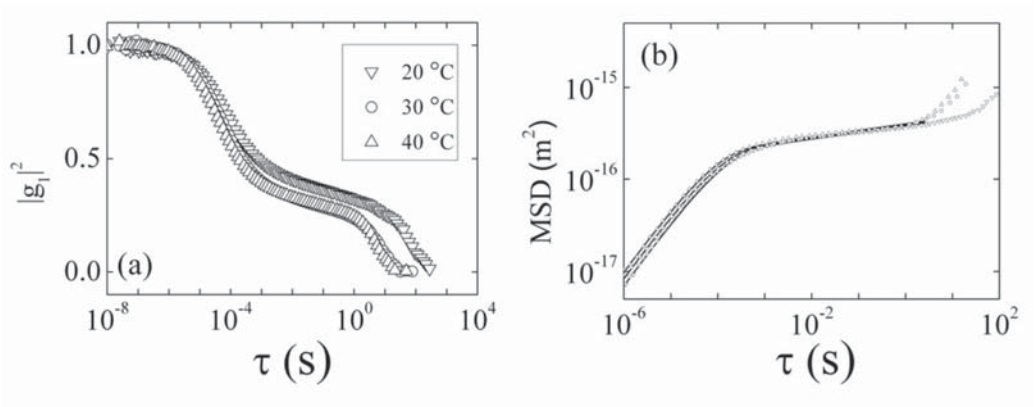

FIGURE 3.7: (a) De-correlation of scattered laser light induced by the movement microspheres within a sample of the engineered DM42 blocky-pectin recorded 24 hours after the introduction of GDL. After the gel had formed experiments were carried out as a function of temperature between 20 and 40 °C. (b) The corresponding mean square displacement of the probe particles for the data shown in (a). Mean-square displacement as a function of time at different temperatures, 20, 30, 40°C (bottom to top), fitted with the GWLC using the same values for $L, l_p, \xi, \mathcal{E}, \zeta_\perp, \Lambda$ as for the nonlinear fits in the preceding section.

$\mathcal{E} \propto T^{-1}$. We do not attempt here to model the terminal relaxation for τ>10 s, the investigation of which remains a focus for our continued investigations. It is clear that the otherwise relative insensitivity of the linear microrheological properties on temperature is well captured within the GWLC framework, despite its prediction of the substantial temperature dependence of the non-linear properties.

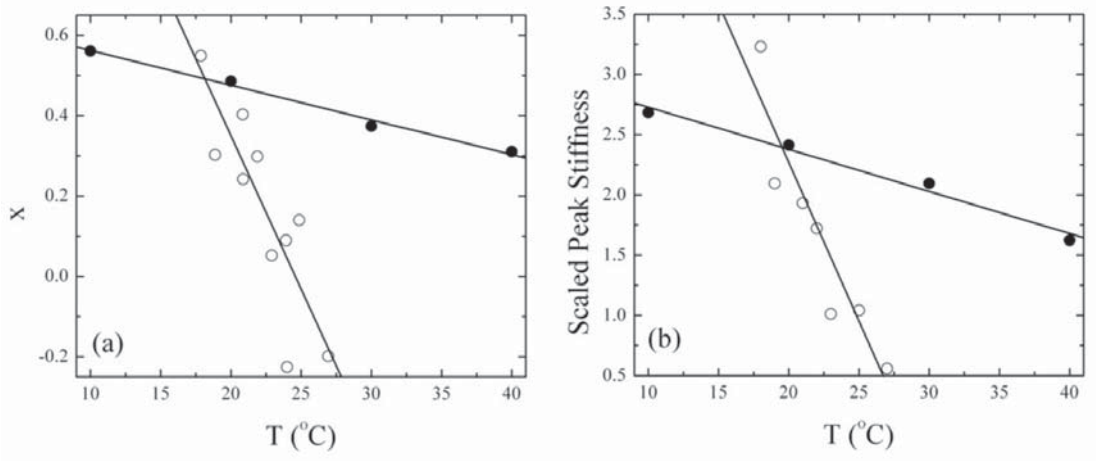

FIGURE 3.8: (a) Slope of the normalized inverse creep compliance and differential modulus, respectively, plotted against the temperature for actin (open circles) and pectin (filled circles). (b) Scaled peak stiffness plotted against the temperature for actin (open circles) and pectin (filled circles).

3.3.4.1 Comparison with experimental data from other systems

As for pectin, the stiffness of F-actin decreases with temperature [114]. To compare the actin data to the pectin data recorded for the acid-induced gels investigated here, the slope x of the scaled normalized differential shear modulus has been determined for the data shown in Fig. 3.5 and plotted alongside the normalized inverse of the creep compliance of F-actin measured in previous work (Fig. 3.8(a)). On average, a temperature increase of 10°C causes a decrease of the slope by about 18 % for this pectin system, compared to about 150 % for F-actin. Additionally, we determined the scaled peak stiffness for the F-actin and the pectin data, shown in Fig. 3.8(b). For F-actin, a temperature increase of 10°C decreases the peak value of the normalized inverse creep compliance by about 90%, while for pectin, a temperature increase of 10°C causes a decrease of the scaled peak stiffness by about 13 %.

A decrease of stiffness with temperature has also been observed in non-adherent cells [149]. In this work the Young's modulus, which was determined from AFM force measurements, decreased from 3.2 kPa to 0.5 kPa within a temperature range of 21°C, so that for a temperature change of 10°C, the stiffness decreased by around 60 %. In summary, it can be stated that an increase in temperature causes a decrease of the stiffness of these acid-pectin gels, as well as of F-actin networks and non-adherent cells, but that the temperature effect at least for these particular pectin systems, is less pronounced. The different extent to which temperature changes affect the nonlinear rheology in pectin, actin and cellular systems is of fundamental interest. It is, to date, unclear whether these differences arise on the microscopic scale or rather depend on the mesoscale network architecture. Interestingly the analysis in our paper shows that the temperature effects for acid-induced pectin gels are quantitatively explained by a generic polymer-based model (the GWLC), and could be indicative of a somewhat special mechanism at work in F-actin and cells.

3.4 Conclusion and outlook

The pursuit to understand the mechanics of the cytoskeleton has already driven forward great advances in experimental and theoretical areas of microrheology and semi-flexible network theories. Herein we have studied a polysaccharide network, whose understanding promises to enlighten another considerably less-studied, but arguably just as important, biopolymer matrix, that of the plant cell wall. It has been shown that the study of these systems too can benefit hugely from what has already been achieved in the understanding of reconstituted protein matrices and the application of mesoscopic models of semi-flexible filaments and glassy dynamics. We have revealed striking analogies between the rheological behaviour of acid pectin gels with molecularly highly dissimilar polymeric systems such as F-actin, intermediate filament and collagen networks. We rationalized the discovered similarity and the corresponding redundancy with respect to the molecular structure within a schematic mesoscopic polymer model that provides a faithful and consistent parametrisation of our linear and nonlinear rheological data, obtained by various measurement techniques. Furthermore, at least for pectin and F-actin, the nonlinear response is found to be much more sensitive to temperature changes than their linear response, a property that is well reproduced by the GWLC model.

As an outlook, this work suggests that polysaccharide networks such as the pectin gels studied here are also promising model systems in their own right for testing and developing mesoscopic theories such as the GWLC model, with their own set of control parameters. In particular, the ability to modify the molecular architecture of the extended cross-linking sites (via the manipulation of the methylester pattern) holds the tantalizing possibility of controlling the junction zone "stickiness" in a systematic way. Additionally using different assembly modalities offers the potential of modifying the mesoscopic network architecture in a controlled way while studying the resulting effects on the temperature sensitivity of the nonlinear rheology. In general, mesoscopic physical models offer the potential to understand how, in principle, mechanical functionality at the cellular level arises from microscopic interactions. They aim to elucidate how a myriad of available molecular level control parameters, ranging from enzymatic modification of polymeric structure to local manipulation of pH and ionic strength, act within a unified framework to achieve the manipulation of the free-energy landscape governing the strength and dynamics of stress-bearing associations. In this way the apparent complexity of the biological can be seen as ensuring the provision of multiple pathways for controlling the same essential physics, with the redundancy not only introducing robustness in the system, but providing mechanisms for compensation, adaptation and homeostasis.

Acknowledgments

We would like to thank Christian Secker for help in the early acid-gel work and Jens Glaser for initial work on the application of the GWLC. RRRV would like to acknowledge AMI (Fribourg) for the use of the ARG2 rheometer. Allan Raudsepp and Yacine Hemar are gratefully acknowledged for interesting discussions.

DRC 16

MASSEY UNIVERSITY
GRADUATE RESEARCH SCHOOL

STATEMENT OF CONTRIBUTION
TO DOCTORAL THESIS CONTAINING PUBLICATIONS

(To appear at the end of each thesis chapter/section/appendix submitted as an article/paper or collected as an appendix at the end of the thesis)

We, the candidate and the candidate's Principal Supervisor, certify that all co-authors have consented to their work being included in the thesis and they have accepted the candidate's contribution as indicated below in the *Statement of Originality*.

Name of Candidate: Brad William Mansel

Name/Title of Principal Supervisor: Martin Williams

Name of Published Research Output and full reference:

R R Vincent, B W Mansel, A Kramer, K Kroy, and M A K Williams. Micro- rheological behaviour and nonlinear rheology of networks assembled from polysaccharides from the plant cell wall. New Journal of Physics, 15(3):035002, March 2013. ISSN 1367-2630. doi: 10.1088/1367-2630/15/3/035002.

In which Chapter is the Published Work: 2

Please indicate either:

- The percentage of the Published Work that was contributed by the candidate: 30%

  and / or

- Describe the contribution that the candidate has made to the Published Work:

  The candidate performed microrheology experiments, and analysis, created key figures and helped with the writing.

Brad Mansel — Digitally signed by Brad Mansel DN: cn=Brad Mansel, o, ou, email=bmansel@gmail.com, c=NZ Date: 2015.05.19 14:17:53 +12'00'

Candidate's Signature — 19/05/2015 — Date

Williams, Martin — Digitally signed by Williams, Martin DN: cn=Williams, Martin, o, ou, email=m.williams@massey.ac.nz, c=US Date: 2015.05.19 12:24:57 +12'00'

Principal Supervisor's signature — 19/05/2015 — Date

GRS Version 3– 16 September 2011

4. Structural and Rheological Characterization of an Acid-Induced Pectin Gel

As submitted in:

B W Mansel, C-Y Chu, A Leis, Y Hemar, H-L Chen, M A K Williams, Zooming In: Structural Investigations of Rheologically Characterized Hydrogen-Bonded Polysaccharide Networks, submitted to *Biomacromolecules*

Abstract

Physical gels are an important class of soft condensed matter, exhibiting complex material properties that differ over a large range of length and time-scales. Self-assembled hydrogen-bonded networks of the polysaccharide pectin, a mechanically functional component of plant cell walls, have been of recent interest as biomimetic exemplars of physical gels, and the micro-rheological and strain-stiffening behaviour have been previously investigated. Despite this detailed rheological characterisation of pre-formed gels, little is known about the fundamental arrangement of the polymers into cross-linking junction zones, the size of these bonded regions, and the resultant network architecture in these hydrogen-bonded materials, especially in contrast to the plethora of such information available for their well-known calcium-assembled counterparts.

In this work, in concert with pertinent rheological measurements, an in-depth structural study of the hydrogen-bond-mediated gelation of pectins is provided. Gels were realised

by using glucona-delta-lactone (GDL) to decrease the pH of solutions of pectic polymers that had a (blockwise) low degree of methylesterification (low DM). Small-angle x-ray scattering (SAXS) and transmission electron microscopy (TEM) were utilized to access structural information on length scales on the order of nanometres to hundreds of nanometres, while complementary mechanical properties were measured, predominantly using small amplitude oscillatory shear rheology. Time resolved SAXS and rheological measurements were performed across the acid induced sol-gel transition and revealed changes in the network architecture, across all accessible length scales, as the mechanical properties evolved. Frequency-sweep and strain-stiffening rheological measurements were performed on cured gels, showing well-formed networks with moduli of several hundred Pascals that strain-stiffened by nearly an order of magnitude. Finally, temperature resolved SAXS measurements were carried out on gels formed in both H_2O and D_2O in order to further investigate structural changes induced on melting and those resulting from subtle changes in solvent-substrate hydrogen bonding. Interestingly, and particularly noteworthy for the interpretation of neutron scattering experiments, measurements showed substantial differences in the clusters formed as part of the gel structure in these different solvents. The study provides new structural information on these biomimetic polysaccharide networks, building bridges from molecular assembly to macroscopic materials properties.

4.1 Introduction

Pectin is a polysaccharide of considerable structural importance in the plant cell wall [25, 26, 57, 116]. In tandem with the fundamental biophysical interest in its native mechanical role, there is also significant interest in pectin-based biomaterials from many different industries due, in-part, to its ability to form a solid material with tuneable mechanical properties [150]. While divalent-ion-chelating pectin gels have been exploited for many decades here we report on the structure and mechanical properties of less-exploited hydrogen-bonded pectin gels that can be formed under acidic conditions. In the spirit of traditional soft matter physics we aim to understand the relationship between structure and mechanical properties. Measurements on the structural aspects of such biopolymer materials are typically experimentally challenging in comparison to mechanical measurements and as such there are considerably fewer structural studies

reported in the literature. In particular there is presently a complete lack of structural data on the acid-induced pectin networks of interest here.

Pectin, as found in the plant cell wall, is a complex hetero-polysaccharide consisting of several domains, predominantly homo- and rhamno-galacturonan (RGI and RGII), the disposition of which is still a matter of debate to some extent [42]. It is clear however that the homogalacturonan (HG) backbone is connected through alpha 1-4 linkages and that it is the intermolecular association of this part of the polymer that is primarily responsible for pectin's ion-binding and gel forming capacity [151]. RGI contains rhamnose residues, alternating with those of galacturonic acid, that act as sites of neutral sugar side chain attachment. However, these branches are often removed during extraction procedures that are used to purify pectin and are consequently not usually present in significant amounts in commercially available samples. In the plant cell pectin is biosynthesised as a weak acid with around 20 percent of the monomers in each homogalacturanan chain bearing an unesterified carboxyl group, with the remaining groups carrying a methyl ester [30]. The ratio of methyl ester groups to acid groups is referred to as the degree of methyl esterification (DM) and can be modified using chemical or enzymatic procedures. Modifying the degree or pattern of methyl esterification can radically alter the gel forming abilities and mechanical properties of the subsequent gels formed. This makes pectin a particularly attractive biopolymer to design and create soft materials with tailored mechanical properties.

Physical gels are formed through dynamic cross-linking, typically involving ionic interactions, hydrogen bonding, van der Waals interactions or topological entanglements, and are commonly weaker than gels formed by permanent covalent bonding [152]. Hydrogen bonding between protonated and un-protonated carboxyl groups on neighbouring chains has been hypothesised to be involved in the formation of acid-induced low DM pectin gels [34]. In order to form a stable junction with a binding energy of several kT requires the concerted action of many such bonds, thus explaining the propensity of substrates with very blockwise patterns of de-methylesterification and of low DM to form acid gels. While a low DM is required for gel formation, it should be noted that if the degree of methyl esterification is too low the pectin can precipitate out of solution rather than forming a stable gel. When acid gels do form they are typically comparatively weak, having storage moduli that rarely exceed hundreds of Pascal [35, 37]. This fact, together with the less clear biomimetic relevance of these acid-induced gels mean the majority of

research on pectin gels to date has focused on their better known ionotropic networks in which the carboxyl groups chelate divalent metal ions. In this work pectin is gelled, at ambient temperature, using the hydrolysis and concomitant release of protons from glucono-delta-lactone (GDL) to reduce the solution pH in a controlled manner.

The polyelectrolytic properties, or more precisely the charge density of the pectin polymer, plays an important role in determining the physical properties of both its solution and gel states. The linear charge density is a result of the number of unmethylesterified carboxyl groups displayed by the substrate, their distribution along a chain, the protonation state of these groups and any counter-ion condensation or screening effects. In general, polyelectrolyte solution behaviour can be complex, with much discussion in the literature as to the effects on both the polymer structure and dynamics [153–155]. The Coulomb interaction is long ranged, so that both the intra- and inter-molecular interactions of the polymer are expected to be modified by the charge density and distribution. This is exemplified by the conformational change from a 2,1 to 3,1 helix that accompanies the protonation of the carboxyl groups in low DM pectin which has been detected by circular dichroism and x-ray diffraction [34]. It is thought that the placement of the carboxyl groups induced by this conformational change, facing them out from the polymer backbone, facilitates inter-chain hydrogen bonding and is key to the acid-induced gelation mechanism.

In the first part of this study the effects of pH on the structural and viscoelastic properties of a block-wise de-esterified, low DM, pectin solution were explored. Experiments were carried out at pH values both at, and below, the pKa, over a range that covers the sol-gel transition (between pH 2 to 3 for this particular sample). Small angle oscillatory shear rheology and small-angle x-ray scattering (SAXS) were used to examine the evolution of mechanical and structural properties during the sol-gel transition and SAXS was further utilized to explore the effects of temperature and solvent on the large scale structure of the system. For a complete overview of the structure present in an acid-induced pectin gel TEM tomography was carried out, on a plastic embedded gel sample, while small-angle x-ray scattering (SAXS) experiments were performed on the corresponding unadulterated gel. Small angle scattering techniques provide a unique approach to access the structural properties of soft materials free from freezing or plastic embedding, as is required with real space electron microscopy imaging techniques such as transmission electron microscopy (TEM) and scanning electron microscopy (SEM),

which could significantly perturb the molecular arrangements in these soft systems. The interpretation of the scattering data, which is measured in reciprocal space, can however be challenging compared to real space techniques and any heterogeneities are pre-averaged over the scattering volume during the measurement itself. To completely characterise the structural properties of biopolymer gels one must not only probe the molecular scale where the individual polysaccharide chains self-assemble, but also the microscale where assemblies typically form a large porous network, and correspondingly we performed SAXS using two different instruments in order to span a larger distance scale and probe large-scale changes in the networks upon heating and cooling.

4.2 Experimental

4.2.1 Polymer and gel preparation

The gelation method exploited herein has been described in detail previously[33]. The polymer fine structure modification was performed by first dissolving dried apple pectin (Sigma) in ultra pure water (milliQ) to a final polymer concentration of 0.25 wt% and then adjusting the pH to 7 using 1N and 0.1N analytical grade sodium hydroxide together with a calibrated digital pH meter. A pH-monitored demethylesterification method was then carried out. The pH of the solution was monitored, and held at 7 by slowly adding known volumes of 0.1N NaOH, to counteract the active PME enzyme liberating galacturonic acid groups on the polymer backbone from their methyl esters, until the DM was lowered to 40 % (as confirmed by capillary electrophoresis). The sample was then heated to 80 ˚C to denature the PME, frozen using liquid nitrogen and finally freeze dried for 24 hours to allow for the long term storage of the dried polymer. Subsequently a solution was made by dissolving 0.02 g of the freeze dried pectin in 1.5 ml of deionized water. Next 0.16 g of glucono delta-lactone (GDL) was dissolved in 0.32 ml of deionized water and mixed with the pectin solution as quickly as possible, in order to minimize any hydrolysis of GDL occurring before mixing, while being careful not to form bubbles. This solution was then either loaded into the requisite sample cells for small-angle x-ray scattering or into the rheometer geometry as described below.

4.2.2 Small-angle X-ray Scattering

Gel structure was characterized using small-angle x-ray scattering experiments that were performed at two different synchrotron facilities. The first experiments were performed at beamline 23A1 at the National Synchrotron Radiation Research Centre (NSRRC) in Hsinchu Taiwan. Here, samples were held in 2.5 mm path-length cells, sealed with Kapton windows, and were irradiated with 15 KeV x-rays. A Dextris Pilatus 1M detector, with a sample to detector distance of 3072 mm, collected the scattered radiation. Further information about the beam-line optics can be found in Liu et al. [156]. For heating experiments acquisitions were made for approximately one minute while moving the sample in the beam in order to reduce the possibility of radiation damage, then the sample was heated in 10 °C increments each of 5 minutes duration, with each heating step followed by 5 minutes equilibration time and the acquisition or a further dataset. For time resolved measurements acquisitions were taken continuously with ten second exposures for a period of 20 minutes.

The second round of experiments were performed at the Australian Synchrotron on the SAXS beamline [157], where samples were prepared in 1.5 mm diameter quartz glass capillary tubes (purchased from Hampton Research or capillarytubes.co.uk) and irradiated with 11 KeV radiation. Multiple exposures were averaged over post-acquisition in order to increase the signal to noise ratio. For temperature measurements samples were heated in 5 °C intervals and allowed to equilibrate for 10 minutes before collecting data between heating steps. Scattered radiation was collected using a Dextrus Pilatus 1M detector as at NSRRC, although in this case a longer sample to detector distance of 7179 mm was taken advantage of in order to access information on larger length scales. It should be noted that care was taken to subtract the scattering from GDL using a series of background experiments and that measurements were carried out to ensure radiation damage was not an issue.

4.2.3 Rheology

Rheology experiments were performed using an Anton Paar MCR 302 rheometer equipped with a Peltier-controlled heating plate and a 50 mm cone and plate geometry. All experiments were performed with the gel formed in-situ on the rheometer. First time-resolved

experiments were performed by imposing a 0.5 % strain at 1 Hz to investigate the evolution of the mechanical properties. Once gelation had been fully realized pre-stress measurements were performed. An oscillatory shear of between 0.1 to 10 Hz at 0.5% strain was superimposed onto a constant stress, P, that was varied from P=0.1 to P=100 Pa to obtain the frequency dependent mechanical properties of the pre-stressed gel.

4.2.4 Transmission Electron Microscopy

Gels were fixed with 0.1% Ruthenium Red and phosphate buffered 2.5% glutaraldehyde prior to dehydration in a graded ethanol series and embedding in an epoxy resin (ProCure 812, ProSciTech, Thuringowa, Australia). Sections with nominal thickness of 150 nm were cut with an ultramicrotome and pre-irradiated for 15 minutes at low magnifcation prior to image acquisition. Two-dimensional micrographs and tomographic tilt series were recorded on a JEOL JEM-1400 transmission electron microscope with a LaB6 cathode operated at 120 kV and under low-dose conditions including using a spot size 3 and synchronised beam blanking and acquisition. Projection images were collected on a Gatan Ultrascan 2K x 2K CCD with a pixel size of 0.86 nm (nominal magnification of 12 000X). The tilt increment was 1 degree, and the tilt range was typically plus/minus 75 degrees. Tomograms were recorded using 'Recorder' software (System in Frontier/JEOL, Japan) and subsequently aligned via fiducial markers using eTomo (NCIM, Boulder, Colorado). The aligned projections were reconstructed using weighted back-projection, again using eTomo.

4.3 Results and discussion

4.3.1 Structural analysis of pectin solutions

Figure 4.1 shows the results obtained from SAXS experiments performed on pectin solutions at a range of concentrations made from the pre-modified, commercially-available, apple pectin that was later demethylesterified and subsequently used to form acid gels. Reassuringly the scattering profiles exhibited by these original pectin solutions are similar to those expected for a semi-dilute semi-flexible polymer solution [76]. It can be clearly seen, particularly as the concentration increases, that the data exhibits 2 distinct

regimes. (Power law behaviours with exponents of -2.1 and -1 are shown as a guide to the eye). In the low q (large length-scale) regime the average fractal dimension of the mesh formed by the overlapping polymer solution can be obtained: -2 would indicate a random arrangement of the polymers in 3D space, and lower fractal dimensions (power law exponents) more expanded arrangements. For the data obtained on these pectin solutions a slope of approximately -2.1 is obtained, indicating instead that the chains have a moderately clustered conformation and do not fill space as efficiently as a simple random walk. The high q (short length scale) linear region with a slope of approximately -1 indicates the rod-like nature of the polymers below the persistence length or mesh-size, so that the q value at which the transition between the regions occurs gives information on the length scale at which the space-filling becomes dominated by the geometrical architecture of the mesh rather than the individual polymers. It should be noted that the relatively long persistence length and small radius of a pectin chain means that the application of many models available for describing polymeric systems would produce redundant parameters, so instead a generalized power law model in the form of a Beaucage model was fitted to the data (Figure 1: Solid Lines). In general

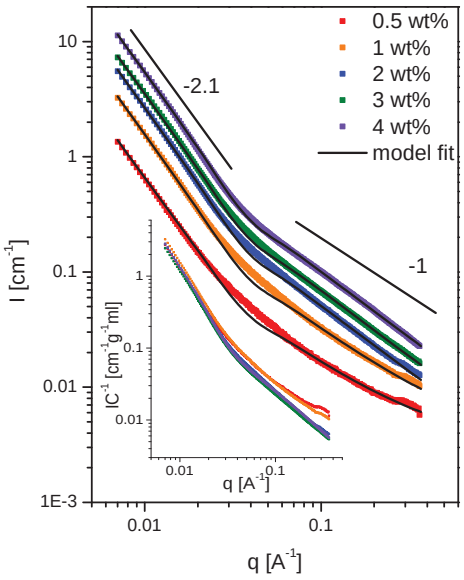

FIGURE 4.1: SAXS data recorded from apple pectin solutions as a function of concentration. Fits to the Beaucage model as described in the text are also shown. Two regimes are present: the lower q data corresponding to the arrangement of pectin chains in space and the higher q, to the rod like behaviour of a single chain. The insert shows the scattering normalized for concentration.

the Beaucage model can be used to describe a system with a Guinier regime describing the average size of the entities comprising the elements of the fractal system, followed by power law regions. Systems such as polymer coils display this type of scattering [158, 159]. The modified Beaucage model was used where the intensity as a function of momentum transfer vector, $q = 4\pi/\lambda \sin(\theta/2)$ is described by [159–161]:

$$I(q) \cong \left\{ G \exp\left(-\frac{q^2 R_g^2}{3}\right) + B \exp\left(\frac{-q^2 R_s^2}{3}\right) \left(\frac{1}{q^*}\right)^p \right\} + \left\{ G_s \exp\left(\frac{-q^2 R_s^2}{3}\right) + B_s \left(\frac{1}{q_s^*}\right)^{p_s} \right\} \tag{4.1}$$

where $q^* = q/[\mathrm{erf}(qR_g/6^{0.5})]^3$, $q_s^* = q/[\mathrm{erf}(qR_s/6^{0.5})]^3$, R_s is the radius of gyration of the sub-unit, G is the Guinier prefactor defined by $G = N_p \Delta\rho^2 V_p^2$, and $\Delta\rho$ is the change in electronic density, where N_p and V_p are the number of particles and the volume of the particles in the scattering volume respectively. B and B_s are given below where Γ is the gamma function and p is the power law exponent of the fractal. This model provided by Hammouda [161], uses the complete expansion of the polymer fractal model.

$$B = \frac{Gp}{{R_g}^p} \left[\frac{6p^2}{(2+p)(2+2p)} \right]^{p/2} \Gamma\left(\frac{p}{2}\right) \tag{4.2}$$

$$B_s = \frac{G_s p_s}{{R_s}^{p_s}} \left[\frac{6p_s^2}{(2+p_s)(2+2p_s)} \right]^{p_s/2} \Gamma\left(\frac{p_s}{2}\right) \tag{4.3}$$

For this semi-flexible polymer system the low q scattering is described by the first term in equation 1 and the second term describes the high q scattering. For an entangled polymer system it is expected that if there are no large scale polymer density fluctuations the low q regime will span all of space up to the size of the container and no Guinier regime will be found.

The fit to the Beaucage model, figure 4.1, shows that as the polymer concentration is increased there is little change in the length scales or mass fractal of the semi-dilute polymer solution. This is further confirmed by the sub-plot which shows the same data as figure 4.1 but normalized for concentration. The only change observed is at the lowest concentration an increase in the high q regime that can be accounted for by the weak scattering being close to the incoherent background of this system. All concentrations could be fitted to a low-q fractal dimension of 2.1, a radius of gyration of the high q

rod-like region of 74 Å and a high-q fractal dimension of 1.1. For a semi-dilute polymer network this length scale physically represents either the mesh size, or the Kuhn length whichever is shorter.

The radius of gyration of the rod-like sub-unit is reflected in figure 4.1 by the q value of the transition from a slope of -2.1 to -1.1, and can be converted into a length scale which for this entangled polymer system corresponds to the length of the constituent rods, l_{rod}, forming the semi-flexible entangled polymer solution. For this system l_{rod} can be calculated through the radius of gyration of a thin rod, $l_{rod} = \sqrt{12R_s^2}$, and is calculated to be 25.6 nm which is approximately twice the length of the previously measured persistence length of pectin [58]. Other measurements, not using small-angle scattering techniques, have reported the persistence length to be between 7 and 9 nm[60, 61]. The only differences seen as the concentration of the polymer was increased were that the model more accurately fits to the measured scattering data. This data shows that pectin in the solution state, in the absence of added salt, does not homogeneously fill space but instead has large regions that are polymer rich and other regions that are solvent rich. These can be thought of as tenuous dynamic aggregates that do not increase in density as the concentration is increased. If pectin homogeneously filled space then the transition between the two power laws would move to a lower q when the concentration is increased. Indeed, dynamic light scattering measurements, performed by the authors (data not shown) and others [59] show a bimodal correlation function, even at concentrations far below the overlap concentration, suggesting tenuous aggregation which has also been shown using other techniques [162, 163].

4.3.2 Rheological and structural evolution during acid-induced gel formation

After demethylesterification of this high DM sample, GDL was introduced into solutions of the resulting blockwise low-DM polymer, as described in the Experimental section, inducing a reduction in pH and concomitant gel formation. Figure 4.2(a) shows the evolution of the rheological properties after the introduction of GDL as its hydrolysis proceeds and the pH falls (See Inset). Interestingly, and particularly evident in the 1% sample, is that before the significant increase, (signalling macroscopic gel-formation) there is a slight decrease in the shear modulus. Figure 4.2(b) shows the corresponding

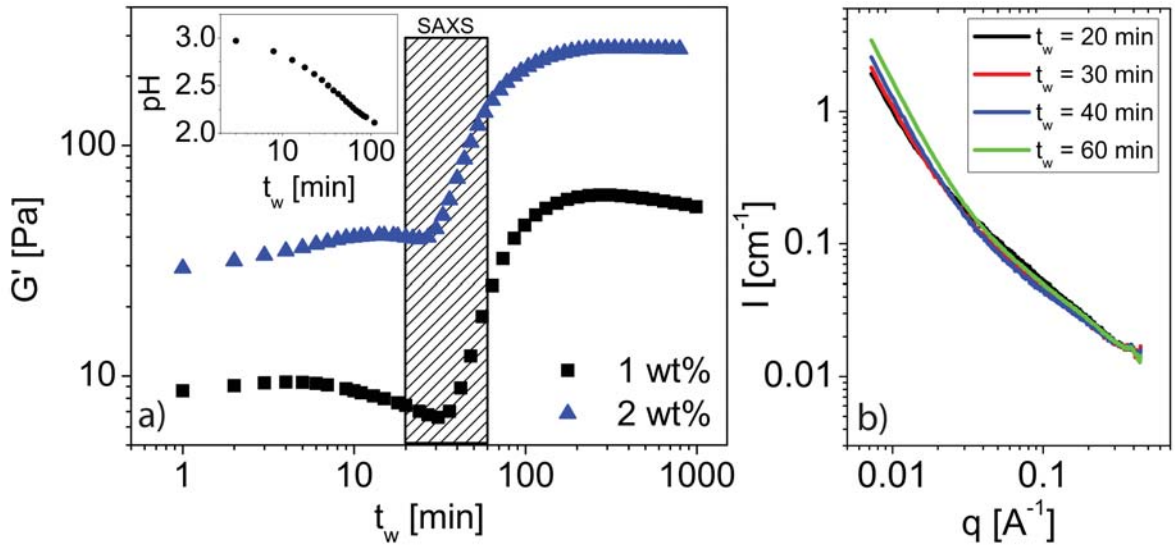

FIGURE 4.2: a)Plot showing the evolution of the storage modulus for 1 and 2 wt% acid gels and b) time resolved SAXS for the corresponding gels recorded at 4 different times after mixing (t_w).

SAXS data, and with time, as the gelation proceeds, it can clearly be seen that the scattering at low q systematically increases in intensity and steepens in slope. This suggests that as the entangled pectin solution starts to associate and form local cross-links, polymer is drawn into more clustered regions that fill space less efficiently than the individual polymers, and offers an explanation of the rheological data. In the early stages of the network formation, before these clusters are connected into a space spanning network, the clustered regions themselves draw polymer together and lower the effective concentration of the solution, temporarily reducing the storage modulus. As more clusters nucleate, grow and connect a space-spanning stress-bearing network is formed reflected in the growth of the storage modulus.

4.3.3 Rheology and TEM of a pre-formed acid-induced Gel

Once gels had reached the maximum strength, frequency-dependent pre-stress rheology experiments were performed in order to further mechanically characterise the system (Figure 4.3). Clear strain-stiffening is observed with the modulus of the systems increasing significantly with applied pre-stress. This behaviour has indeed been reported previously in these acid-induced pectin gels where the data were shown to be consistent with the Glassy Wormlike Chain model [74], which also captured the reported microrheology of the system [33]. In general stress-stiffening of networks has been shown to be

a generic feature of systems in which the fundamental connecting elements deform according to a worm-like chain Hamiltonian [103]. It is worthwhile noting that at least in the accessible pre-stress region that the increase of the differential shear modulus with pre-stress appears to increase linearly rather than with a power of 3/2 as predicted by the simple model [164, 165]. This has been observed not only in acid-induced pectin gels but also in calcium-assembled gels induced by controlled release of ions or the action of demethylesterifying enzymes, where the data was again well modelled [166]. While the rheological response then is highly suggestive of a network assembled from strands whose essential physics can be captured by those of a wormlike chain, several questions do remain including the distribution of sizes of such elements and the three dimensional arrangement of the elastically active network chains in space. In an attempt to gather more information on the network architecture and provide some insight into these questions a TEM tomography study was preformed as described in the Experimental section.

Figures 4.4 and 4.5 show TEM micrographs obtained from the final gelled system (A movie of the tomogram is available in the electronic supplementary information). It can be seen that the network has a somewhat clustered appearance with clusters of approximately a few hundred nanometres. Despite the significant difference in the strength of the fundamental bonding mediating the junction zones in these acid-induced networks and those in ionotropic pectin gels examined previously the network architecture rendered here does not appear significantly different (a quantitative comparison is part of a larger study and will be published elsewhere). This indicates that perhaps the initial architecture of such systems at least is dominated by the nucleation and growth of nodes and less concerned with the strength of the connections (at least above several kT) that might dominate the dynamics and thermal stability to a much larger extent.

4.3.4 Structural characterization of the acid-induced gels as a function of temperature

In general SAXS measurements carried out on the gelled samples (figure 4.6) show a similar scattering profile to that obtained from pectin solutions (figure 4.1), although with a drop in intensity in the high q limit. This can be explained as an increase in the average radius of the scattering entities in the cross-linked system. To help further

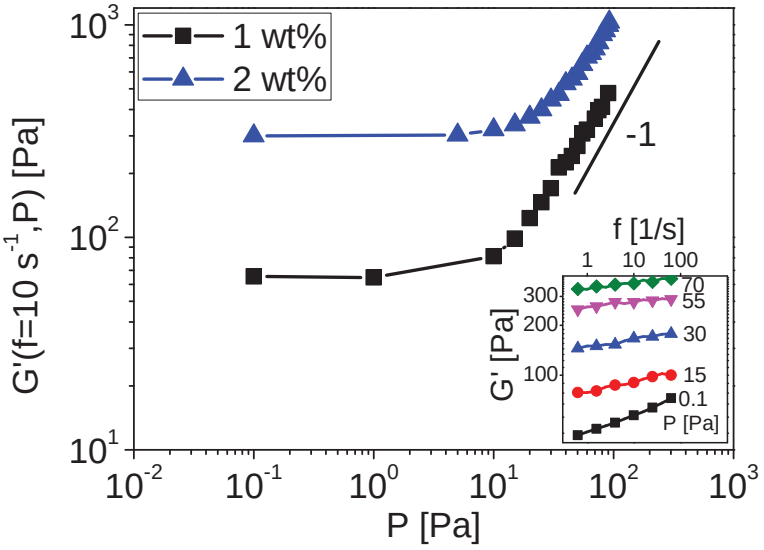

FIGURE 4.3: Plot showing the storage modulus as a function of applied pre-stress, P. The insert shows the frequency dependence of the storage modulus as the pre-stress is applied. The storage modulus shows a power law dependence of one, represented by the solid line guide, with increasing pre-stress.

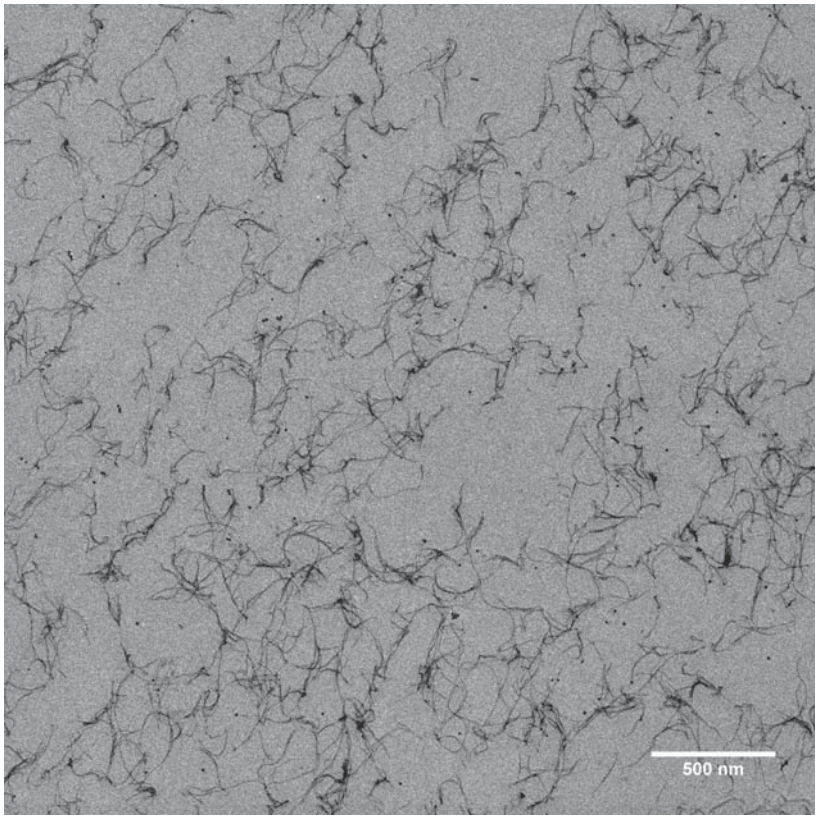

FIGURE 4.4: TEM micrograph of an acid-induced pectin gel prepared using GDL, as described in the text, showing the large scale network architecture.

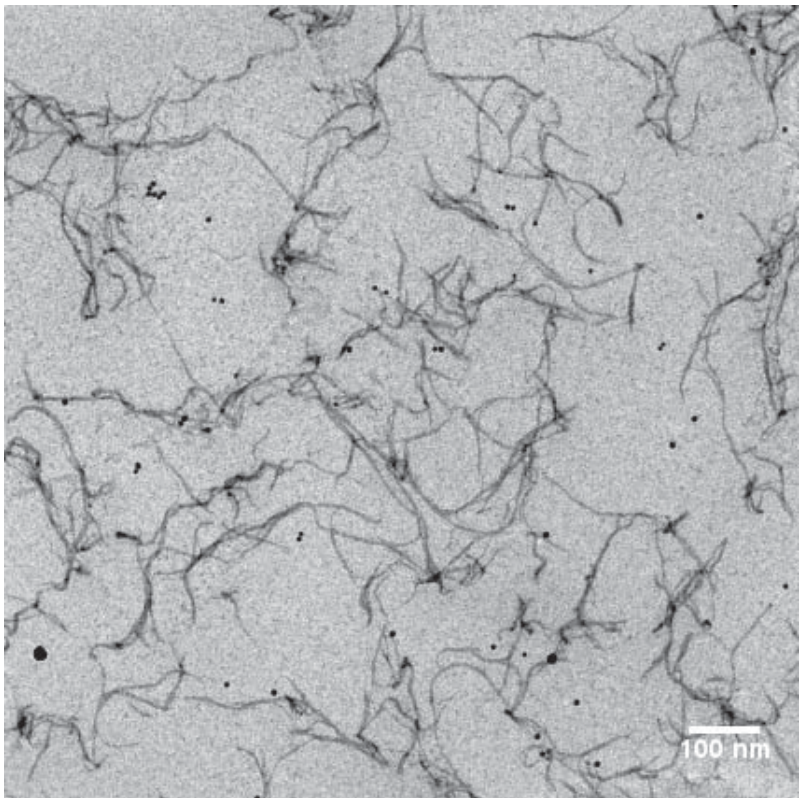

FIGURE 4.5: TEM micrograph of an acid-induced pectin gel prepared using GDL, as described in the text, showing the individual polymer entities forming the gel.The highly contrasted spots are colloidal gold particles added as fiducial markers to assist in the alignment of tomographic tilt series.

quantify the structural properties of this gelled system a fit to a flexible cylinder form factor [167, 168] with a fractal structure factor model [85] has been performed. The model is the same model as the worm like chain model in the intermediate to high q regimes, although it includes a structure factor to take into account the low q scattering and was implemented using NCNR analysis macros for Igor, kindly made available by Steve Kline [169]. This model was chosen as TEM micrographs showed significant bending in the polymeric entities forming the gel and, as described, the rheological properties - in particular the observed strain-stiffening, can be captured by WLC network elements. It can indeed be seen (figure 4.6) to provide an excellent fit to the scattering data obtained from these gels.

These hydrogen-bonded networks are well known for their thermoreversibility and their melting at moderate temperatures ($> 50\,^{\circ}\mathrm{C}$), especially when compared to their calcium-formed cousins, and in order to investigate the structural changes occurring during such

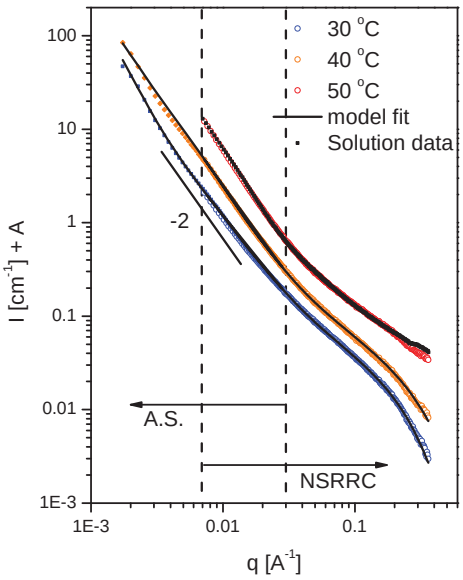

FIGURE 4.6: SAXS data for a 1 wt% acid-induced pectin gel formed with GDL as described in the text, as the temperature is increased. Squares represent data taken at the Australian Synchrotron (AS) and open circles data taken at the NSRRC. It can be seen by 50 °C the scattering from the *melted gel* resembles that taken for apple *solution* data at 30 °C. The solid lines represent a fit to a flexible cylinder form factor with fractal structure factor, refer to table 1 for the fitting parameters. Data for 40 °C and 50 °C have been shifted for clarity, 30 °C is plotted to an absolute intensity scale.

Temperature [°C]	30 ± 1	40 ± 1
Fractal dimension	2.6281 ± 0.0004	2.12 ± 0.01
Kuhn length [Å]	97.5 ± 0.3	93 ± 2
Radius [Å]	7.056 ± 0.002	6.2 ± 0.2

TABLE 4.1: The parameters fitted to the flexible cylinder with fractal structure factor model. Errors are shown as ± one standard deviation.

a process, pre-formed gels were heated in 10 °C increments while performing SAXS experiments, (figure 4.6). At each step the data were also fitted to the same model: at 40 °C there is a significant drop in the size and persistence length of the scattering elements as can be seen from table 1. As the junction zones begin to dissolve above 50 °C the data shows a profile very similar to that observed from the solution scattering of the individual polymers, (for comparison, 1 percent solution data has been plotted in figure 4.6 and shows almost an exact overlap with the melted gel, signalling its complete melting).

Subsequently, further SAXS experiments were performed at the Australian Synchrotron

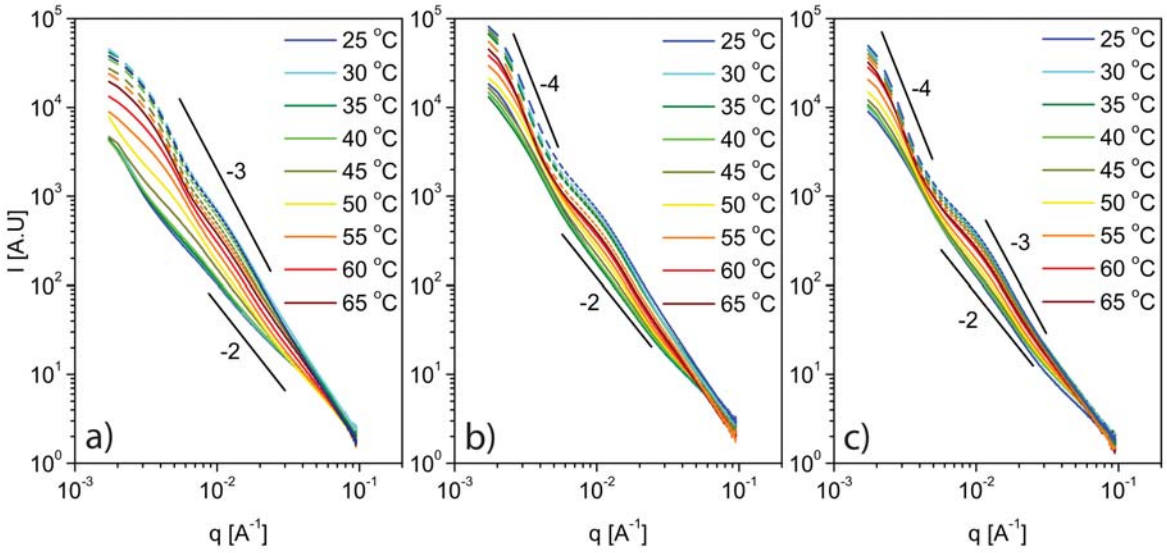

FIGURE 4.7: Plots showing SAXS data from acid-induced pectin gels formed in different solvents: a) H_2O, b) HDO, and c) D_2O. Solid lines represent data recorded as the sample was heated and dashed lines the same sample as the temperature was reduced. The experiment was performed on a time scale of hours. It can be seen that gels formed in deuterated water are structurally different from those formed in water. All three samples appear to undergo aggregation upon heating which is not reversible, as it is still present upon cooling. Solid lines are to guide the eye.

SAXS beamline, an instrument capable of accessing smaller momentum transfer vectors. In overlapping q ranges the data recorded on the different beamlines (NSRRC and AUS-SAXS) agreed well, shown in figure 4.6. Here, in order to manipulate the key hydrogen-bonding strength, and also to make preliminary measurements to test the viability of performing small-angle neutron scattering on this system, we performed SAXS measurements on gels formed in pure D_2O, HDO and H_2O (Figure 4.7). Lines in figure 4.7 are drawn as a guide to the eye and show slopes between -3 to -4 in the low q region indicating the presence of surface scattering form aggregates forming in the gel. These gels were formed at ambient temperatures using GDL in order to reduce the pH as described, and were then heated while acquiring scattering data. Previous rheology measurements have shown that pectin acid gels are highly thermoreversible and can be melted, then cooled and re-set with little hysteresis in the rheological properties.

These SAXS measurements show that if the gels are held above the melting temperature for significant periods of time there are structural changes, that appear to be significant aggregation, on the length scale of the order of hundreds to thousands of Angstrom, as seen by increases in the slopes shown in figures 4.7. Further work here needs to be carried out to investigate these aggregations, as it is not clear if they are influenced by

any chemical changes to the polymer. Chemical changes with heat are expected with pectin but at a pH close to neutral: at an acidic pH, as used here (see insert to figure 4.2(a)) pectin is considered stable to moderate heat [170]. Previous experience with de-esterification methods and pectin chemistry suggests it is unlikely that significant chemical changes are occurring [127, 130]. If chemical changes are not present then clearly highly stable extensive aggregates could be formed at room temperature if they were not hindered by the formation of a network, and if the chains are allowed to interact uninhibited then phase separation might be the ultimate fate of the system. The gelation process kinetically traps the system in a long lived but out of equilibrium state. Indeed, a slow relaxation mode in pectin acid gels [33] and in other polysaccharide networks [16–18], as found experimentally, can then be understood as arising from internal stresses created by the desire of the system to create longer junction zones. The method of de-esterification used to modify the polymer in this study created long runs of de-esterified regions, with few shorter ones. In effect, the lowest energy state of this pectin acid gel would be an aggregate that has completely phase separated into pure polymer and pure solvent regimes. Indeed, this brings to light the importance of knowledge about the esterification pattern along pectin chains, which is commonly overlooked and difficult to measure. Experiments on annealing these gels forms future work.

Also striking is the difference in fractal dimension, at 25 °C, between the gel formed in H_2O and the one formed in D_2O, that shows the gel formed in D_2O is much more clustered. The cause of the difference needs further investigation, as little is known about the bonding in these networks and it is unclear if the difference is due to solvent polymer interaction, stronger binding due to the solvent playing a part in the hydrogen bonding or the conformation of the pectin chain changing. Nevertheless, this highlights the need to be mindful of induced changes when substituting D_2O in systems with significant hydrogen bonding.

4.4 Conclusion

SAXS measurements revealed the structure of acid-induced pectin gels to be clustered networks composed of flexible, cylinder like elements with an average radius of 7 Å, and a Kuhn length of 97.5 Å at 30 °C. The flexible rod-like nature of the network was indeed clearly visible using TEM and despite the similarities in the overall network architecture

the flexibility of the fundamental network elements is in contrast to the more rod like junctions found in pectin calcium gels. Measurements on networks formed in deuterium oxide show substantial differences in the network clustering bringing further to light the importance of hydrogen bond formation in these networks and highlighting that care must be taken when using deuterated solvents if hydrogen bonding is important.

The authors thank Romaric Vincent for interesting discussions, The Royal Society of New Zealand for the Taiwan exchange funding, the Australian synchrotron for proposal 7612 and the New Zealand Synchrotron group for travel funding.

DRC 16

MASSEY UNIVERSITY
GRADUATE RESEARCH SCHOOL

STATEMENT OF CONTRIBUTION
TO DOCTORAL THESIS CONTAINING PUBLICATIONS

(To appear at the end of each thesis chapter/section/appendix submitted as an article/paper or collected as an appendix at the end of the thesis)

We, the candidate and the candidate's Principal Supervisor, certify that all co-authors have consented to their work being included in the thesis and they have accepted the candidate's contribution as indicated below in the *Statement of Originality*.

Name of Candidate: Bradley William Mansel

Name/Title of Principal Supervisor: Martin Williams

Name of Published Research Output and full reference:

B W Mansel, C-Y Chu, A Leis, Y Hemar, H-L Chen, M A K Williams, Zooming In: Rheologically Characterised Hydrogen-Bonded Polysaccharide Networks Studied by SAXS and TEM, submitted to Biomacromolecules

In which Chapter is the Published Work: 3

Please indicate either:

- The percentage of the Published Work that was contributed by the candidate: 80%

  and / or

- Describe the contribution that the candidate has made to the Published Work:

  The candidate did all the experimental work bar a TEM image, the analysis of the data and 80% of the writing.

Brad Mansel — Digitally signed by Brad Mansel DN: cn=Brad Mansel, o, ou, email=bmansel@gmail.com, c=NZ Date: 2015.05.19 14:23:10 +12'00'
Candidate's Signature

19/05/2015
Date

Williams, Martin — Digitally signed by Williams, Martin DN: cn=Williams, Martin, o, ou, email=m.williams@massey.ac.nz, c=US Date: 2015.05.19 12:24:57 +12'00'
Principal Supervisor's signature

19/05/2015
Date

GRS Version 3– 16 September 2011

5. Slow Dynamics and Structural Characterization of Calcium Mediated Pectin Gels

As submitted in:

B W Mansel, M A K Williams, Internal Stress drives slow glassy dynamics and quake-like behaviour in ionotropic pectin gels, submitted to *Soft Matter*

Abstract

Frustrated, out-of-equilibrium materials have been of considerable interest for some time and continue to be some of the least understood materials. Recent measurements have shown that many gelled biopolymer materials display slow dynamics on timescales greater than one second, that are not accessible with typical methods, and are characteristic of glassy trapped systems. In this study we have controlled the fine structure of the anionic polysaccharide pectin in order to construct a series of ionotropic gels having differing binding energies between the constituent chains, in an attempt to further understand the slow dynamical processes occurring. Using multi-speckle light scattering techniques it is shown that the slow dynamics observed in these gelled systems are stress-driven. As the binding lengths, and thus the binding energies, of the junction zones between the polymer chains in these networks increase the long-time dynamics initially slow, as might be expected, until a critical level of internal stress is reached upon which the dynamics increase significantly, with gentle creaking punctuated by localised stress-relieving quakes.

5.1 Introduction

Typically, colloidal gels have been the canonical model for out-of-equilibrium materials that exhibit glassy dynamics and considerable amounts of underlying theory has been developed to describe their behaviour, such as mode coupling theory [171–173]. However, recent measurements on the dynamics of polysaccharide gels showing bi-modal dynamics, with slow modes reminiscent of those seen in other frustrated out of equilibrium systems highlight the breadth of soft materials exhibiting such behaviour [16–18]. It should perhaps not be surprising that such slow behaviour exists in polysaccharide gels, as syneresis, where the gel squeezes water from the network as it slowly pulls together, on time scales of hours or days has long been observed [30, 174]. Typically in colloidal systems one seeks to understand the mechanism behind the slow internal dynamics: are they thermally driven or are they driven by internal-stresses built up as the system approaches the glass transition [7]? Here we investigate the interplay between the inter-polymer binding strength and the observed slow dynamics.

Recent experiments have highlighted many interesting phenomena regarding the slow dynamics in both pectin and alginate gels [16–18]. The slow dynamical processes occurring in pectin networks is an especially important topic, not only to understand the stability of gelled systems for controlled release in the food and pharmaceutical industries, but for the insights it may provide into how the plant cell wall, in which it is a major component, can elongate while maintaining its integrity, or perform directional motion in response to an external stimulus. In light of recent work we have designed three gels using three different pectin fine structures (the same monosaccharide composition of the chains, but different patterns of the cross linking moieties), to give differing binding strengths in a quest to predictably modify the slow dynamics.

Pectin, as found in the plant cell wall, is a complex hetero-polysaccharide consisting of several domains, predominantly homo- and rhamno-galacturonan (RGI and RGII), the disposition of which is still a matter of debate to some extent [42]. It is clear however that the homogalacturonan (HG) backbone is connected through alpha 1-4 linkages and that it is the intermolecular association of this part of the polymer that is primarily responsible for pectin's ion-binding and gel forming capacity [151]. While RGI contains rhamnose residues, alternating with those of galacturonic acid, that act as sites of neutral sugar side chain attachment, these branches are often removed during commercial

extraction procedures that are used to purify pectin and are subsequently not usually present in significant amounts in commercially available samples. In the plant cell pectin is biosynthesised as a weak acid with around 20 percent of the monomers in each homo-galacturanan chain bearing naked carboxyl groups, with the remaining groups carrying a methyl ester. The ratio of methyl ester groups to acid groups is referred to as the degree of methyl esterification (DM) and can be modified using chemical or enzymatic procedures. Modifying the degree or pattern of methyl esterification can radically alter the gel forming abilities and mechanical properties of the subsequent gels formed. This makes pectin a particularly attractive biopolymer from which to create soft materials with designed mechanical properties.

Ionotropic pectin gels are formed when divalent ions, most commonly calcium, chelate a series of carboxyl groups on two different pectin chains, forming a bond between them. Two carboxyl groups binding a single calcium ion has a binding energy that is much lower than the thermal energy and hence cannot form a stable junction between chains. It has been calculated that between 8 and 15 consecutive bonds of this type are required to form a stable junction, and, as such, the distribution of the calcium chelating acid groups along a pectin chain is crucial in determining the gel-forming capacity. A higher degree of blockiness means that most of the acid groups are arranged in blocks along the chain, while a lower degree of blockiness means that most of the acid groups are more randomly distributed [175]. As described, the degree of blockiness plays a large role in determining the mechanical properties of a gel, as the number of binding groups in each junction defines the binding strength [36]. Indeed, a qualitative method used to categorise different pectins is to group them either as blocky pectins, forming stronger inter-chain junctions, or random pectins, forming weaker inter-chain associations. The number of ions available to form bonds is clearly another critical consideration in forming a gel: the number of ions relative to the number of pairs of carboxyl groups is typically defined as the R value:

$$R = \frac{2\mathrm{Ca}^{2+}}{\mathrm{COO}^{-}} \tag{5.1}$$

with a value of one being where all the ions in the system have a pair of carboxyl groups potentially available to bind. The lowest R value that can form a gel depends on the degree of blockiness with typical R values for pectin gels being between 0.2 to 0.8, and a value greater than one meaning that there are more ions than binding sites, a situation that is not generally desirable.

Frustrated, out-of-equilibrium systems that display slow dynamics generally have similar dynamical behaviour: ultra slow relaxation that is often the result of internal stress and spatially and temporally heterogeneous dynamics that slow as the gel ages [8, 176, 177]. The understanding of these phenomena have been of considerable interest in recent years and they have been shown to exist in many soft systems. For this study we investigate these properties for 3 different ionotropic pectin gels assembled with calcium using the same R value, from polymers having the same DM but with different levels of blockiness, in a quest to modify the long-time dynamics. To verify that the different pectin samples studied did indeed form gels where the only predominant difference was the length of the inter-polymer junction-zone lengths we utilized Small-Angle X-ray scattering. Slow dynamical processes in these systems were studied using time-resolved multi-speckle dynamic light scattering techniques which offered simple and robust techniques to measure behaviour from non-ergodic samples, and achieve good statistics. Two different, albeit similar techniques, namely Photon Correlation Imaging (PCI) and multi-angle multi-speckle dynamic light scattering (MAMS DLS) were applied. PCI measures spatial information about the dynamics, which is particularly important for out-of-equilibrium systems, on length scales from around 50 μm to 6 millimetres. MAMS DLS provides information on the mechanism driving the dynamics, by measuring how they scale with the scattering vector q. Where q is related to the angle between incident and scattered radiation, θ, the refractive index of the medium, n and the wavelength of the radiation λ by: $q = 4\pi n \sin(\theta/2)/\lambda$. For out-of-equilibrium soft materials at large length scales the characteristic decay time, τ_f of the slow mode generally scales with the scattering vector as a power law with an exponent of -1, $\tau_f \propto q^{-1}$, indicating stress driven dynamics. In contrast, for systems with negligible internal stress the dynamics have been found to scale with a power law of exponent -2, $\tau_f \propto q^{-2}$, indicating thermally driven dynamics. For polysaccharide gels in general there has been some debate about the mechanism driving the slow dynamics, with speculation that if interchain binding strengths are near that of thermal energy the dynamics could indeed be thermally, and not stress, driven [18].

5.2 Materials and methods

5.2.1 Materials

Three pectin samples with a known degree of methylesterification (DM) and de-esterification methodology (that controls the intramolecular pattern of charged residues) were used for this study, two of which were purchased from CP Kelco and the other modified from apple pectin. The two purchased samples had: a DM of 43 and a random intramolecular charge pattern (R40), and a DM of 40 and a blockwise de-esterification pattern (B40) respectively. The other sample was modified from an apple pectin sample that had a starting DM of 75 (Sigma), by reducing the DM to 40 (P40), using pectin methylesterase (PME) extracted from orange (Sigma), under ideal conditions to produce a very blocky sample. The polymer fine structure modification was performed by first dissolving dried apple pectin in ultra pure water (milliQ) to a final polymer concentration of 0.25 wt% and then adjusting the pH to 7 using 1N and 0.1N analytical grade sodium hydroxide together with a calibrated digital pH meter. A pH-monitored demethylesterification method was then carried out. The pH of the solution was monitored, and held at 7 by slowly adding known volumes of 0.1N NaOH, to counteract the active PME enzyme liberating galacturonic acid groups on the polymer backbone from their methyl esters, until the DM was lowered to 40 %. The sample was then heated to 80 °C to denature the PME, frozen using liquid nitrogen and finally freeze dried for 24 hours to allow for the long term storage of the dried polymer.

Gels with a final polymer concentration of 1 wt% were formed from the different polymers using the well-studied controlled calcium release gelation method, that introduces calcium using the dissolution of initially insoluble calcium carbonate. Gels were formed by dissolving 30 mg of the dried pectin in 2.37 ml ultra pure water (MilliQ) by mixing the suspended pectin with a magnetic stirrer for approximately 6 hours, then heating the solution to 50 °C for less than 30 minutes to ensure complete dissolution. To initiate gelation 2.32 mg of calcium carbonate with a nominal diameter of one micron was suspended in a solution consisting of 8.25 mg of glucono-δ-lactone (GDL) in 0.593 ml of ultra pure water. This gave a ration of calcium ions to GDL of 1:2 which ensured that the pH of the solution was unchanged. The calcium carbonate and GDL solution was

quickly added, within the order of tens of seconds, and mixed through the pectin solution to make a homogeneous solution, that was initially turbid owing to the inclusion of the calcium carbonate particles. The final sample weight was 3 grams. For samples with added tracer particles, 0.505 micron diameter polystyrene particles (Polysciences) were added to the calcium carbonate suspension to make the final phase volume of spheres in the sample 0.0013 %. Samples were left for 12 hours to gel in a 1.5 mm diameter quartz glass capillary for small-angle x-ray scattering measurements, a 10 mm path length cylindrical cuvette for dynamic light scattering, or a 10 mm path length rectangular cuvette for photon correlation imaging. After gelation the samples without added tracers had an almost transparent appearance with a low turbidity.

5.2.2 Small-angle X-ray Scattering.

SAXS measurements were performed at the Australian Synchrotron on the SAXS beamline [157], where samples were prepared in 1.5 mm quartz glass capillary tubes (purchased from Hampton Research or capillarytubes.co.uk) and irradiated with 11 keV ($\lambda = 1.127$ Å) radiation. For this high-flux undulator-beamline a slit was used to attenuate the beam and multiple 1 second exposures were averaged over in order to increase the signal to noise ratio. Scattered radiation was collected using a Dextrus Pilatus 1M detector with the detector positioned either at 7179 or 719 mm from the sample which corresponds to a scattering vector, q, of 0.001-1 Å^{-1}. The scattering vector is defined as: $q = 4\pi\lambda^{-1}\sin(\theta/2)$, where θ is the angle between incident and scattered radiation. Absolute scattering intensities were measured using water as a standard scatterer.

5.2.3 Multiple-angle Multi-speckle Photon Correlation Spectroscopy.

MAMS PCS was used to measure the dynamics at multiple angles simultaneously. A setup with four CMOS detectors (Basler AG, model no. acA2040-90um) positioned around a sample formed in a 10mm path length cylindrical cuvette was illuminated with $\lambda = 532$ nm wavelength light, emitted from a 300 mW ultra-low-noise diode-pumped solid state laser (Cobolt Samba). The scattering vector is calculated from the scattering angle and is defined as: $q = 4\pi n\lambda^{-1}\sin(\theta/2)$, where n is the refractive index of the solvent. Laser light was attenuated using a neutral density (ND) filter which reduced the power to levels where a good signal to noise ratio was observed

but heating effects were minimised. We estimate the power at the sample to be less than 100 mW. The setup was mounted on a large-area rotation stage (Thorlabs, model RBB18A), for ease of detector alignment, which was then positioned on an air damped optical table (Photon Control). The sample to detector distance was modified to adjust the speckle size to approximately the size of one pixel. Measurements were performed after allowing the sample to equilibrate for at least one hour in the sealed, temperature regulated, laboratory, with no other activity present and surrounded by curtains to further minimise low frequency air vibrations. Data were collected and post processed using the MATLAB programming environment.

The formalism outlined by ref. [178] was used in the analysis, with the time resolved degree of correlation defined as:

$$c_I(t,\tau) = \frac{\langle I_p(t) I_p(t+\tau)\rangle_p}{\langle I_p(t)\rangle_p \langle I_p(t+\tau)\rangle_p} - 1 \tag{5.2}$$

where $I_p(t)$ is the intensity recorded at the p$^{\text{th}}$ pixel at time t and τ is the time lag. To improve statistics c_I is averaged over a period of time to give:

$$g_2(t_w,\tau) - 1 = \langle c_I(t,\tau)\rangle_{t_w \le t \le t_w + t_{av}} \tag{5.3}$$

where t_w is the time between making the sample and performing the measurement. In addition

$$\chi(\tau) = \langle c_I(t,\tau)^2\rangle_t - \langle c_I(t,\tau)\rangle_t^2 \tag{5.4}$$

where $\chi(\tau)$ is the variance of the correlation function, which is similar to the dynamical susceptibility as is often calculated in numerical work [100].

5.2.4 Photon Correlation Imaging.

PCI measurements were performed using the laser and ND filter as described above, although, for these experiments the 2mm diameter beam (at sample) was sent through a beam expander consisting of a pair of plano-cylindrical lenses to expand the beam into a vertical sheet with a height of 10mm. This line collimated beam was used to illuminate the sample which was gelled in a 10mm path length square cuvette (Hellma-Analytics) and scattered light was collected using a zoom lens (thorlabs, MVL7000) with internal

aperture and a CMOS camera (Pixelink PL-B741) with a resolution of 1280 by 1024 pixels. The imaged area was 6.40 mm wide by 5.12 mm high, and each pixel at the detector corresponded to 5 μm in real space. Data was collected then post processed using the MATLAB environment.

5.3 Results

5.3.1 Gel structure

Measurements using SAXS, carried out to resolve and compare the structure of the three gels, all showed scattering profiles characterised by three different power law regimes, clearly indicated by the different slopes of these regions on a log-log plot. Broadly speaking, such plots reveal: in the low q region, a slope of -2.9; in the intermediate q regime a slope of -1; and at the highest accessible q values a slope of -3 (tending towards -4 for the P40 sample), although this is limited by the instrument background (figure 5.1). The low q results indicate highly clustered arrangements of the polymers in space. The intermediate and high q regimes display the scattering from the singular subunits, in this case a slope of around -1 indicating rod like entities compose the polymer network. The high q slope of -3 is consistent with the scattering from a rough surface fractal, as the interrogated length-scale becomes smaller than the diameter of the network strands. A model, in the form of a fractal structure factor with cylinder form factor was chosen to fit all three regimes simultaneously and is shown in figure 5.1 as solid black lines. The model accounts well for the scattering at the low and intermediate q regimes although it does not account for the rough surface fractal, represented by a slope of -3 in the high q regime. A model based on a rough cylinder form factor could be used, but is beyond the scope of this work. Using the standard scattering formalism, the measured intensity can be decomposed into three parts, a form factor, $P(q)$, which describes the form of the individual scatterers, a structure factor, $S(q)$, which describes the assembly of individual scatterers and a parameter $\Delta\rho$ which describes how strongly such a system should scatter and is related to the difference in electron density between the solvent and scatterer. A final parameter n describes the number of scatterers in a volume, and

TABLE 5.1: Parameters used for the fitting of SAXS data shown in figure 5.1

Parameter fitted	R40	B40	P40
r [Å]	12 ± 1	11.8 ± 0.7	12.3 ± 0.2
L [Å]	70 ± 20	238 ± 4	300 ± 30
D	2.911 ± 0.005	2.9355 ± 0.0006	2.7 ± 0.2
r_0 [Å]	78 ± 2	112.4 ± 0.3	150 ± 20

these parameters are related by:

$$I(q) = n\Delta\rho P(q)S(q) \tag{5.5}$$

For our system a cylinder form factor fitted the scattering profile well, as one would expect for rigid calcium-pectin junction zones. It contains a length, L and radius, r and is given by [78]:

$$P(q) = \int_0^{\pi/2} \left[2\frac{\sin(qL\cos(\alpha)/2)}{(qL\cos(\alpha)/2)} \frac{J_1(qr\sin(\alpha))}{(qr\sin(\alpha))} \right]^2 \sin\alpha d\alpha \tag{5.6}$$

where J_1 is the Bessel function of the first kind. The fractal structure factor is described by three parameters, r_0 describes the smallest length scale where the scattering becomes self similar, D the fractal dimension and ξ is the correlation length which describes a Guinier type behaviour at low q [85]:

$$S(q) = 1 + \frac{1}{(Qr_0)^D} \frac{D\Gamma(D-1)}{1 + 1/(q^2\xi^2)^{(d-1)/2}} \times \sin[(D-1)\tan^{-1}(q\xi)] \tag{5.7}$$

For the gels shown here, no Guinier type behaviour was seen and ξ was set to a value larger than the lowest q. It can in any case be clearly seen that the three different ionotropic pectin gels produced similar scattering profiles in which the main difference is seen in the intermediate regime, reflecting the length-scale of the rod-like subunits. The model fitting confirmed that, as hypothesised, gels made from pectins with blockier intramolecular charge distributions indeed form longer rod-shaped structures (calcium-chelating junction zones), see table 5.1. Furthermore there is little difference in the radius of these junction-zones or their arrangement in space. The SAXS structural analysis confirms therefore that changes in the long-time dynamics of these different gels might safely be attributed to changes in the junction-zone strengths, and concomitantly their binding energies, as opposed to changes in the overall network architecture.

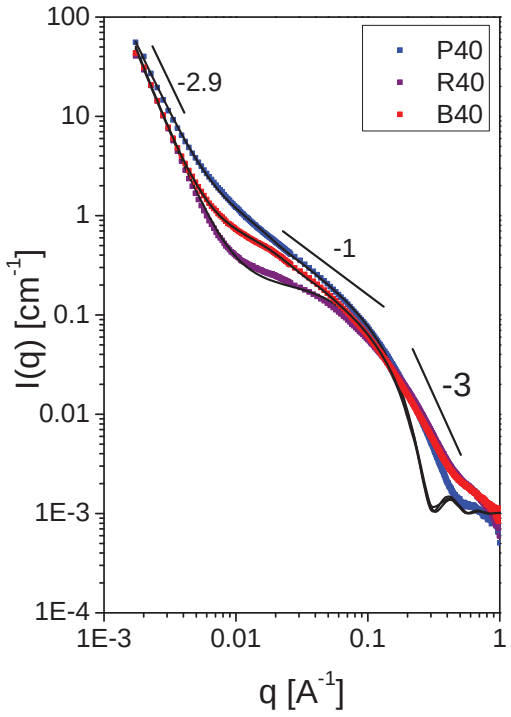

FIGURE 5.1: Small-angle x-ray scattering log-log plot showing the intensity (I) measured on an absolute scale as a function of scattering vector (q) for the three different gels. Small square symbols are the measured results and the solid lines are fits to a fractal structure factor with cylinder form factor model as described in the text.

5.3.2 Slow dynamics

To investigate the internal network dynamics the gels were either seeded with 505 nm diameter polystyrene spheres (for the MAMS DLS), or studied as-is (for PCI). In MAMS DLS experiments the additional spheres provided strong scattering centres to reduce the possibility that different sized heterogeneities in the gel network might produce angle-dependent scattering and complicate the analysis. Figure 5.2 shows correlation data and fits to an exponential function of the form: $g_2 - 1 \propto \exp[-(t/\tau_f)^{\beta}]$ where β acts to either stretch, or compress the exponential decay depending on if it is less than or greater than one. It can be seen that the dynamics from the R40 and B40 gels show good fits to compressed exponential functions with compressing factor, β, between 1.3-1.7, depending on the sample, (values that are commonly seen in other soft glassy systems). The results for the P40 sample, figure 5.2, however, did not show a (compressed or stretched) exponential decay in the correlation function: while periodically the P40 gel could be described by a smooth exponential decay, most often the dynamics were highly

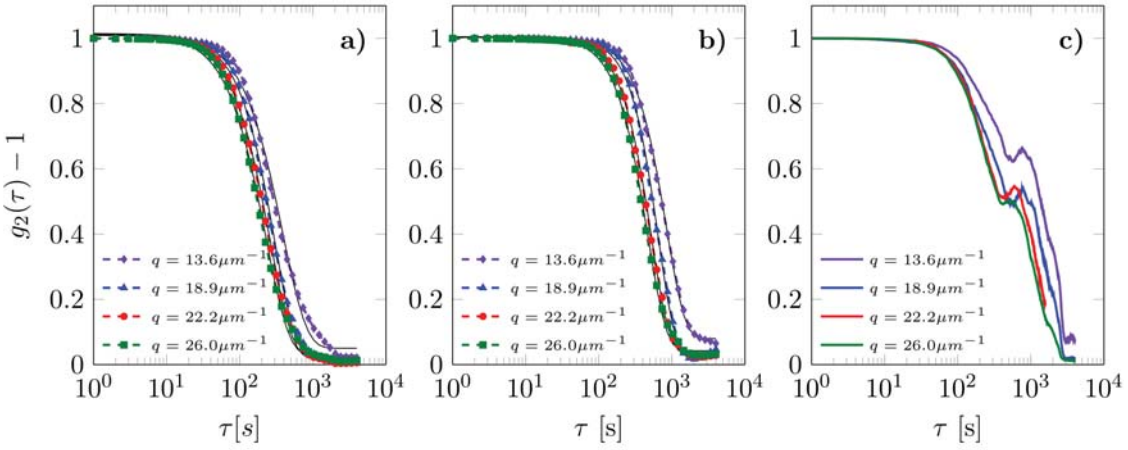

FIGURE 5.2: MAMS DLS for the three different gels seeded with 0.505 micron diameter polystyrene probe particles. Solid lines represent compressed exponential fits with a compressing factor β of between 1.3 and 1.7. figure a) is data recorded from the R40 sample, b) the B40 sample and c) the P40 sample.

heterogeneous and showed non-exponential decay behaviour as is shown in 5.2. Similar non-exponential decay behaviour has been observed for alginate gels [18]. While the other two pectin gels investigated here also showed non-exponential decay behaviour on occasion they predominantly showed a compressed exponential decay in the average degree of correlation.

Commonly in soft solids one tries to understand the driving mechanism behind the measured dynamics, which can be either stress or thermally driven. This can be done by measuring how the characteristic time associated with the slow dynamics scales with the scattering vector, in a similar way to distinguishing between ballistic and diffusive motion by observing how the mean-square-displacement scales with time. For this study four different scattering vectors were used to investigate the dynamics. A plot of the characteristic time corresponding to the slow dynamics, τ_f, against scattering vector is shown in figure 5.3. It can be seen that the characteristic time clearly scales with the scattering vector as a power law with an exponent close to 1 (and not to 2), indicating that even for the gel composed of the smallest junction lengths the dynamics are driven by internal stresses and not thermally activated fluctuations of the junction-zone integrity. This should not be too surprising as these structures can easily support their own weight: evidence that a majority of bonds are stronger than thermal fluctuations, so that they do not slowly creep and flow. For these gels, even in the R40 sample which appears to be significantly softer than the others, the slow dynamics cannot be

controlled by the thermally activated breaking of the weakest bonds, but instead is governed by collective rearrangements of the structure driven by stronger longer junctions continuing to "zip up".

To gain further insights into these slow dynamical processes the time-resolved degree of correlation, c_I, has been plotted for the $q = 18.9\mu m^{-1}$ data shown in figures 5.2, for different lag times, as shown in figures 5.4, 5.5 and 5.6. This angle was chosen as it probes intermediate length scales compared to the other angles. The dynamics appear to be stochastic; there is some probability that the internal stresses will build up sufficiently to trigger a phase of heterogeneous dynamics. Dynamical processes in these gels appear to fall broadly into three different categories; 1) at the shortest time scales there are "quake-like" fluctuations that yield intermittent sudden spikes in the degree of correlation; 2) on time scales of around 1000 seconds larger longer-lasting fluctuations reminiscent of creaking are evident, and 3) a universal decrease in the degree of correlation is also evident, that stays constant in time, as the time lag increases. The spiking and fluctuations are heterogeneous dynamics, and appear to be features of high levels of internal stress. The gels can enter a period of this type of dynamics then revert back to a temporally homogeneous regime as shown for the B40 gel in figure 5.5 where at a time of around 2000 seconds the dynamics switch from temporally heterogeneous to homogeneous. Figure 5.6 shows that most commonly the high levels of internal stress in the P40 gel make it predominantly display temporally heterogeneous dynamics. It can also be seen in figures 5.4, 5.5 and 5.6 that the time resolved degrees of correlation, $c_I(\tau)$, appear to increase following the highest frequency of quake-like events. This appears to be evidence of the build up and subsequent release of internal stresses, where the slow, steady drop in correlation signifies prolonged periods in which many small dynamical events occur as the internal stress increases, that are punctuated by larger length-scale rapid quake-like events signifying a large release of the internal stress. Finally a drop in the number of small stress-building events events appears to be manifest following each series of quake-mediated relaxations, as shown by a gradual increase in $c_I(\tau)$. Plots of the variance of the degree of correlation,$\chi(\tau)$, figure 5.8 show a single peak corresponding to the time lag where there is maximum variation in the time resolved degree of correlation. The three gels show similar profiles, although the P40 sample displays significantly larger quake-like events at short time lags compared to the other gels.

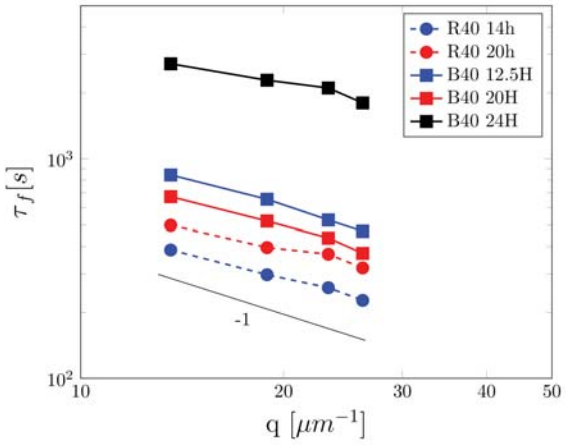

FIGURE 5.3: q vs. τ_f plots for the R40 and B40 pectin calcium gels at different ages. It can be seen that the characteristic times for the correlation functions scale with the scattering vector (q) with an exponent of approximately -1.

While it has been proposed that the mechanism responsible for slow dynamics seen in calcium-assembled alginate gels could be the thermally-activated separation of junction-zones in contrast to the stress-driven dynamics observed herein, further experimental evidence supports the minimal involvement of the opening of unstressed junction-zones in these gels. Firstly, upon heating the gels to 80 °C there was no observed melting. Certainly for the R40 gel some softening of the gel was observed, but a solid, minimally-creeping structure seemed to be preserved. Upon heating the B40 gel, many small non-spherical "bubbles" became evident that are suggested to be the result of the higher temperature "annealing" whereupon larger junctions formed at the expense of shorter ones, thus increasing the internal stress to such high levels that weaknesses in the gel structure alleviate internal stress and "bubbles" are formed as a result of micro-fractures. For the P40 gel, upon heating, as well as the formation of these micro-fractures the gel underwent significant levels of syneresis, in which the gel structure shrank in size to approximately half its pre-heated size. The non-melting and syneresis of these gels suggests that bond-breaking has little to do with the slow dynamics that we have observed at ambient temperatures, and instead that the continual rearrangements are driven not by thermal effects but by internal stresses resulting from larger junctions further associating. This hypothesis is in line with the results, that the polymer with the longest block length, that forms the longest junction zones, as confirmed by SAXs, does not have the slowest dynamics, but on the contrary, the fastest most heterogeneous dynamics in many measurements.

Finally, the spatial extent of the correlations in the dynamics is investigated using

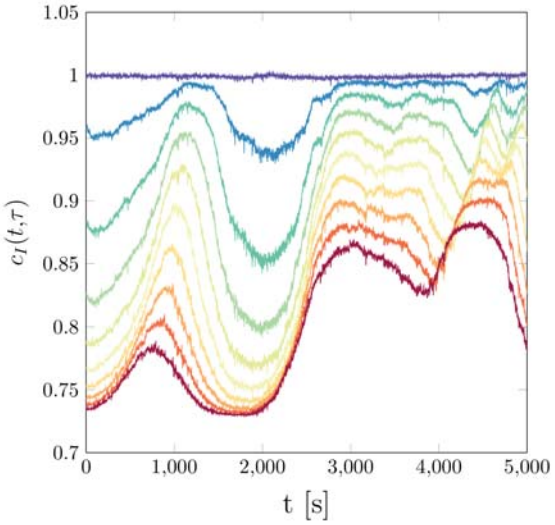

FIGURE 5.4: R40 time resolved correlation for 11 different lag times (from top to bottom, 1, 100, 200, 300, 400, 500, 600, 700, 800, 900 and 1000 seconds). The plot reveals a host of time scales over which the decorrelation of light occurs characteristic of heterogeneous dynamics.

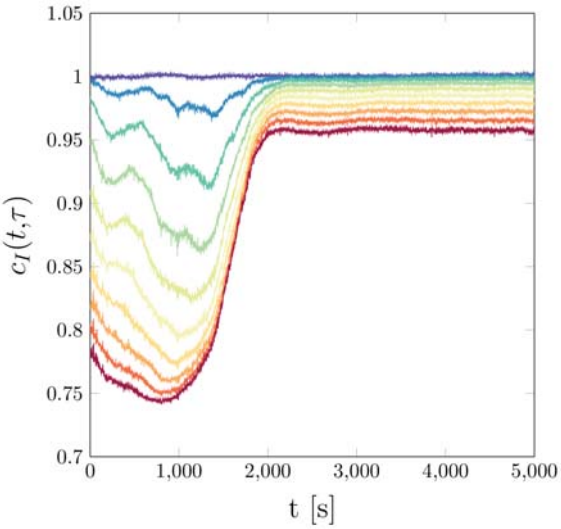

FIGURE 5.5: B40 time resolved correlation for 11 different lag times (from top to bottom, 1, 100, 200, 300, 400, 500, 600, 700, 800, 900 and 1000 seconds). This plot reveals that this sample undergoes a phase of temporally homogeneous dynamics where the correlation function has a flat response in time but decreases as the lag time increases.

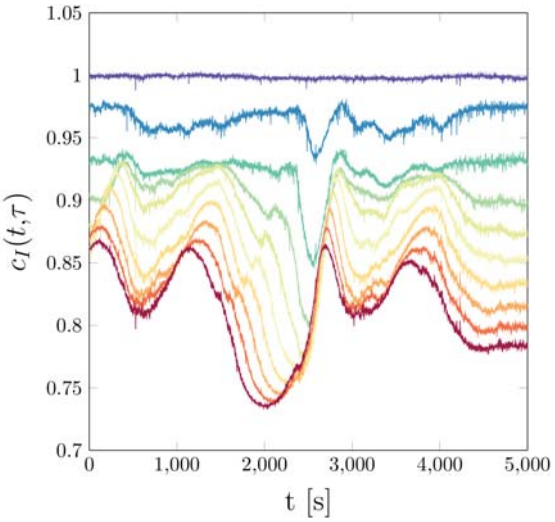

FIGURE 5.6: P40 time resolved correlation for 10 different lag times (from top to bottom, 1, 100, 200, 300, 400, 500, 600, 700, 800, 900 and 1000 seconds). It can be seen that the decorrelation of light evolves in a similar manner to the other gels, although some larger quake-like events are present.

photon-correlation imaging (PCI). PCI is a technique that spatially maps the decorrelation of light using a lens with an aperture to spatially filter and image the speckle pattern onto a CMOS detector (figure 5.7). For the set-up used during this study each pixel represents 5 μm at the imaging plane, as described in the experimental section. To improve the signal to noise ratio, each pixel shown in figure 5.7 is a 10x10 pixel average of the recorded scattering image, corresponding to 50 μm in the imaging plane. The colour in the false colour images corresponds to the value of the correlation function (dark red = 1, dark blue =0). It can be seen in figure 5.7 that the dynamics are spatially heterogeneous and the dynamics show, as has previously been documented in other soft systems, ultra long-range spatial correlations [100]. The ultra long-range correlation is an interesting phenomenon that has been reported to be a feature of enthalpic elasticity, which would be consistent with the SAXS structural analysis, which suggests the network is formed by rigid, rod like entities [100]. Little difference is seen between the three samples, but it should be noted that once again the sample constructed from the most blocky fine structure, that possesses the longest most thermally-stable junction zones shows the most varied dynamics (Movies Available On-Line).

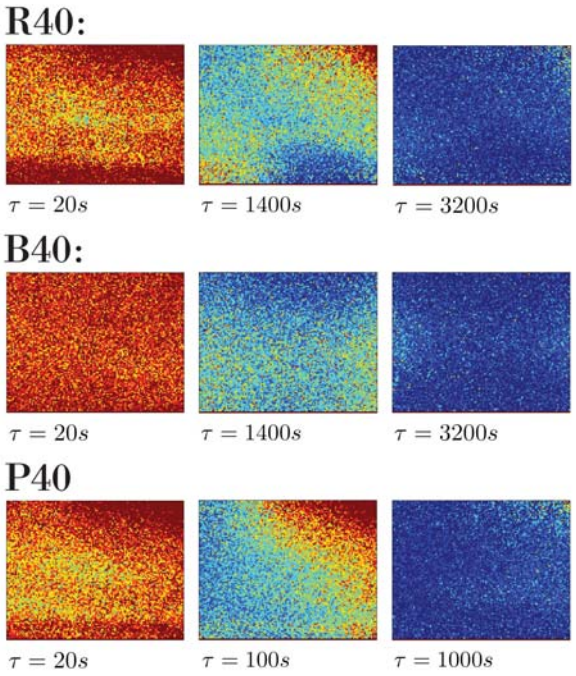

FIGURE 5.7: Photon-correlation images of the three different gels at different times. The colour in the false colour images corresponds to the value of the correlation function (dark red = 1, dark blue =0). One pixel corresponds to a measurement of the decorrelation averaged across an area of ten by ten pixels, or spatially $50 \times 50 \mu m$. The three gels show similar spatially resolved dynamics, although the P40 sample showed significantly faster dynamics during this measurement where the light was decorrelated after approximately 1000 seconds. It can also be seen that the gels have large scale spatial heterogeneities of the order of many millimetres.

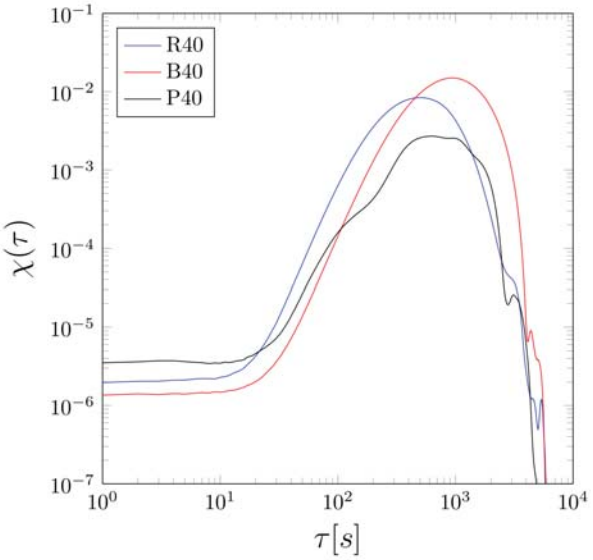

FIGURE 5.8: The variance of the time resolved dynamics for the three gels. The size of the fluctuations are similar as expected from the time resolved dynamics shown in figures 5.4, 5.5, 5.6, although it can be seen that at short times the P40 sample shows larger quake-like events compared to the other two gels.

5.3.3 Ageing

As is seen in other soft systems that display slow dynamical processes these pectin gels show dynamics that on average slow as the system ages. However, this ageing process is not at all linear. The relaxation processes occurring often appear to become jammed, and build internal stresses, the release of which causes the slowing of the dynamics to be punctuated by rapid quake-like fluctuations that are spatially heterogeneous but sweep over large distances in a correlated manner. As these systems go through such stochastic phases the dynamics are found to be highly temporally heterogeneous and exhibit correlation functions that have complicated non-exponential forms which may even increase before the correlation eventually decays to zero.

5.4 Conclusions

Three ionotropic gels of the polysaccharide pectin were assembled with calcium, using polymers that contained the same number of charged residues, but with different intramolecular distributions. As successful calcium-binding, which bridges chains and is the molecular process underlying successful network formation, requires a contiguous stretch of the charged galacturonic acid residues, the blockiness or otherwise of the pattern of charged groups along the backbone can be expected to be a crucial factor in gel formation. SAXS studies elucidated the calcium-mediated junction-zone lengths of the three gels created, and confirmed that using polymers with more blocky intramolecular charge distributions indeed provides longer inter-chain binding regions that can form longer, more thermally stable, junctions. However, rather than increasing the stability of the networks, if the junction-zone length is significantly increased, the internal dynamics can become driven by increasing internal stresses and become faster and more temporally heterogeneous. Imaging the dynamics, using PCI, showed that there are long range correlations in the dynamics, over several millimetres, many orders of magnitude larger than the rod-like entities forming the gel or the solid calcium carbonate particles that act as nuclei in the gel-formation process. Angle-resolved multi-speckle dynamic light scattering revealed that indeed the dynamics scale with a power law exponent of approximately -1 (and not -2) when changing the scattering vector, confirming that the dynamics in these systems are stress-driven for all gels measured. Increasing the

junction zone length can increase the average characteristic time associated with these long timescale dynamics for intermediate blocklength pectin samples, but on the contrary, when very long junction zones can form, the dynamics often increase indicating that indeed long time internal network dynamics are not controlled by the thermally activated breakage of weaker junctions, but rather by their stress-induced disassembly driven by the propensity of larger junctions-zones to continue to assemble.

The authors acknowledge Dr. Allan Raudsepp for many discussions and valuable input to this work. Dr Che-Yi Chu and Prof. Hsin-Lung Chen for discussions about SAXS of biopolymer networks. Pablo Hernandez-Cerdan and Dr Stephen Keen for their critical reading of the manuscript. Funding for the SAXS section from the New Zealand Synchrotron group, the MacDiarmid institute for the PhD studentship (BWM) and Massey University for equipment Funding.

DRC 16

MASSEY UNIVERSITY
GRADUATE RESEARCH SCHOOL

STATEMENT OF CONTRIBUTION
TO DOCTORAL THESIS CONTAINING PUBLICATIONS

(To appear at the end of each thesis chapter/section/appendix submitted as an article/paper or collected as an appendix at the end of the thesis)

We, the candidate and the candidate's Principal Supervisor, certify that all co-authors have consented to their work being included in the thesis and they have accepted the candidate's contribution as indicated below in the *Statement of Originality*.

Name of Candidate: Bradley William Mansel

Name/Title of Principal Supervisor: Martin Williams

Name of Published Research Output and full reference:

B W Mansel, M A K Williams, Internal Stress drives slow glassy dynamics and quake-like behaviour in ionotropic pectin gels, submitted to Softmatter

In which Chapter is the Published Work: 4

Please indicate either:

- The percentage of the Published Work that was contributed by the candidate: 90%

  and / or

- Describe the contribution that the candidate has made to the Published Work:

  The candidate did 100% of the experimental work and data processing and 90% of the writing.

Brad Mansel — Digitally signed by Brad Mansel DN: cn=Brad Mansel, o, ou, email=bmansel@gmail.com, c=NZ Date: 2015.05.19 14:26:18 +12'00'

Candidate's Signature — 19/05/2015 Date

Williams, Martin — Digitally signed by Williams, Martin DN: cn=Williams, Martin, o, ou, email=m.williams@massey.ac.nz, c=US Date: 2015.05.19 12:24:57 +12'00'

Principal Supervisor's signature — 19/05/2015 Date

GRS Version 3– 16 September 2011

6. Annex A: Further Structural Characterization of Pectin Gels

6.1 Introduction

In addition to the work reported in chapter 4 the structure of pectin gels formed under a variety of conditions, with different divalent ions, and with the addition of monovalent ions was investigated. Furthermore, different gelation protocols for the introduction of ions to the polymer were investigated. In earlier chapters the gelation is performed through the hydrolysis of GDL to form an acid-induced gel or through the dissolution of solid calcium carbonate to form a calcium ionotropic gel. While these two methods are highly favoured for the proposed ability to produce a homogeneous gel at room temperature, other techniques do exist. A common, and less complex method to form pectin calcium gels is using a heat-set gelation method which involves heating pectin and calcium chloride solutions, mixing them while hot, and subsequently allowing to cool. A similar procedure can be used to form an acid-induced gel - which involves lowering the pH of the pectin solution below that which would cause gelation at room-temperature, while holding the temperature above the melting point, and finally cooling to room temperature. This work was undertaken as few previous studies have been carried out to investigate the structural properties of pectin gels, and it was expected that the gelation procedure as well as the conditions under which the gel was formed would have significant effects on the structure. Here we investigate structural differences between gels formed at room temperature and those formed at high temperatures, as well as the effects of adding monovalent salt and different divalent binding ions.

6.2 Method and materials

6.2.1 Small-angle X-ray Scattering

Small-angle x-ray scattering was performed at the Australian synchrotron and the National Centre for Synchrotron Radiation Research in Taiwan. For a complete methodology see the SAXS section of chapters 2 and 3.

6.2.2 Controlled release gelation

The method entails suspending solid carbonate salt in a pectin solution and then solubilizing the ions using an acidifying agent to dissolve the solid carbonate particles. In this section either calcium carbonate, strontium carbonate, or lead carbonate were solubilized using glucono-δ-lactone. The ratio of divalent ions per two carboxyl groups, the R value, was kept constant at 0.5 for the different ions. After initiating gelation the samples were left for 24 hours before measurements were performed. For the complete control release methodology see chapter 4.

6.2.3 Heat-set calcium gelation

Calcium heat-set gels were formed by first dissolving 20mg of dried pectin in 1.58 ml of milliQ water, to give a final concentration of 1 wt %. The pectin solution was heated to 80 °C then mixed with 0.395 ml of 3.5 mM calcium chloride solution at 80 °C. The number of calcium ions gives an R value of 0.25. The solutions were transferred into the requisite sample holder where it solidified upon cooling.

6.2.4 Heat-set acid-induced gelation

Firstly 10 mg of P40 pectin was dissolved in 0.791 ml of milliQ water, this solution was then heated to 50 °C. A magnetic stirrer was added to the heated solution and the temperature corrected pH monitored as 0.1 mol HCl was added to lower the pH to either 2.6 or 2. The solution was topped up to 1 ml with 50 °C milliQ water. Finally, the heated solutions were loaded into the requisite sample holder.

6.3 Results and discussion

6.3.1 Structural characterization of pectin networks formed with different divalent ions

Pectin is most commonly gelled using calcium ions, which is the mechanism of binding in the plant cell wall, although it has long been known that other divalent ions can bind pectin [39]. In an effort to modify the energy of association between chains ionotropic control release gels using strontium and lead carbonates were formed. SAXS measurements were made on gels formed from the three different pectins studied throughout (random, partially blocky and more blocky DM40) with either strontium or lead ions are shown in fig. 6.1. It can be seen that for strontium the scattering strongly resembles that of gels formed with calcium shown in fig. 5.1. The scattering from lead-induced gels shows that the R40 and B40 pectin samples form a gel with a similar scattering profile to calcium, although the most blocky pectin (P40) shows a significant increase in the low q intensity. This increase appears to be the formation of large-scale aggregates and it should be noted that the sample had a significantly higher turbidity compared to the other two samples. Measurements on the binding affinity for pectin and various divalent ions has shown that copper and lead have the highest binding affinity of all divalent ions investigated [179]. We conclude that the P40 pectin, which has the highest affinity to divalent ions, and the high binding affinity of lead has resulted in larger structures and some of the polymer precipitating out of solution.

6.3.2 Concentration and monovalent salt effects on the structure of pectin calcium gels

In figure 6.2 the effects of added sodium chloride and polymer concentration on SAXS scattering vector versus intensity plots are shown. It can be seen that added monovalent salt affects the mid to low-q regimes but has little affect on the high-q regime. In the mid q regime a steady increase in the fractal dimension is seen, while the low-q regime shows a decrease in the fractal dimension from 3 to 2 as the concentration of sodium chloride is increased. The change in scattering intensity of pectin gels from the addition of monovalent salt is a convoluted problem due to the salt changing the conformation of the polymer, the assembly of the junctions, and also introducing scattering resulting

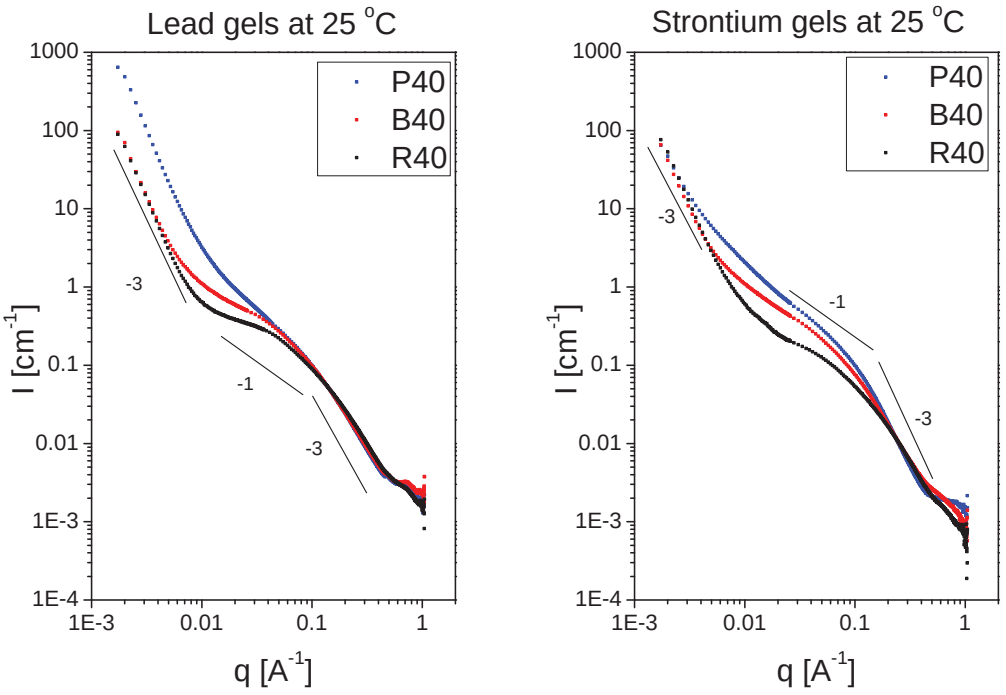

FIGURE 6.1: SAXS scattering vector vs intensity plots for pectin lead (left figure) and strontium (right figure) control release ionotropic gels. It can be seen that generally pectin gels formed with different ions via the control release method have similar structures.

from density fluctuations of the salt ions. The polyelectrolytic properties of pectin cause positively charged ions to congregate around charged regions of the polymer, which are known as ion condensates. At large length scales (or at low-q) it is clear that the change in scattering intensity is from a change in polymer conformation or the junction zone assembly and not ion condensates, due to the ion condensates being considerably smaller than the length scales in the low-q regime. In the low-q regime a fractal dimension of 3 corresponds to a highly clustered conformation of the pectin chains and 2 is the fractal dimension of a random walk. The increase in fractal dimension of the intermediate regime would be considered consistent with the polymer becoming more flexible, although this cannot be the only effect as the upturn would be expected to move to higher q values as the polymer becomes more flexible. It can be seen in fig. 6.2 that there is no change in the q value of the increase in fractal dimension, meaning that ion condensates are affecting the intermediate-q regime, coupled with any effects on the polymer flexibility.

Previous studies on pectin with the addition of monovalent ions have shown that gels

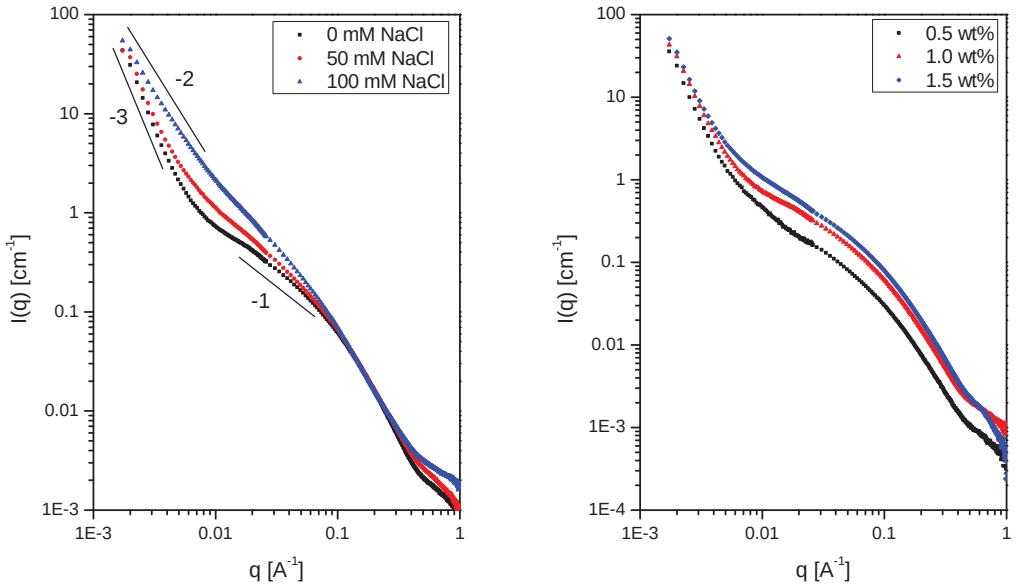

FIGURE 6.2: SAXS scattering vector vs intensity plots for pectin control release gels with added monovalent salt (left figure) and a variety of concentrations (right figure). It can be seen that adding monovalent salt has a significant effect on the gel structure at mid to large length scales.

typically become stronger as the concentration of monovalent salts is increased up to a molarity of a few hundred millimoles, as shown in figure 6.3. In ref. [180] the explanation given for the increase in the storage modulus is "the counter ions suppress the electrostatic repulsion between pectin chains". While this statement is true, our measurements, shown in figure 6.2, reveal that adding monovalent salts forms a more homogeneous, or less clustered random walk network. It is thought that a random walk network will form a more elastic network for the same amount of polymer, as this is the most efficient way to fill space and we show in figure 4.2 that indeed the storage modulus drops as a pectin solution becomes more clustered. It is surprising that the addition of monovalent salt forms a less clustered gel structure as the solution conformation of pectin with added salt turns out to be highly clustered (figures 7.5 and 7.6). This means that the added salt affects the interaction between pectin and calcium, and it does not appear that the solution conformations are fixed when the addition of divalent ions arrests the system.

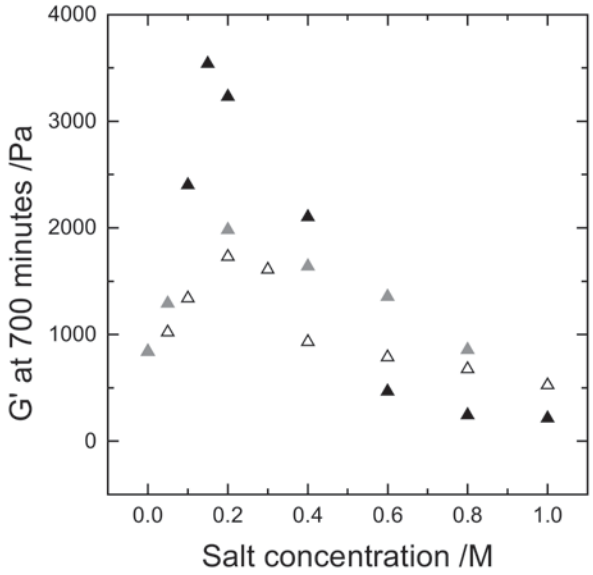

FIGURE 6.3: Storage modulus of a 2 wt % pectin control release calcium gels for a range of added monovalent salts and salt concentrations. Black symbols represent KCl, grey symbols NaCl, and open symbols LiCl. It can be seen that for all ions, up to 200 mM, there is an increase in the storage modulus. Graph reproduced from [180].

6.3.3 Structure of heat-set pectin networks

The SAXS data recorded from heat-set calcium pectin gels, figure 6.4, shows considerably different scattering behaviour compared to those formed using a control release method. Compared to the previously studied controlled release gels the heat-set gels do show a similar low-q regime with a fractal dimension of 3, although this region extends to higher q values that results in the intermediate regime covering a far smaller q range, while the high-q regime has a lower fractal dimension of 2. The high-q regime of heat-set κ-carrageenan gels (data not shown) has also been measured to have a fractal dimension of 2, this work will form part of a larger body of work. While there is a large structural change between heat-set and controlled release gels for each polymer it can be seen in fig. 6.4 that there is little difference between heat-set gels formed with different pectin samples, in stark contrast to the controlled release gels.

Previous experimental studies using rheology and TEM on the difference between pectin controlled release and heat-set calcium gels have shown different structures and melting properties [180]. The authors of the work draw the conclusion that the heat-set calcium gels form many different junction lengths that depends on the cooling rate, while the controlled release protocol predominantly forms one average junction length and a more

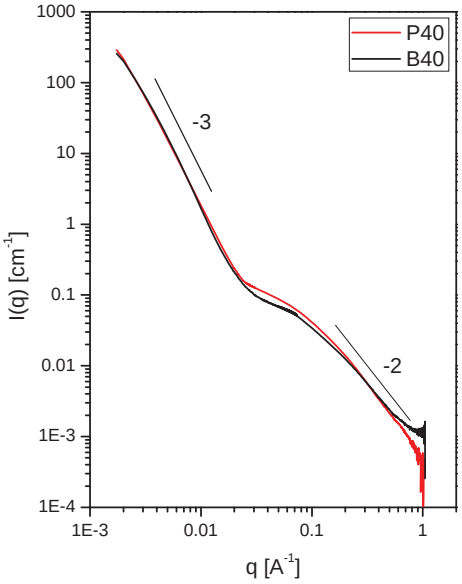

FIGURE 6.4: The scattering profile of B40 and P40 heat-set calcium gels. It can be seen that there is a significant difference in the structure of heat-set gels compared to control release gels, although little difference between heat-set gels formed with different polymers.

trapped network. The formation of a larger variation in junction lengths for the heat-set gel results from the fact that at higher temperatures only the longer and more stable junctions can form, then as the sample cools progressively shorter junctions can form. These results agree well with those we have obtained with SAXS and the ambiguous scattering of the heat-set gels could be the result of poly-disperse length-scales being present. Unfortunately, it is not possible to fit SAXS data to both polydispersity and shape, unless the shape is predetermined, therefore no length scales could be extracted.

The SAXS data obtained from heat-set acid-induced pectin gels, shown in figure 6.5, do show considerably different scattering compared to that seen from those formed using a slow acidification method. It is clear from fig. 6.5 that pH plays an important role in determining the structure of the gel: this was also clear from the turbidity of the sample that at pH 2.0 had far larger associations. The scattering of the heat-set acid-induced gels show fractal dimensions that span large length scales and the data shows little structure. Fig. 6.5 shows fits to a fractal model with fractal dimensions of 1.8 ± 0.3 for the pH 2.5 sample and 2.22 ± 0.04 in the low-q regime for the pH 2 sample. It should be noted that a fractal dimension of 1.76 is close to the fractal dimension of a self avoiding

walk which has a fractal dimension of 1.67. It is also interesting to note that both the heat-set acid gels are less clustered than the slow acidification method.

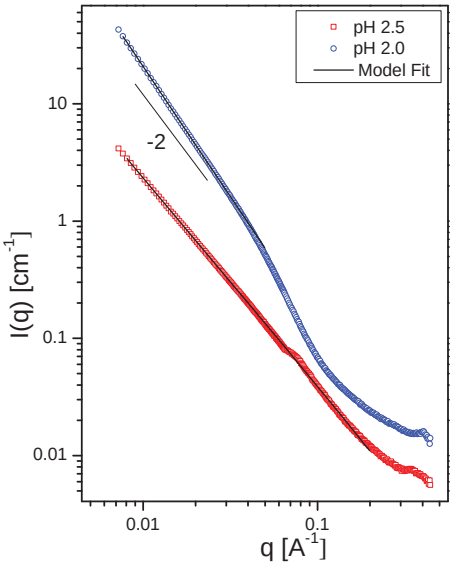

FIGURE 6.5: Scattering profile of heat-set acid induced pectin gels. A fit to a fractal model has been applied to the low q regions and represented by a line on the plot. The different pH of the samples results in different fractal dimensions. The pH 2.5 sample fits to a fractal dimension of 1.8 ± 0.3 and the pH 2.0 sample fractal dimension 2.22 ± 0.04.

6.4 Conclusion

Changes in the gelation method, the way the ions are "introduced" to the polymer and the addition of monovalent ions have significant effects on the structure of the gels formed. Changing the divalent binding ions had little effect on the structure of control release pectin gels, except for the P40 sample with lead ions, which showed larger large-scale structures. Monovalent ions had a significant effect on the mid and large size structures in the gel, with little effect on the smaller scale structure. The change in structure at the largest length scale was a decrease in the fractal dimension of the mesh formed by the polymer network (the polymer appears to fill space more efficiently when monovalent salt is added). At intermediate length scales there is also a change in fractal dimension, although the change is an increase in the fractal dimension from 1 to 2. Heat-set acid gels form a gel that is self-similar across a large range of length scales, which is

considerably different in comparison to those formed at room temperature with a slow acidification method when as the gel tries to form the dynamics are more restricted.

7. Annex B: Conformations of Pectin and Homogalacturonan in the Solution State

7.1 Introduction

We aim to further understand the solution conformations of pectin in a range of different environments. Pectin has been described as a semi-flexible polymer with a persistence length of approximately 10 nm and it has been shown that the mechanical properties of a single pectin chain can be described by the worm-like chain model. While the mechanical properties are well described by the worm-like chain model [181] the solution state small-angle scattering of pectin is expected to be affected by polyelectrolyte effects. Understanding the solution conformations of polyelectrolytes is a complicated problem, with the complexity resulting from many competing effects, which include: polymer stiffness, effects of counter-ion condensates, intra- and inter-chain electrostatic repulsion [182–184]. In the absence of excess salt the solution-state scattering of polyelectrolytes does not resemble that of a worm-like chain, which is a highly successful model to describe many aspects of a semi-flexible polymer unaffected by charge[167, 168, 185]. Currently, polyelectrolytes are not well understood and much effort has been put into understanding these systems using small-angle scattering [153, 186, 187].

Small-angle scattering is a commonly utilized technique to measure the conformation of polymers in the solution state. There are a plethora of different models and methods to analyse small angle scattering data, although a basic method, which still produces significant insights into the structure of the sample is fractal analysis. It involves measuring

the slope of the scattering vector versus scattered intensity on a log-log plot, where the slope describes the average fractal dimension of the scatterers. For polymer-like systems fractal analysis is especially important due to the self-similarity these systems display across a range of length scales [159, 160]. Typically, there are 3 different regimes that describe the scattering of polymer-like systems with a small polymer radius: at the smallest length scales a fractal dimension of 1, which represents the rod-like entities of the local structure; at larger length scales a fractal dimension of 2 is predicted if the polymer exhibits random walk behaviour or 5/3 for a self-avoiding walk. Finally, at length scales larger than the radius of gyration, a plateau is predicted, where the intensity is related to the molecular weight of the polymer [188]. The low-q regime is especially important for polymers in the solution state as it reveals inter-chain interactions or effects related to the solvent. Figure 7.1 shows the predicted scattering from a worm-like chain with excluded volume effects, the two different fractal regimes are shown along with the low q plateau. The model shown in fig. 7.1 can be fitted to experimental data, although it is challenging to obtain a system that experimentally reproduces the predicted scattering.

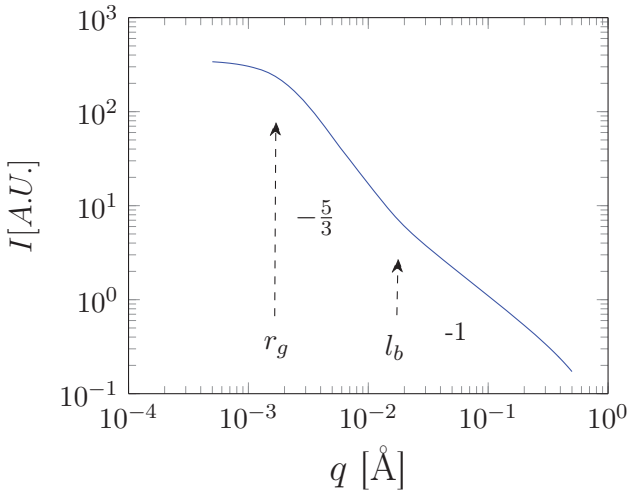

FIGURE 7.1: Scattered intensity as a function of scattering vector for a $l_b = 200$ Å, $l_c = 10000$ Å, $r = 2$ Å worm-like chain with excluded volume effects. Data calculated using SASView software.

In contrast to electrically neutral polymers small-angle scattering from polyelectrolytes in the absence of salt does not resemble the scattering of a worm-like chain and typically displays a large peak in the low to mid-q scattering that is related to the repulsion of the chains from one another, see fig. 7.2 [189]. While pectin is a polyelectrolyte, a more

accurate description is a complex heteropolysaccharide with charged and uncharged regions that can be described by charge distributions which depend on the method with which the sample was demethylesterified (see figures 7.3 and 7.4). The scattering from pectin in the solution state is thus expected to be a combination of both the worm-like chain and polyelectrolyte scattering, although the exact cause of different aspects of the scattering are difficult to predict.

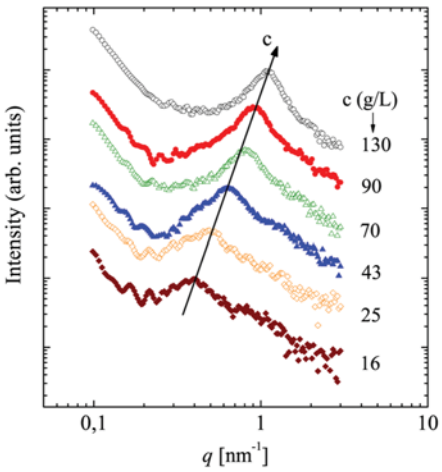

FIGURE 7.2: SAXS from DNA in pure water from ref. [190]. It can be seen that the scattering in this q range has a large peak and does not resemble the worm-like chain model shown in figure 7.1.

Pectin can be refined into pure homogalacturonan (HG) using acidic conditions or RG1ase enzymes to de-polymerize the rhamnogalacturonan-homogalacturonan linkages leaving short blocks of pure HG. These HG chains are approximately 100 residues, which is about one fifth of the size of a pectin chain of 500 residues. The removal of the rhamnose groups groups, further sample purification and the complete chemical knowledge of these samples makes them ideal to further understand the solution conformations of pectin. The HG samples are also ideal to study using SAXS due to their small size being well within the largest accessible length scales. The radius of gyration, r_g for a rod shaped object is related to the length l and radius r by: $r_g^2 = r^2/2 + l^2/12$. A completely extended HG chain of $r = 2.25$ Å and $l = 1000$ Å , corresponds to an $r_g = 289$ Å, which is well within the maximum length scale accessible by the SAXS instruments we used (6000 Å), so that any aggregation should be easily discernible from the measured r_g of an HG chain. The solution conformation of pectin has also been reported to change due to the presence of RG groups which have more flexible linkages

compared to those of HG, and as a result one would expect that samples composed of a higher proportion of RG groups would have a smaller persistence length [60].

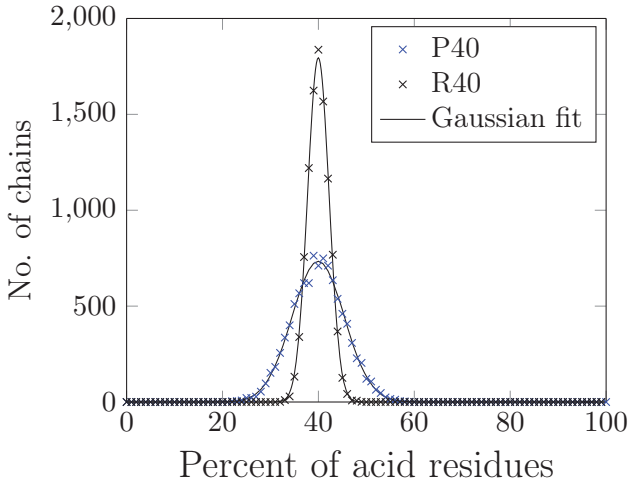

FIGURE 7.3: The distribution of the degree of methylesterification for a random 40%, R40, and PME modified 40%, P40 samples calculated using a Monte Carlo simulation with the software written by J. Owen [191]. It can be seen that the random sample has a far narrower distribution, as is displayed by fits to a Gaussian function (solid lines) with parameters: $\mu = 39.95 \pm 0.08$, $\sigma = 7.7 \pm 0.1$ for the P40 sample and $\mu = 39.98 \pm 0.01$, $\sigma = 3.16 \pm 0.02$ for the R40 sample.

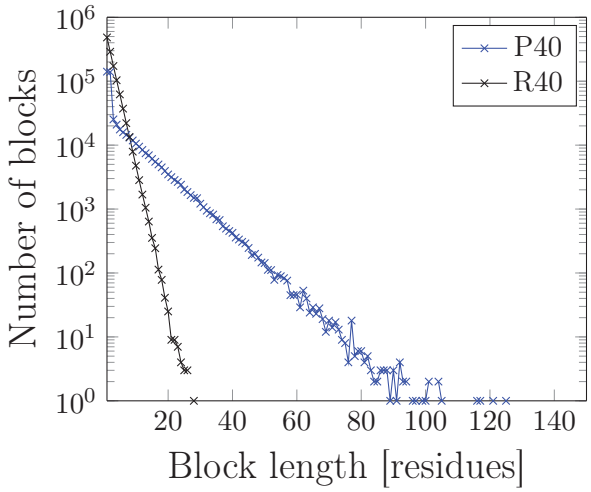

FIGURE 7.4: The distribution of charged block lengths for an R40 and B40 sample calculated using a Monte Carlo simulation written by J. Owen [191].

7.2 Method and materials

7.2.1 Small-angle X-ray Scattering

Small-angle x-ray scattering was performed at the Australian synchrotron and has been described in detail in chapter 4. All samples were filtered through a 500 nm pore size syringe filter to remove any large aggregates or undissolved pectin.

7.2.2 Static Light Scattering

Static light scattering was performed using a goniometer (Malvern) mounted with a gradient-index lens and fibre optic coupled to a photo-multiplier tube. Samples were held in a 10 mm diameter cylindrical cuvette that was placed in an index matching bath. A toluene standard was used to check the alignment before performing experiments on the pectin samples.

7.2.3 Homogalacturonan samples

HG samples were kindly provided by M.C. Ralet(INRA Nantes) and solutions were prepared by dissolving the required amount of dried sample in milliQ water to form a final concentration of 0.2 wt%. Samples were filtered through 0.45 μm pore size syringe filters before adding to the required sample holder.

7.2.4 Pectin samples

Pectin solutions were made by dissolving the required amount of dried pectin powder, obtained from CP Kelco, in either water or a salt solution containing 100 mM of sodium chloride (Sigma). Solutions were made at a concentration of either 0.1, 0.2, 0.3, or 0.4 wt%. For this study solutions in the dilute regime were required to investigate the aggregation properties of pectin solutions therefore 0.2 wt% was typically utilized as this was a low enough concentration to be far enough below the overlap concentration while still providing a good signal to noise. Samples were filtered through 0.45 μm pore size syringe filters before adding to the required sample holder.

7.3 Results

7.3.1 Dilute pectin solutions

SAXS revealed that the scattering from pectin in the dilute solution state, figures 7.5 and 7.6, predominantly shows the following regimes; a high q slope of approximately -1 and a low q slope of -3, although the scattering varies depending on the pH and added salt. Unexpectedly, the low q, or large length-scale, the conformation of the polymer appears highly clustered for all samples. While the propensity for pectin to aggregate is well known, it was thought that pectin would fill space in a more homogeneous manner as the associations forming the clusters are presumed to be weak and dynamic. At intermediate-q values the scattering is highly variable depending on ionic conditions and pH. Finally at high-q values the scattering resembles rod-like objects with a fractal dimension of 1.

As the pH is increased clear trends in the solution conformations (figures 7.5 and 7.6) can be observed for both samples in the presence and absence of salt. In the absence of salt the random and blocky sample behave differently due to the high local charge density of the blocky sample having a higher propensity to form counter ion condensations and stronger attraction and repulsion effects. Added salt appears to predominantly screen out these effects, except at pH 3 or 6 where a significant change in the scattered intensity is observed mostly in the mid-q regime. This mid-q effect is an increase at pH 3, with no change observed in the low or high q, while at pH 6 there is a significant decrease in the mid q and an increase in the low q. Further experiments would be required to understand this complex system.

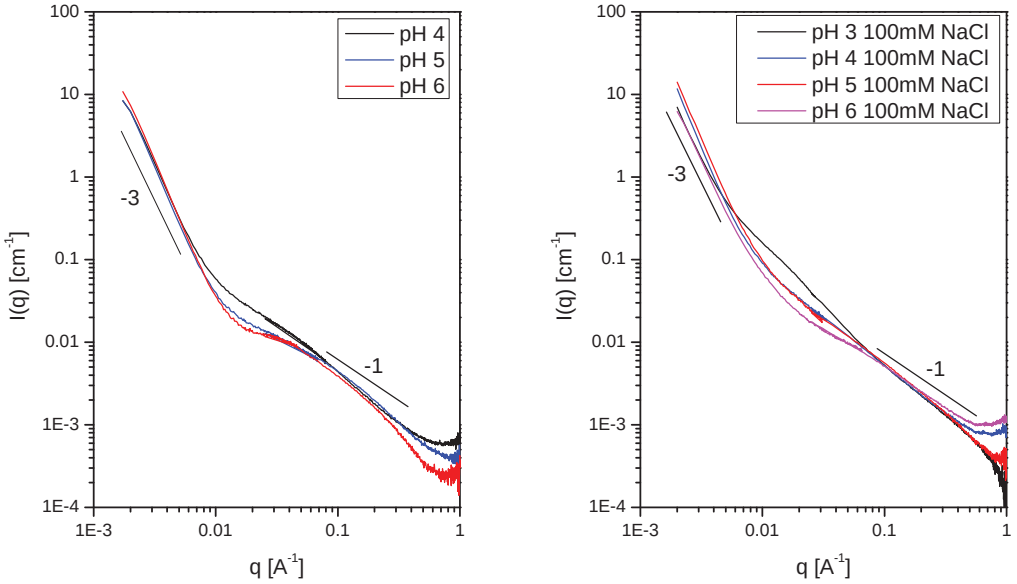

FIGURE 7.5: SAXS results for a 0.2 wt% R40 solution at different pH values and in the absence of salt (left), or with 100 mM of sodium chloride (right).

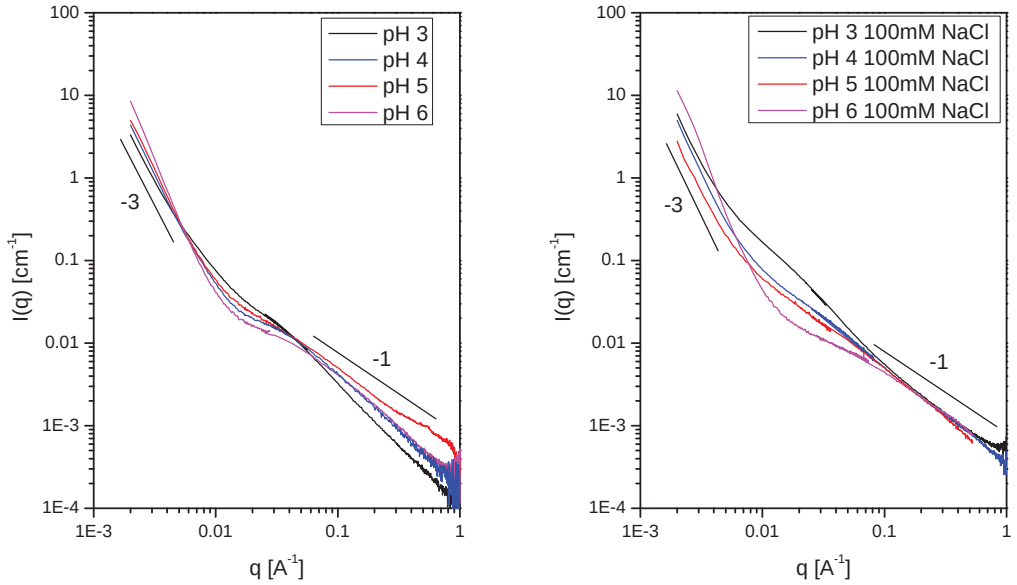

FIGURE 7.6: SAXS results for a 0.2 wt% B40 solution at different pH values and in the absence of salt (left), or with 100 mM of sodium chloride (right).

7.3.2 Dilute homogalacturonan solutions

Dilute solutions of homogalacturonan in purified water were investigated using SAXS and in a quest to access even larger length scales static light scattering (SLS) was performed. The two samples investigated here are called B76 and P79, B76 is a moderately blocky sample with a DM of 76% and the P79 sample is a very blocky sample with a DM of 79%. The SAXS results, see figure 7.7, show a similar trends to pectin in the mid to high q regime, although the HG solutions produce a lower low-q fractal dimension of 2. In the mid-q regime the HG solutions show an increase in scattered intensity at low pH values, similar to the pectin solutions. The two different samples also show a similar trend to pectin in that the more blocky samples are more sensitive to changes in the pH. SLS measurements generally agree with the SAXS measurements and confirm that the low q slope is not an artefact due to radiation damage.

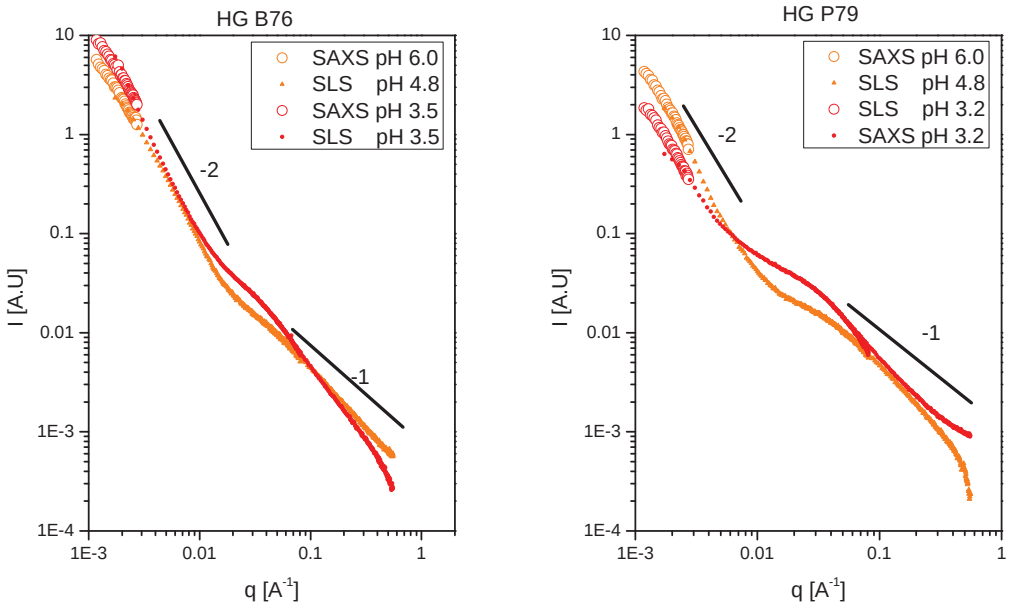

FIGURE 7.7: SAXS results for a 0.2 wt% HG solutions in pure water at different pH values.

7.4 Conclusion

We performed a series of scattering experiments on dilute pectin and HG solutions using SAXS and SLS. While clear trends are present, the solution conformation of

pectin is complicated and the results differ from other polymer-like systems, therefore it was not possible to extract length scales from the data. It was clearly observed that pectin in the dilute solution state forms highly clustered conformations that remain with modifying the pH or the addition of salt. The capability of pectin to aggregate in all environments was clear and no Guinier regime was observed in the low-q regime, even for the low molecular weight HG samples. The HG samples displayed a lower low-q fractal dimension of 2 compared to pectin which had a fractal dimension of 3, which warrants further investigation. The addition of salt screens out some of the effects seen at intermediate length scales, although at low pH values it introduces a curious increase in the scattering intensity at intermediate-q values. Samples with a longer block length are more sensitive to pH changes and display more significant structural changes upon modifying the pH.

To further understand the dilute solution state of pectin and HG further complimentary experiments are needed. Dynamic light scattering could provide significant insights into the size of the aggregates and it has long been speculated that the low-q upturn in small-angle scattering data is related to the slow mode seen in DLS.

8. Conclusion and Future Work

8.1 Scope of thesis

The general aim of this thesis was to further understand the structure, dynamics and material properties of pectin gels. We employed traditional soft matter physics ideas and state-of-the-art experimental techniques to understand how the constituents behave in the solutions state; the mechanism that drives their self-assembly; and finally how modifying the self-assembled entities affects the structure, dynamics and material properties of the resulting gel. Few previous studies have been performed on the structure and dynamics of pectin gels, although work has been carried out that focuses on the fast dynamics and structure of junction zones. We extend measurements of the dynamics out to long times, up to the order of hours, and structural measurements have extended over the range of one to hundreds of nanometres. Long time measurements are particularly interesting as they provide insights into the non-equilibrium state of the system. These gels are typically far from their equilibrium state and can be considered a soft glass.

8.2 Summary

Chapter 2 focus on dynamical and rheological measurements on pectin acid gels. Diffusing wave spectroscopy and non-linear rheology measurements were performed on acid-induced pectin gels. These measurements were fitted to a phenomenological model, called the glassy wormlike chain model, that provided insights into the glass-like behaviour that acid-induced gels display. The short time data provided insights into the bundle size of the associated polymeric entities forming the network. At long times

measurements revealed that there was a further, unexpected, de-correlation in the scattered light. This so called slow-mode moved to faster times upon heating and became the major focus of this thesis.

Chapter 3 focuses on further characterizing the structure and mechanical properties of acid-induced pectin gels and solutions. The chapter can be divided into 4 parts which cover: measurements of the structure and mechanical properties from the solution state to the gel state, structural measurements on heating and melting, and finally structural studies on the thermo-reversibility and solvent effects. Initially, the pre-modified pectin was structurally characterized using small-angle x-ray scattering (SAXS) which showed a slightly clustered conformation of the chains in the semi-dilute state. Next we focussed on measuring time-resolved rheological and structural properties as we induced gelation of the modified pectin solution using a slow acidification technique. It was found that initially the dynamic moduli dropped before a major increase corresponding to the sol-gel transition. SAXS revealed that the decrease was due to the large scale confirmation of the polymer solution becoming more clustered and filling space less efficiently. Frequency-dependent pre-stress rheology experiments were performed on acid-induced gels and it was found that the networks could stress stiffen to around ten times the unstressed moduli. The structure of the acid-induced gel was characterized using SAXS and the result was fitted to a flexible cylinder model. The model extracted a persistence length that was 5 nm. Finally SAXS measurements investigating thermo-reversibility and the effect of deuterated water were performed. It was found that gels formed in deuterated water showed different structural properties compared to hydrogenated water. These results displayed the importance of hydrogen bonding in these systems. It was also found that if one holds the temperature of the sample above the gel-sol transition temperature there are significant amounts of aggregation, suggesting that kinetic entrapment is highly important in forming spatially homogeneous acid-induced pectin gels.

Chapter 4 answers questions proposed during the initial DWS experiments, pertaining to the long-time dynamics. Firstly, we designed a series of pectin calcium ionotropic gels that we suspected would present differing long-time dynamics. We predicted that if we formed calcium pectin gels under the same conditions, with the same constituents, although changing the distribution of the binding regions on the pectin chains, we could produce gels with differing long-time dynamics. This was performed by using

three different pectins with different degrees of blockiness. To ensure that the different block lengths translated into different junction zones SAXS was performed on the gels and the data fitted to a cylinder form factor with fractal structure factor. The results of the model fitting showed that the more blocky samples had longer junction lengths, as hoped. To quantify the long-time dynamics two different scattering techniques were built. The first technique called photon correlation imaging(PCI), spatially resolved the dynamics. The second technique, multi-angle multi-speckle dynamic light scattering (MAMS DLS) resolved the angular dependence of the long-time dynamics. PCI revealed that the gels are highly spatially heterogeneous with heterogeneities on the scale of millimetres. MAMS DLS showed that internal stress was driving the long-time dynamics in all three gels. Both techniques showed that gels formed with the shortest junction-zones typically had the fastest dynamics and while increasing the length of junction-zones initially gave slower dynamics, junction-zones that were too long saw the dynamics increase and were often the fastest. MAMS DLS further revealed, using time-resolved correlation plots, that the gels displayed three types of dynamics, the shortest was a quake-like temporally heterogeneous dynamics, at intermediate times an oscillation in the correlation, synonymous with creaking, was observed and as the time-lag was increased a steady decrease in the time resolved degree of correlation was observed.

Chapters 5 and 6, which are presented as annexes, describe further structural characterization of pectin gels and solutions. In Chapter 5 the structure of gels formed under a variety of conditions was investigated. It was found that pectin gels could be formed using a controlled-release gelation method using different divalent binding ions and generally a similar structure to calcium controlled-release gels was observed. In contrast, calcium gels formed using a heat-set method formed gels with significantly different structures, as did systems with the addition of monovalent salt. Small-angle x-ray scattering from dilute solutions of pectin revealed that pectin forms highly clustered conformations in solution that remained upon changing the ionic conditions or pH. Purified homogalacturonan samples showed random-walk network behaviour that indicated tenuous aggregation which remained, as for the pectin samples, upon changing the pH or ionic conditions despite the low molecular weight and low concentration.

8.3 Conclusions

- Diffusing wave spectroscopy measurements on pectin acid gels revealed a second slow mode in the correlation that had not previously been reported.
- Structural and rheological measurements of a pectin acid gel were performed which revealed the size of the network architecture on scales of a few Angstrom to several thousand Angstrom and rheology measurements revealed a network that could significantly strain stiffen.
- Angle-resolved dynamic measurements revealed that internal stress drives the slow dynamics in pectin gels and internal stress appears to increase when the junction lengths are made excessively long. Gels formed with intermediate length junction zones display the slowest dynamics.
- SAXS measurements on the structure of pectin gels formed under a variety of conditions and gelation protocols revealed that many different gel architectures can be formed depending on the gelation conditions.
- SAXS measurements on dilute pectin solutions showed that pectin in solution does not typically reside as a single entity but rather as tenuous aggregates that persist upon changing the pH or ionic conditions.

8.4 Future work

Studying slow dynamical processes in gelled materials is still a new area of research and many experiments are possible to get a more complete understanding of relaxation processes in soft matter. Significant insights could be obtained if one could monitor the internal stress as the gel evolves. One possible method to achieve this is to monitor the slope of the short-time regime of the time-lag versus mean-square displacement plot from DWS. Previous microrheological measurements and theory have shown that the initial decay in the correlation, at short times, can provide information on the bundle size and internal stress in the system. It has been shown that this short time decay, when converted to a mean-square displacement, scales as a function of the lag-time with a power law of 3/4, if the internal stress is low. If there is significant amounts of internal stress the power law is predicted to change and scale with 1/2. The short time

dynamics could then be used to monitor the internal stress in the gel and the change in internal stress related to changes in the long time dynamics as the gel ages. One could also introduce stress using a shear cell and monitor how the dynamics respond. This would also be a method to test the theoretical prediction that describes the scaling of the MSD.

Dynamical measurements on gels formed with different divalent binding ions could provide significant insights into how the binding energy of junction zones affects the long-time dynamics. We have shown that lead and strontium divalent ions can produce controlled-release gels with similar structures. Investigating gels formed with divalent ions could provide insights into how the gel structure affects the non-equilibrium state of the system.

We have shown that vastly different gel structures can be formed by varying the gelation protocol or with the addition of monovalent ions. To the authors knowledge there is no study, to date, that relates the structure measured using small-angle scattering to the mechanical properties of the gel formed. It was shown in chapter 6 that the low-q fractal dimension can be modified using monovalent ions and it is known that added monovalent ions form a gel with a higher storage modulus, although little is known about the other rheological parameters of the gels. A random walk network fills space most efficiently and would be the most well connected network, which should not only be stronger but also exhibit significantly different stress stiffening. These measurements could provide significant insights and further work should be performed to investigate a correlation between the yield stress and fractal dimension of the network. The author predicts that a random walk network would have a lower yield stress and would be less susceptible to network deformation for a given stress compared to a more clustered network. It has been speculated, on the basis of temperature dependent rheological measurements, that heat-set gels have a larger range of junction lengths than controlled-release pectin gels. Results from annex 6 appear to further confirm this speculation, although scattering measurements on poly-disperse systems cannot reveal a significant amount of information about the system. Non-linear rheology would provide significant insights, as the heat-set gel has poly-disperse junction zone lengths, with some very large junctions. One would expect the differential shear modulus to increase at a lower rate with increasing pre-stress, although have a higher failure stress, compared to the same gel with a more average distribution of junction lengths.

Structural measurements on dilute pectin solutions have uncovered many currently unexplainable features in the measurements. Small-angle scattering measurements that can discern between scattering from the counter ions and the polymer would provide significant insights into these measurements. However, in this case SANS would not be appropriate as it requires deuterated water that, as we have shown, affects the conformation of pectin in solution. One technique that makes this possible is anomalous-SAXS which uses the absorption edge of certain elements to provide some contrast between the ions and polymer, although the anomalous scattering is typically only a few percent of the total scattering intensity making the measurements difficult. Another technique which makes this possible is resonant soft x-ray scattering (RSOXS). For soft x-rays there is an element dependent enhancement of the scattering at certain resonant frequencies. This can be utilized to add contrast to certain elements and the effect is a significant increase in the scattered intensity, although this technique must be performed under ultra-high vacuum making the measurement of solution state samples difficult, and it must be performed at a highly specialized beamline.

While this thesis has answered questions pertaining to the structure, dynamics and rheological properties of pectin networks it has raised many more and much work remains to be done.

References

[1] Pierre-Gilles de Gennes. Soft Matter (Nobel Lecture). *Angewandte Chemie International Edition in English*, 31(7):842–845, July 1992. ISSN 0570-0833, 1521-3773. doi: 10.1002/anie.199208421. URL http://doi.wiley.com/10.1002/anie.199208421.

[2] Ronald G. Larson. *The structure and rheology of complex fluids*. Topics in chemical engineering. Oxford University Press, New York, 1999. ISBN 019512197X.

[3] R Edgeworth, B J Dalton, and T Parnell. The pitch drop experiment. *European Journal of Physics*, 5(4):198–200, October 1984. ISSN 0143-0807, 1361-6404. doi: 10.1088/0143-0807/5/4/003. URL http://stacks.iop.org/0143-0807/5/i=4/a=003?key=crossref.b3147ae4c286a1f7123a407128757db6.

[4] C. A. Angell, K. L. Ngai, G. B. McKenna, P. F. McMillan, and S. W. Martin. Relaxation in glassforming liquids and amorphous solids. *Journal of Applied Physics*, 88(6):3113, 2000. ISSN 00218979. doi: 10.1063/1.1286035. URL http://scitation.aip.org/content/aip/journal/jap/88/6/10.1063/1.1286035.

[5] Mi D. Ediger. Spatially heterogeneous dynamics in supercooled liquids. *Annual review of physical chemistry*, 51(1):99–128, 2000. URL http://www.annualreviews.org/doi/abs/10.1146/annurev.physchem.51.1.99.

[6] Pablo G. Debenedetti and Frank H. Stillinger. Supercooled liquids and the glass transition. *Nature*, 410(6825):259–267, 2001. URL http://www.nature.com/articles/doi:10.1038%2F35065704.

[7] Luca Cipelletti and Laurence Ramos. Slow dynamics in glassy soft matter. *Journal of Physics: Condensed Matter*, 17(6):R253–R285, February 2005. ISSN 0953-8984, 1361-648X. doi: 10.1088/0953-8984/17/6/

R01. URL http://stacks.iop.org/0953-8984/17/i=6/a=R01?key=crossref.5310ed6e85c7a827417472cb491223ae.

[8] Luca Cipelletti, Laurence Ramos, S. Manley, E. Pitard, D. A. Weitz, Eugene E. Pashkovski, and Marie Johansson. Universal non-diffusive slow dynamics in aging soft matter. *Faraday Discussions*, 123:237–251, January 2003. ISSN 13596640, 13645498. doi: 10.1039/b204495a. URL http://xlink.rsc.org/?DOI=b204495a.

[9] Predrag Bursac, Guillaume Lenormand, Ben Fabry, Madavi Oliver, David A. Weitz, Virgile Viasnoff, James P. Butler, and Jeffrey J. Fredberg. Cytoskeletal remodelling and slow dynamics in the living cell. *Nature Materials*, 4(7):557–561, July 2005. ISSN 1476-1122, 1476-4660. doi: 10.1038/nmat1404. URL http://www.nature.com/doifinder/10.1038/nmat1404.

[10] Ranjini Bandyopadhyay, Dennis Liang, James L. Harden, and Robert L. Leheny. Slow dynamics, aging, and glassy rheology in soft and living matter. *Solid state communications*, 139(11):589–598, 2006. URL http://www.sciencedirect.com/science/article/pii/S0038109806005229.

[11] Linhong Deng, Xavier Trepat, James P. Butler, Emil Millet, Kathleen G. Morgan, David A. Weitz, and Jeffrey J. Fredberg. Fast and slow dynamics of the cytoskeleton. *Nature Materials*, 5(8):636–640, August 2006. ISSN 1476-1122. doi: 10.1038/nmat1685. URL http://www.nature.com.ezproxy.massey.ac.nz/nmat/journal/v5/n8/full/nmat1685.html.

[12] Tadeusz Pakula, Dimitris Vlassopoulos, George Fytas, and Jacques Roovers. Structure and Dynamics of Melts of Multiarm Polymer Stars. *Macromolecules*, 31 (25):8931–8940, December 1998. ISSN 0024-9297. doi: 10.1021/ma981043r. URL http://dx.doi.org/10.1021/ma981043r.

[13] Luca Cipelletti and Laurence Ramos. Slow dynamics in glasses, gels and foams. *Current Opinion in Colloid & Interface Science*, 7(34):228–234, August 2002. ISSN 1359-0294. doi: 10.1016/S1359-0294(02)00051-1. URL http://www.sciencedirect.com/science/article/pii/S1359029402000511.

[14] Andrei Fluerasu, Abdellatif Moussaïd, Anders Madsen, and Andrew Schofield. Slow dynamics and aging in colloidal gels studied by x-ray photon correlation spectroscopy. *Physical Review E*, 76(1), July 2007. ISSN 1539-3755, 1550-2376.

doi: 10.1103/PhysRevE.76.010401. URL http://link.aps.org/doi/10.1103/PhysRevE.76.010401.

[15] Emanuela Del Gado, Annalisa Fierro, Lucilla de Arcangelis, and Antonio Coniglio. Slow dynamics in gelation phenomena: From chemical gels to colloidal glasses. *Physical Review E*, 69(5):051103, 2004. URL http://journals.aps.org/pre/abstract/10.1103/PhysRevE.69.051103.

[16] Eleonora Secchi, Tommaso Roversi, Stefano Buzzaccaro, Laura Piazza, and Roberto Piazza. Biopolymer gels with physical cross-links: gelation kinetics, aging, heterogeneous dynamics, and macroscopic mechanical properties. *Soft Matter*, 9(15):3931–3944, March 2013. ISSN 1744-6848. doi: 10.1039/C3SM27153F. URL http://pubs.rsc.org.ezproxy.massey.ac.nz/en/content/articlelanding/2013/sm/c3sm27153f.

[17] E Secchi, F Munarin, M D Alaimo, S Bosisio, S Buzzaccaro, G Ciccarella, V Vergaro, P Petrini, and R Piazza. External and internal gelation of pectin solutions: microscopic dynamics versus macroscopic rheology. *Journal of Physics: Condensed Matter*, 26(46):464106, November 2014. ISSN 0953-8984, 1361-648X. doi: 10.1088/0953-8984/26/46/464106. URL http://stacks.iop.org/0953-8984/26/i=46/a=464106?key=crossref.2ba6e4e347c4dcd41b544d2b5af94444.

[18] Domenico Larobina and Luca Cipelletti. Hierarchical cross-linking in physical alginate gels: a rheological and dynamic light scattering investigation. *Soft Matter*, 9(42):10005–10015, October 2013. ISSN 1744-6848. doi: 10.1039/C3SM52006D. URL http://pubs.rsc.org.ezproxy.massey.ac.nz/en/content/articlelanding/2013/sm/c3sm52006d.

[19] GM Pajonk. Aerogel catalysts. *Applied Catalysis*, 72(2):217–266, 1991.

[20] International Union of Pure and Applied Chemistry. *Compendium of polymer terminology and nomenclature: IUPAC recommendations, 2008*. RSC Pub. : IUPAC, Cambridge, 2009. ISBN 9780854044917.

[21] AR Bausch and K Kroy. A bottom-up approach to cell mechanics. *Nature physics*, 2(4):231–238, 2006.

[22] Wolfgang Kabsch, Hans Georg Mannherz, Dietrich Suck, Emil F Pai, and Kenneth C Holmes. Atomic structure of the actin: DNase I complex. *Nature*, (347): 37–44, 1990.

[23] Chris T Brett and John R Hillman. *Biochemistry of plant cell walls*, volume 70. CUP Archive, 1985.

[24] Daniel J. Cosgrove. Growth of the plant cell wall. *Nature Reviews Molecular Cell Biology*, 6(11):850–861, November 2005. ISSN 1471-0072, 1471-0080. doi: 10.1038/nrm1746. URL http://www.nature.com/doifinder/10.1038/nrm1746.

[25] William G. T. Willats, Lesley McCartney, William Mackie, and J. Paul Knox. Pectin: cell biology and prospects for functional analysis. In N. C. Carpita, M. Campbell, and M. Tierney, editors, *Plant Cell Walls*, pages 9–27. Springer Netherlands, January 2001. ISBN 978-94-010-3861-4, 978-94-010-0668-2. URL http://link.springer.com/chapter/10.1007/978-94-010-0668-2_2.

[26] William G. T Willats, J. Paul Knox, and Jørn Dalgaard Mikkelsen. Pectin: new insights into an old polymer are starting to gel. *Trends in Food Science & Technology*, 17(3):97–104, March 2006. ISSN 0924-2244. doi: 10.1016/j.tifs.2005.10.008. URL http://www.sciencedirect.com/science/article/pii/S0924224405002517.

[27] K. J. Pienta, H. Nailk, A. Akhtar, K. Yamazaki, T. S. Replogle, J. Lehr, T. L. Donat, L. Tait, V. Hogan, and A. Raz. Inhibition of Spontaneous Metastasis in a Rat Prostate Cancer Model by Oral Administration of Modified Citrus Pectin. *JNCI Journal of the National Cancer Institute*, 87(5):348–353, March 1995. ISSN 0027-8874, 1460-2105. doi: 10.1093/jnci/87.5.348. URL http://jnci.oxfordjournals.org/cgi/doi/10.1093/jnci/87.5.348.

[28] P. Nangia-Makker, V. Hogan, Y. Honjo, S. Baccarini, L. Tait, R. Bresalier, and A. Raz. Inhibition of Human Cancer Cell Growth and Metastasis in Nude Mice by Oral Intake of Modified Citrus Pectin. *JNCI Journal of the National Cancer Institute*, 94(24):1854–1862, December 2002. ISSN 0027-8874, 1460-2105. doi: 10.1093/jnci/94.24.1854. URL http://jnci.oxfordjournals.org/cgi/doi/10.1093/jnci/94.24.1854.

[29] M. K. Chourasia and S. K. Jain. Pharmaceutical approaches to colon targeted drug delivery systems. *Journal of Pharmacy & Pharmaceutical Sciences: A Publication of the Canadian Society for Pharmaceutical Sciences, Société Canadienne Des Sciences Pharmaceutiques*, 6(1):33–66, April 2003. ISSN 1482-1826.

[30] D.A. Rees. Structure, Conformation, and Mechanism in the Formation of Polysaccharide Gels and Networks. In *Advances in Carbohydrate Chemistry and Biochemistry*, volume 24, pages 267–332. Elsevier, 1969. ISBN 9780120072248. URL http://linkinghub.elsevier.com/retrieve/pii/S0065231808603522.

[31] Apicius, Barbara Flower, Elisabeth Alföldi-Rosenbaum, and Katerina Wilczynski. *The Roman Cookery Book: A Critical Translation of" The Art of Cooking" by Apicius for Use in the Study and the Kitchen*. GG Harrap & Company, 1961.

[32] Donatella Bulone, Vincenzo Martorana, Caide Xiao, and Pier Luigi San Biagio. Role of Sucrose in Pectin Gelation: Static and Dynamic Light Scattering Experiments. *Macromolecules*, 35(21):8147–8151, October 2002. ISSN 0024-9297, 1520-5835. doi: 10.1021/ma0205109. URL http://pubs.acs.org/doi/abs/10.1021/ma0205109.

[33] R R R Vincent, B W Mansel, A Kramer, K Kroy, and M A K Williams. Micro-rheological behaviour and nonlinear rheology of networks assembled from polysaccharides from the plant cell wall. *New Journal of Physics*, 15(3):035002, March 2013. ISSN 1367-2630. doi: 10.1088/1367-2630/15/3/035002. URL http://stacks.iop.org/1367-2630/15/i=3/a=035002?key=crossref.e6989d93080c6c493cc8652c637ffdb7.

[34] P. M. Gilsenan, R. K. Richardson, and E. R. Morris. Thermally reversible acid-induced gelation of low-methoxy pectin. *Carbohydrate Polymers*, 41(4):339–349, April 2000. ISSN 0144-8617. doi: 10.1016/S0144-8617(99)00119-8. URL http://www.sciencedirect.com/science/article/pii/S0144861799001198.

[35] Petter Stang Holst, Anna-Lena Kjøniksen, Huaitian Bu, Sverre Arne Sande, and Bo Nyström. Rheological properties of pH-induced association and gelation of pectin. *Polymer Bulletin*, 56(2-3):239–246, February 2006. ISSN 0170-0839, 1436-2449. doi: 10.1007/s00289-005-0489-8. URL http://link.springer.com/article/10.1007/s00289-005-0489-8.

[36] Anna Ström, Pascual Ribelles, Leif Lundin, Ian Norton, Edwin R. Morris, and Martin A. K. Williams. Influence of Pectin Fine Structure on the Mechanical Properties of Calcium-Pectin and Acid-Pectin Gels. *Biomacromolecules*, 8(9): 2668–2674, September 2007. ISSN 1525-7797. doi: 10.1021/bm070192r. URL http://dx.doi.org/10.1021/bm070192r.

[37] Anna Ström, Erich Schuster, and Suk Meng Goh. Rheological characterization of acid pectin samples in the absence and presence of monovalent ions. *Carbohydrate Polymers*, 113:336–343, November 2014. ISSN 0144-8617. doi: 10.1016/j.carbpol.2014.06.090. URL http://www.sciencedirect.com/science/article/pii/S0144861714006894.

[38] Michael C. Jarvis. Structure and properties of pectin gels in plant cell walls. *Plant, Cell and Environment*, 7(3):153–164, April 1984. ISSN 0140-7791, 1365-3040. doi: 10.1111/1365-3040.ep11614586. URL http://doi.wiley.com/10.1111/1365-3040.ep11614586.

[39] Maxim Khotimchenko, Valeri Kovalev, and Yuri Khotimchenko. Equilibrium studies of sorption of lead(II) ions by different pectin compounds. *Journal of Hazardous Materials*, 149(3):693–699, November 2007. ISSN 03043894. doi: 10.1016/j.jhazmat.2007.04.030. URL http://linkinghub.elsevier.com/retrieve/pii/S0304389407005158.

[40] Rudolf Kohn. Binding of toxic cations to pectin, its oligomeric fragments and plant tissues. *Carbohydrate Polymers*, 2(4):273–275, January 1982. ISSN 01448617. doi: 10.1016/0144-8617(82)90030-3. URL http://linkinghub.elsevier.com/retrieve/pii/0144861782900303.

[41] Debra Mohnen. Pectin structure and biosynthesis. *Current Opinion in Plant Biology*, 11(3):266–277, June 2008. ISSN 1369-5266. doi: 10.1016/j.pbi.2008.03.006. URL http://www.sciencedirect.com/science/article/pii/S1369526608000630.

[42] Jean-Paul Vincken, Henk A. Schols, Ronald J. F. J. Oomen, Maureen C. McCann, Peter Ulvskov, Alphons G. J. Voragen, and Richard G. F. Visser. If Homogalacturonan Were a Side Chain of Rhamnogalacturonan I. Implications for Cell Wall Architecture. *Plant Physiology*, 132(4):1781–1789, August 2003. ISSN 0032-0889,

1532-2548. doi: 10.1104/pp.103.022350. URL http://www.plantphysiol.org/content/132/4/1781.

[43] Marshall L Fishman and Joseph J Jen. Chemistry and function of pectins. 1986.

[44] A. Cesàro, A. Ciana, F. Delben, G. Manzini, and S. Paoletti. Physicochemical properties of pectic acid. I. Thermodynamic evidence of a pH-induced conformational transition in aqueous solution. *Biopolymers*, 21(2):431–449, February 1982. ISSN 1097-0282. doi: 10.1002/bip.360210214. URL http://onlinelibrary.wiley.com/doi/10.1002/bip.360210214/abstract.

[45] M. D. Walkinshaw and Struther Arnott. Conformations and interactions of pectins: I. X-ray diffraction analyses of sodium pectate in neutral and acidified forms. *Journal of Molecular Biology*, 153(4):1055–1073, December 1981. ISSN 0022-2836. doi: 10.1016/0022-2836(81)90467-8. URL http://www.sciencedirect.com/science/article/pii/0022283681904678.

[46] M. D. Walkinshaw and Struther Arnott. Conformations and interactions of pectins: II. Models for junction zones in pectinic acid and calcium pectate gels. *Journal of Molecular Biology*, 153(4):1075–1085, December 1981. ISSN 0022-2836. doi: 10.1016/0022-2836(81)90468-X. URL http://www.sciencedirect.com/science/article/pii/002228368190468X.

[47] M Bosco, S Miertus, S Turchini, T Prosperi, I Ascone, and R Rizzo. Structural studies on polygalacturonate gels: an EXAFS investigation combined with molecular modelling. *Carbohydrate Polymers*, 47(1):15–26, January 2002. ISSN 0144-8617. doi: 10.1016/S0144-8617(00)00339-8. URL http://www.sciencedirect.com/science/article/pii/S0144861700003398.

[48] Liangbin Li, Yapeng Fang, Rob Vreeker, Ingrid Appelqvist, and Eduardo Mendes. Reexamining the Egg-Box Model in Calcium-Alginate Gels with X-ray Diffraction. *Biomacromolecules*, 8(2):464–468, February 2007. ISSN 1525-7797, 1526-4602. doi: 10.1021/bm060550a. URL http://pubs.acs.org/doi/abs/10.1021/bm060550a.

[49] Isabelle Braccini and Serge Pérez. Molecular basis of Ca2+-induced gelation in alginates and pectins: the egg-box model revisited. *Biomacromolecules*, 2(4):

1089–1096, December 2001. ISSN 1525-7797. doi: 10.1021/bm010008g. URL http://dx.doi.org/10.1021/bm010008g.

[50] Gregor T. Grant, Edwin R. Morris, David A. Rees, Peter J. C. Smith, and David Thom. Biological interactions between polysaccharides and divalent cations: The egg-box model. *FEBS Letters*, 32(1):195–198, May 1973. ISSN 0014-5793. doi: 10.1016/0014-5793(73)80770-7. URL http://www.sciencedirect.com/science/article/pii/0014579373807707.

[51] Ali Assifaoui, Adrien Lerbret, Uyen Thi Diem Huynh, Fabrice Neiers, Odile Chambin, Camille Loupiac, and Fabrice Cousin. Structural behaviour differences in low methoxy pectin solutions in presence of divalent cations (Ca2+ and Zn2+): a process driven by the binding mechanism of the cation with the galacturonate unit. *Soft Matter*, November 2014. ISSN 1744-6848. doi: 10.1039/C4SM01839G. URL http://pubs.rsc.org/en/content/articlelanding/2014/sm/c4sm01839g.

[52] M. A. V. Axelos, J. F. Thibault, and J. Lefebvre. Structure of citrus pectins and viscometric study of their solution properties. *International Journal of Biological Macromolecules*, 11(3):186–191, June 1989. ISSN 0141-8130. doi: 10.1016/0141-8130(89)90066-4. URL http://www.sciencedirect.com/science/article/pii/0141813089900664.

[53] H. Anger and G. Berth. Gel permeation chromatography and the Mark-Houwink relation for pectins with different degrees of esterification. *Carbohydrate Polymers*, 6(3):193–202, 1986. ISSN 0144-8617. doi: 10.1016/0144-8617(86)90019-6. URL http://www.sciencedirect.com/science/article/pii/0144861786900196.

[54] H. Anger and G. Berth. Gel permeation chromatography of sunflower pectin. *Carbohydrate Polymers*, 5(4):241–250, 1985. ISSN 0144-8617. doi: 10.1016/0144-8617(85)90033-5. URL http://www.sciencedirect.com/science/article/pii/0144861785900335.

[55] M Doi and S. F Edwards. *The theory of polymer dynamics*. Clarendon Press, Oxford, 1986. ISBN 0198519761 9780198519768 0198520336 9780198520337.

[56] Paul J. Flory. *Statistical mechanics of chain molecules*. Interscience Publishers, New York, 1969. ISBN 0470264950.

[57] Beli R. Thakur, Rakesh K. Singh, Avtar K. Handa, and M. A. Rao. Chemistry and uses of pectin A review. *Critical Reviews in Food Science and Nutrition*, 37(1):47–73, February 1997. ISSN 1040-8398. doi: 10.1080/10408399709527767. URL http://dx.doi.org/10.1080/10408399709527767.

[58] Soizic Cros, Catherine Garnier, Monique A. V. Axelos, Anne Imberty, and Serge Pérez. Solution conformations of pectin polysaccharides: Determination of chain characteristics by small angle neutron scattering, viscometry, and molecular modeling. *Biopolymers*, 39(3):339–351, September 1996. ISSN 1097-0282. doi: 10.1002/(SICI)1097-0282(199609)39:3<339::AID-BIP6>3.0.CO;2-P. URL http://onlinelibrary.wiley.com/doi/10.1002/(SICI)1097-0282(199609)39:3<339::AID-BIP6>3.0.CO;2-P/abstract.

[59] Aline M. F. Lima, Valdir Soldi, and Redouane Borsali. Dynamic light scattering and viscosimetry of aqueous solutions of pectin, sodium alginate and their mixtures: effects of added salt, concentration, counterions, temperature and chelating agent. *Journal of the Brazilian Chemical Society*, 20(9):1705–1714, January 2009. ISSN 0103-5053. doi: 10.1590/S0103-50532009000900020. URL http://www.scielo.br/scielo.php?script=sci_abstract&pid=S0103-50532009000900020&lng=en&nrm=iso&tlng=en.

[60] M. A. Axelos and J. F. Thibault. Influence of the substituents of the carboxyl groups and of the rhamnose content on the solution properties and flexibility of pectins. *International Journal of Biological Macromolecules*, 13(2):77–82, April 1991. ISSN 0141-8130.

[61] Anna Malovikova, Marguerite Rinaudo, and Michel Milas. On the characterization of polygalacturonate salts in dilute solution. *Carbohydrate Polymers*, 22(2):87–92, 1993. ISSN 0144-8617. doi: 10.1016/0144-8617(93)90070-K. URL http://www.sciencedirect.com/science/article/pii/014486179390070K.

[62] D. I Svergun, L. A Feigin, and George W Taylor. *Structure Analysis by Small-Angle X-Ray and Neutron Scattering*. 1987. ISBN 9781475766240 1475766246. URL http://dx.doi.org/10.1007/978-1-4757-6624-0.

[63] Harold P. Klug. *X-ray diffraction procedures for polycrystalline and amorphous materials*. Wiley, New York, 2d ed edition, 1974. ISBN 0471493694.

[64] O. Glatter and O. Kratky, editors. *Small angle x-ray scattering*. Academic Press, London ; New York, 1982. ISBN 0122862805.

[65] Anna Ström and Martin A. K. Williams. Controlled Calcium Release in the Absence and Presence of an Ion-Binding Polymer. *The Journal of Physical Chemistry B*, 107(40):10995–10999, 2003. ISSN 1520-6106. doi: 10.1021/jp034322b. URL http://dx.doi.org/10.1021/jp034322b.

[66] R. R. Vincent, A. Cucheval, Y. Hemar, and M. a. K. Williams. Bio-inspired network optimization in soft materials Insights from the plant cell wall. *The European Physical Journal E*, 28(1):79–87, January 2009. ISSN 1292-8941, 1292-895X. doi: 10.1140/epje/i2008-10416-2. URL http://link.springer.com/article/10.1140/epje/i2008-10416-2.

[67] Erich Schuster, Aurelie Cucheval, Leif Lundin, and Martin A. K. Williams. Using SAXS to Reveal the Degree of Bundling in the Polysaccharide Junction Zones of Microrheologically Distinct Pectin Gels. *Biomacromolecules*, 12(7):2583–2590, July 2011. ISSN 1525-7797. doi: 10.1021/bm200578d. URL http://dx.doi.org/10.1021/bm200578d.

[68] Irit Ventura, Joanna Jammal, and Havazelet Bianco-Peled. Insights into the nanostructure of low-methoxyl pectincalcium gels. *Carbohydrate Polymers*, 97(2):650–658, September 2013. ISSN 0144-8617. doi: 10.1016/j.carbpol.2013.05.055. URL http://www.sciencedirect.com/science/article/pii/S0144861713005304.

[69] P. Lunkenheimer, U. Schneider, R. Brand, and A. Loid. Glassy dynamics. *Contemporary Physics*, 41(1):15–36, January 2000. ISSN 0010-7514. doi: 10.1080/001075100181259. URL http://dx.doi.org/10.1080/001075100181259.

[70] W. Gotze and L. Sjogren. Relaxation processes in supercooled liquids. *Reports on Progress in Physics*, 55(3):241, March 1992. ISSN 0034-4885. doi: 10.1088/0034-4885/55/3/001. URL http://iopscience.iop.org/0034-4885/55/3/001.

[71] David R Reichman and Patrick Charbonneau. Mode-coupling theory. *Journal of Statistical Mechanics: Theory and Experiment*, 2005(05):P05013, May 2005. ISSN 1742-5468. doi: 10.1088/1742-5468/2005/05/

P05013. URL http://stacks.iop.org/1742-5468/2005/i=05/a=P05013?key=crossref.8f695c4085fd6e0414c41732d2643ffb.

[72] Jean Louis Viovy, Michael Rubinstein, and Ralph H. Colby. Constraint release in polymer melts: tube reorganization versus tube dilation. *Macromolecules*, 24 (12):3587–3596, June 1991. ISSN 0024-9297. doi: 10.1021/ma00012a020. URL http://dx.doi.org/10.1021/ma00012a020.

[73] Peter Sollich, François Lequeux, Pascal Hébraud, and Michael E. Cates. Rheology of soft glassy materials. *Physical review letters*, 78(10):2020, 1997. URL http://journals.aps.org/prl/abstract/10.1103/PhysRevLett.78.2020.

[74] Klaus Kroy and Jens Glaser. The glassy wormlike chain. *New Journal of Physics*, 9(11):416, November 2007. ISSN 1367-2630. doi: 10.1088/1367-2630/9/11/416. URL http://iopscience.iop.org/1367-2630/9/11/416.

[75] Cécile Monthus and Jean-Philippe Bouchaud. Models of traps and glass phenomenology. *Journal of Physics A: Mathematical and General*, 29(14):3847–3869, July 1996. ISSN 0305-4470, 1361-6447. doi: 10.1088/0305-4470/29/14/012. URL http://arxiv.org/abs/cond-mat/9601012. arXiv: cond-mat/9601012.

[76] Thomas Zemb and Peter Lindner. *Neutrons, X-rays and light: scattering methods applied to soft condensed matter*. North Holland, 2002.

[77] Bruce J. Berne. *Dynamic light scattering: with applications to chemistry, biology, and physics*. Dover Publications, Mineola, N.Y, dover ed edition, 2000. ISBN 0486411559.

[78] ANDRE Guimer and Gérard Fournet. *Small angle scattering of X-rays*.

[79] Boualem Hammouda. The SANS toolbook. 2000. URL http://www.ncnr.nist.gov/staff/hammouda/the_SANS_toolbox.pdf.

[80] Jerome K Percus and George J Yevick. Analysis of classical statistical mechanics by means of collective coordinates. *Physical Review*, 110(1):1, 1958.

[81] LS Ornstein and F Zernike. Die linearen dimensionen der dichteschwankungen. *Phys. Zeit*, 19:134–7, 1918.

[82] Jean-Pierre Hansen and Ian R McDonald. *Theory of simple liquids*. Elsevier, 1990.

[83] Benoit B Mandelbrot. *Fractals: form, chance, and dimension*. WH Freeman San Francisco, 1977.

[84] Janine L Burns, Yao-de Yan, Graeme J Jameson, and Simon Biggs. A light scattering study of the fractal aggregation behavior of a model colloidal system. *Langmuir*, 13(24):6413–6420, 1997.

[85] J. Teixeira. Small-angle scattering by fractal systems. *Journal of Applied Crystallography*, 21(6):781–785, December 1988. ISSN 0021-8898. doi: 10.1107/S0021889888000263. URL http://scripts.iucr.org/cgi-bin/paper?S0021889888000263.

[86] Paul W. Schmidt. Small-angle scattering studies of disordered, porous and fractal systems. *Journal of Applied Crystallography*, 24(5):414–435, 1991. URL http://scripts.iucr.org/cgi-bin/paper?S0021889891003400.

[87] Sow-Hsin Chen and José Teixeira. Structure and fractal dimension of protein-detergent complexes. *Physical review letters*, 57(20):2583, 1986.

[88] Benjamin Chu. *Laser light scattering*. Quantum electronics–principles and applications. Academic Press, New York, 1974. ISBN 0121745503.

[89] Bivash R. Dasgupta, Shang-You Tee, John C. Crocker, B. J. Frisken, and D. A. Weitz. Microrheology of polyethylene oxide using diffusing wave spectroscopy and single scattering. *Physical Review E*, 65(5):051505, May 2002. doi: 10.1103/PhysRevE.65.051505. URL http://link.aps.org/doi/10.1103/PhysRevE.65.051505.

[90] AJF Siegert. Massachusetts Institute of Technology. *Rad. Lab. Rep*, (465), 1943.

[91] Erich O Schulz-Dubois. *Photon correlation techniques in fluid mechanics: proceedings of the 5th international conference at Kiel-Damp, Fed. Rep. of Germany, May 23-26, 1982*, volume 38. Springer Verlag, 1983.

[92] P.N. Pusey and W. Van Megen. Dynamic light scattering by non-ergodic media. *Physica A: Statistical Mechanics and its Applications*, 157(2):705–741, June 1989.

ISSN 03784371. doi: 10.1016/0378-4371(89)90063-0. URL http://linkinghub.elsevier.com/retrieve/pii/0378437189900630.

[93] DJ Pine, DA Weitz, PM Chaikin, and E Herbolzheimer. Diffusing wave spectroscopy. *Physical Review Letters*, 60(12):1134, 1988.

[94] Wyn Brown. *Dynamic light scattering: the method and some applications*, volume 49. Oxford University Press, USA, 1993.

[95] W. Van Megen and P. N. Pusey. Dynamic light-scattering study of the glass transition in a colloidal suspension. *Physical review A*, 43(10):5429, 1991. URL http://journals.aps.org/pra/abstract/10.1103/PhysRevA.43.5429.

[96] J.L. Harden and V. Viasnoff. Recent advances in DWS-based micro-rheology. *Current Opinion in Colloid & Interface Science*, 6(5-6):438–445, November 2001. ISSN 13590294. doi: 10.1016/S1359-0294(01)00115-7. URL http://linkinghub.elsevier.com/retrieve/pii/S1359029401001157.

[97] P. Zakharov, F. Cardinaux, and F. Scheffold. Multispeckle diffusing-wave spectroscopy with a single-mode detection scheme. *Physical Review E*, 73(1), January 2006. ISSN 1539-3755, 1550-2376. doi: 10.1103/PhysRevE.73.011413. URL http://link.aps.org/doi/10.1103/PhysRevE.73.011413.

[98] A. Raudsepp, A.J. Sutherland Smith, and M.A.K. Williams. Rotating angled plate diffusing wave spectroscopy. *International Journal of Nanotechnology*, 11 (5/6/7/8):573, 2014. ISSN 1475-7435, 1741-8151. doi: 10.1504/IJNT.2014.060579. URL http://www.inderscience.com/link.php?id=60579.

[99] Apollo P. Y. Wong and P. Wiltzius. Dynamic light scattering with a CCD camera. *Review of Scientific Instruments*, 64(9):2547, 1993. ISSN 00346748. doi: 10.1063/1.1143864. URL http://scitation.aip.org/content/aip/journal/rsi/64/9/10.1063/1.1143864.

[100] S. Maccarrone, G. Brambilla, O. Pravaz, A. Duri, M. Ciccotti, J.-M. Fromental, E. Pashkovski, A. Lips, D. Sessoms, V. Trappe, and L. Cipelletti. Ultra-long range correlations of the dynamics of jammed soft matter. *Soft Matter*, 6(21): 5514, 2010. ISSN 1744-683X, 1744-6848. doi: 10.1039/c0sm00155d. URL http://xlink.rsc.org/?DOI=c0sm00155d.

[101] Christopher W Macosko and Ronald G Larson. Rheology: principles, measurements, and applications. 1994.

[102] R. R. Vincent, D. N. Pinder, Y. Hemar, and M. A. K. Williams. Microrheological studies reveal semiflexible networks in gels of a ubiquitous cell wall polysaccharide. *Physical Review E*, 76(3):031909, September 2007. doi: 10.1103/PhysRevE.76.031909. URL http://link.aps.org/doi/10.1103/PhysRevE.76.031909.

[103] Cornelis Storm, Jennifer J. Pastore, F. C. MacKintosh, T. C. Lubensky, and Paul A. Janmey. Nonlinear elasticity in biological gels. *Nature*, 435(7039): 191–194, May 2005. ISSN 0028-0836. doi: 10.1038/nature03521. URL http://www.nature.com/nature/journal/v435/n7039/full/nature03521.html.

[104] Joshua Apgar, Yiider Tseng, Elena Fedorov, Matthew B. Herwig, Steve C. Almo, and Denis Wirtz. Multiple-Particle Tracking Measurements of Heterogeneities in Solutions of Actin Filaments and Actin Bundles. *Biophysical Journal*, 79(2):1095–1106, August 2000. ISSN 0006-3495. doi: 10.1016/S0006-3495(00)76363-6. URL http://www.sciencedirect.com/science/article/pii/S0006349500763636.

[105] M. L. Gardel, J. H. Shin, F. C. MacKintosh, L. Mahadevan, P. Matsudaira, and D. A. Weitz. Elastic Behavior of Cross-Linked and Bundled Actin Networks. *Science*, 304(5675):1301–1305, May 2004. ISSN 0036-8075, 1095-9203. doi: 10.1126/science.1095087. URL http://www.sciencemag.org/content/304/5675/1301.

[106] Andre Palmer, Thomas G. Mason, Jingyuan Xu, Scot C. Kuo, and Denis Wirtz. Diffusing Wave Spectroscopy Microrheology of Actin Filament Networks. *Biophysical Journal*, 76(2):1063–1071, February 1999. ISSN 0006-3495. doi: 10.1016/S0006-3495(99)77271-1. URL http://www.sciencedirect.com/science/article/pii/S0006349599772711.

[107] T. G. Mason, T. Gisler, K. Kroy, E. Frey, and D. A. Weitz. Rheology of F-actin solutions determined from thermally driven tracer motion. *Journal of Rheology (1978-present)*, 44(4):917–928, July 2000. ISSN 0148-6055, 1520-8516. doi: 10.1122/1.551113. URL http://scitation.aip.org.ezproxy.massey.ac.nz/content/sor/journal/jor2/44/4/10.1122/1.551113.

[108] F. C. MacKintosh, J. Käs, and P. A. Janmey. Elasticity of Semiflexible Biopolymer Networks. *Physical Review Letters*, 75(24):4425–4428, December 1995. doi: 10.1103/PhysRevLett.75.4425. URL http://link.aps.org/doi/10.1103/PhysRevLett.75.4425.

[109] T. Mason, K. Ganesan, J. van Zanten, D. Wirtz, and S. Kuo. Particle Tracking Microrheology of Complex Fluids. *Physical Review Letters*, 79(17):3282–3285, October 1997. ISSN 0031-9007, 1079-7114. doi: 10.1103/PhysRevLett.79.3282. URL http://link.aps.org/doi/10.1103/PhysRevLett.79.3282.

[110] N. Willenbacher, C. Oelschlaeger, M. Schopferer, P. Fischer, F. Cardinaux, and F. Scheffold. Broad Bandwidth Optical and Mechanical Rheometry of Wormlike Micelle Solutions. *Physical Review Letters*, 99(6):068302, August 2007. doi: 10.1103/PhysRevLett.99.068302. URL http://link.aps.org/doi/10.1103/PhysRevLett.99.068302.

[111] Peter Sollich and Michael E. Cates. Thermodynamic interpretation of soft glassy rheology models. *Physical Review E*, 85(3):031127, March 2012. doi: 10.1103/PhysRevE.85.031127. URL http://link.aps.org/doi/10.1103/PhysRevE.85.031127.

[112] J. Glaser, O. Hallatschek, and K. Kroy. Dynamic structure factor of a stiff polymer in a glassy solution. *The European Physical Journal E*, 26(1-2):123–136, May 2008. ISSN 1292-8941, 1292-895X. doi: 10.1140/epje/i2007-10321-2. URL http://www.springerlink.com/index/10.1140/epje/i2007-10321-2.

[113] Klaus Kroy. Dynamics of wormlike and glassy wormlike chains. *Soft Matter*, 4(12):2323, 2008. ISSN 1744-683X, 1744-6848. doi: 10.1039/b807018k. URL http://xlink.rsc.org/?DOI=b807018k.

[114] Christine Semmrich, Tobias Storz, Jens Glaser, Rudolf Merkel, Andreas R. Bausch, and Klaus Kroy. Glass transition and rheological redundancy in F-actin solutions. *Proceedings of the National Academy of Sciences*, 104(51):20199–20203, December 2007. ISSN 0027-8424, 1091-6490. doi: 10.1073/pnas.0705513104. URL http://www.pnas.org/content/104/51/20199.

[115] Lars Wolff, Pablo Fernandez, and Klaus Kroy. Inelastic mechanics of sticky biopolymer networks. *New Journal of Physics*, 12(5):053024, May 2010. ISSN

1367-2630. doi: 10.1088/1367-2630/12/5/053024. URL http://iopscience.iop.org.ezproxy.massey.ac.nz/1367-2630/12/5/053024.

[116] Alexis Peaucelle, Siobhan Braybrook, and Herman Höfte. Cell wall mechanics and growth control in plants: the role of pectins revisited. *Frontiers in Plant Science*, 3, June 2012. ISSN 1664-462X. doi: 10.3389/fpls.2012.00121. URL http://www.ncbi.nlm.nih.gov/pmc/articles/PMC3368173/.

[117] M. J. Gidley, E. R. Morris, E. J. Murray, D. A. Powell, and D. A. Rees. Evidence for two mechanisms of interchain association in calcium pectate gels. *International Journal of Biological Macromolecules*, 2(5):332–334, October 1980. ISSN 0141-8130. doi: 10.1016/0141-8130(80)90060-4. URL http://www.sciencedirect.com/science/article/pii/0141813080900604.

[118] E. R. Morris, M. J. Gidley, E. J. Murray, D. A. Powell, and D. A. Rees. Characterization of pectin gelation under conditions of low water activity, by circular dichroism, competitive inhibition and mechanical properties. *International Journal of Biological Macromolecules*, 2(5):327–330, October 1980. ISSN 0141-8130. doi: 10.1016/0141-8130(80)90058-6. URL http://www.sciencedirect.com/science/article/pii/0141813080900586.

[119] E. R. Morris, D. A. Powell, M. J. Gidley, and D. A. Rees. Conformations and interactions of pectins: I. Polymorphism between gel and solid states of calcium polygalacturonate. *Journal of Molecular Biology*, 155(4):507–516, March 1982. ISSN 0022-2836. doi: 10.1016/0022-2836(82)90484-3. URL http://www.sciencedirect.com/science/article/pii/0022283682904843.

[120] Elodie Parre and Anja Geitmann. Pectin and the role of the physical properties of the cell wall in pollen tube growth of Solanum chacoense. *Planta*, 220(4):582–592, September 2004. ISSN 0032-0935, 1432-2048. doi: 10.1007/s00425-004-1368-5. URL http://link.springer.com.ezproxy.massey.ac.nz/article/10.1007/s00425-004-1368-5.

[121] Romaric R. Vincent and Martin A. K. Williams. Microrheological investigations give insights into the microstructure and functionality of pectin gels. *Carbohydrate Research*, 344(14):1863–1871, September 2009. ISSN 0008-6215. doi: 10.1016/

j.carres.2008.11.021. URL http://www.sciencedirect.com/science/article/pii/S0008621508005600.

[122] Aileen B. OBrien, Kevin Philp, and Edwin R. Morris. Gelation of high-methoxy pectin by enzymic de-esterification in the presence of calcium ions: a preliminary evaluation. *Carbohydrate Research*, 344(14):1818–1823, September 2009. ISSN 0008-6215. doi: 10.1016/j.carres.2008.09.029. URL http://www.sciencedirect.com/science/article/pii/S0008621508005387.

[123] Anton Slavov, Catherine Garnier, Marie-Jeanne Crépeau, Sylvie Durand, Jean-François Thibault, and Estelle Bonnin. Gelation of high methoxy pectin in the presence of pectin methylesterases and calcium. *Carbohydrate Polymers*, 77(4): 876–884, July 2009. ISSN 0144-8617. doi: 10.1016/j.carbpol.2009.03.014. URL http://www.sciencedirect.com/science/article/pii/S0144861709001337.

[124] G. Ravanat and M. Rinaudo. Investigation on oligo- and polygalacturonic acids by potentiometry and circular dichroism. *Biopolymers*, 19(12):2209–2222, December 1980. ISSN 1097-0282. doi: 10.1002/bip.1980.360191206. URL http://onlinelibrary.wiley.com/doi/10.1002/bip.1980.360191206/abstract.

[125] A. Cesàro, A. Ciana, F. Delben, G. Manzini, and S. Paoletti. Physicochemical properties of pectic acid. I. Thermodynamic evidence of a pH-induced conformational transition in aqueous solution. *Biopolymers*, 21(2):431–449, February 1982. ISSN 0006-3525, 1097-0282. doi: 10.1002/bip.360210214. URL http://doi.wiley.com/10.1002/bip.360210214.

[126] Michael C. Jarvis and David C. Apperley. Chain conformation in concentrated pectic gels: evidence from 13c NMR. *Carbohydrate Research*, 275(1):131–145, September 1995. ISSN 0008-6215. doi: 10.1016/0008-6215(95)00033-P. URL http://www.sciencedirect.com/science/article/pii/000862159500033P.

[127] Martin A. K. Williams, Tim J. Foster, and Henk A. Schols. Elucidation of Pectin Methylester Distributions by Capillary Electrophoresis. *Journal of Agricultural and Food Chemistry*, 51(7):1777–1781, 2003. ISSN 0021-8561. doi: 10.1021/jf0259112. URL http://dx.doi.org/10.1021/jf0259112.

[128] Martin A. K. Williams, Aurélie Cucheval, Anna Ström, and Marie-Christine Ralet. Electrophoretic Behavior of Copolymeric Galacturonans Including Comments on the Information Content of the Intermolecular Charge Distribution. *Biomacromolecules*, 10(6):1523–1531, June 2009. ISSN 1525-7797. doi: 10.1021/bm900119u. URL http://dx.doi.org/10.1021/bm900119u.

[129] Florence Goubet, Anna Ström, Paul Dupree, and Martin A. K. Williams. An investigation of pectin methylesterification patterns by two independent methods: capillary electrophoresis and polysaccharide analysis using carbohydrate gel electrophoresis. *Carbohydrate Research*, 340(6):1193–1199, May 2005. ISSN 0008-6215. doi: 10.1016/j.carres.2005.01.037. URL http://www.sciencedirect.com/science/article/pii/S0008621505000819.

[130] Anna Ström and Martin A. K Williams. On the separation, detection and quantification of pectin derived oligosaccharides by capillary electrophoresis. *Carbohydrate Research*, 339(10):1711–1716, July 2004. ISSN 0008-6215. doi: 10.1016/j.carres.2004.05.010. URL http://www.sciencedirect.com/science/article/pii/S0008621504002113.

[131] Jonathan J. Hunt, Randall Cameron, and Martin A. K. Williams. On the simulation of enzymatic digest patterns: The fragmentation of oligomeric and polymeric galacturonides by endo-polygalacturonase II. *Biochimica et Biophysica Acta (BBA) - General Subjects*, 1760(11):1696–1703, November 2006. ISSN 0304-4165. doi: 10.1016/j.bbagen.2006.08.022. URL http://www.sciencedirect.com/science/article/pii/S0304416506002327.

[132] Patrick J.B. Edwards, Motoko Kakubayashi, Robin Dykstra, Steven M. Pascal, and Martin A.K. Williams. Rheo-NMR Studies of an Enzymatic Reaction: Evidence of a Shear-Stable Macromolecular System. *Biophysical Journal*, 98(9):1986–1994, May 2010. ISSN 0006-3495. doi: 10.1016/j.bpj.2010.01.022. URL http://www.ncbi.nlm.nih.gov/pmc/articles/PMC2862195/.

[133] T. A. Waigh. Microrheology of complex fluids. *Reports on Progress in Physics*, 68(3):685, March 2005. ISSN 0034-4885. doi: 10.1088/0034-4885/68/3/R04. URL http://iopscience.iop.org.ezproxy.massey.ac.nz/0034-4885/68/3/R04.

[134] F. Gittes, B. Schnurr, P. D. Olmsted, F. C. MacKintosh, and C. F. Schmidt. Microscopic Viscoelasticity: Shear Moduli of Soft Materials Determined from Thermal Fluctuations. *Physical Review Letters*, 79(17):3286–3289, October 1997. ISSN 0031-9007, 1079-7114. doi: 10.1103/PhysRevLett.79.3286. URL http://arxiv.org/abs/cond-mat/9709228. arXiv: cond-mat/9709228.

[135] Y. Hemar and D. N. Pinder. DWS Microrheology of a Linear Polysaccharide. *Biomacromolecules*, 7(3):674–676, February 2006. ISSN 1525-7797. doi: 10.1021/bm050566l. URL http://pubs.acs.org/doi/citedby/10.1021/bm050566l.

[136] Pablo Fernández, Pramod A. Pullarkat, and Albrecht Ott. A Master Relation Defines the Nonlinear Viscoelasticity of Single Fibroblasts. *Biophysical Journal*, 90(10):3796–3805, May 2006. ISSN 0006-3495. doi: 10.1529/biophysj.105.072215. URL http://www.cell.com/article/S0006349506725590/abstract.

[137] F. Gittes and F. C. MacKintosh. Dynamic shear modulus of a semiflexible polymer network. *Physical Review E*, 58(2):R1241–R1244, August 1998. doi: 10.1103/PhysRevE.58.R1241. URL http://link.aps.org/doi/10.1103/PhysRevE.58.R1241.

[138] Wolfgang Götze. *Complex dynamics of glass-forming liquids: a mode-coupling theory*. Number 143 in International series of monographs on physics. Oxford Univ. Press, Oxford, 2009. ISBN 0199656142 0199235341 9780199235346 9780199656141.

[139] G. H. Koenderink, M. Atakhorrami, F. C. MacKintosh, and C. F. Schmidt. High-Frequency Stress Relaxation in Semiflexible Polymer Solutions and Networks. *Physical Review Letters*, 96(13):138307, April 2006. doi: 10.1103/PhysRevLett.96.138307. URL http://link.aps.org/doi/10.1103/PhysRevLett.96.138307.

[140] David C. Morse. Viscoelasticity of tightly entangled solutions of semiflexible polymers. *Physical Review E*, 58(2):R1237–R1240, August 1998. doi: 10.1103/PhysRevE.58.R1237. URL http://link.aps.org/doi/10.1103/PhysRevE.58.R1237.

[141] Philip Kollmannsberger and Ben Fabry. Linear and Nonlinear Rheology of Living Cells. *Annual Review of Materials Research*, 41(1):75–97, 2011. doi:

10.1146/annurev-matsci-062910-100351. URL http://dx.doi.org/10.1146/annurev-matsci-062910-100351.

[142] I. Y. Wong, M. L. Gardel, D. R. Reichman, Eric R. Weeks, M. T. Valentine, A. R. Bausch, and D. A. Weitz. Anomalous Diffusion Probes Microstructure Dynamics of Entangled F-Actin Networks. *Physical Review Letters*, 92(17):178101, April 2004. doi: 10.1103/PhysRevLett.92.178101. URL http://link.aps.org/doi/10.1103/PhysRevLett.92.178101.

[143] L Piculell, J Borgström, I. S Chronakis, P. O Quist, and C Viebke. Organisation and association of κ-carrageenan helices under different salt conditions. *International Journal of Biological Macromolecules*, 21(12):141–153, August 1997. ISSN 0141-8130. doi: 10.1016/S0141-8130(97)00054-8. URL http://www.sciencedirect.com/science/article/pii/S0141813097000548.

[144] Z. H. Mohammed, M. W. N. Hember, R. K. Richardson, and E. R. Morris. Kinetic and equilibrium processes in the formation and melting of agarose gels. *Carbohydrate Polymers*, 36(1):15–26, May 1998. ISSN 0144-8617. doi: 10.1016/S0144-8617(98)00011-3. URL http://www.sciencedirect.com/science/article/pii/S0144861798000113.

[145] Michael Schopferer, Harald Bär, Bernhard Hochstein, Sarika Sharma, Norbert Mücke, Harald Herrmann, and Norbert Willenbacher. Desmin and vimentin intermediate filament networks: their viscoelastic properties investigated by mechanical rheometry. *Journal of Molecular Biology*, 388(1):133–143, April 2009. ISSN 1089-8638. doi: 10.1016/j.jmb.2009.03.005.

[146] Yi-Chia Lin, Norman Y. Yao, Chase P. Broedersz, Harald Herrmann, Fred C. MacKintosh, and David A. Weitz. Origins of Elasticity in Intermediate Filament Networks. *Physical Review Letters*, 104(5):058101, February 2010. doi: 10.1103/PhysRevLett.104.058101. URL http://link.aps.org/doi/10.1103/PhysRevLett.104.058101.

[147] Yi-Chia Lin, Gijsje H. Koenderink, Frederick C. MacKintosh, and David A. Weitz. Control of non-linear elasticity in F-actin networks with microtubules. *Soft Matter*, 7(3):902–906, 2011. ISSN 1744-683X, 1744-6848. doi: 10.1039/C0SM00478B. URL http://xlink.rsc.org/?DOI=C0SM00478B.

[148] Nicholas A. Kurniawan, Long Hui Wong, and Raj Rajagopalan. Early Stiffening and Softening of Collagen: Interplay of Deformation Mechanisms in Biopolymer Networks. *Biomacromolecules*, 13(3):691–698, March 2012. ISSN 1525-7797. doi: 10.1021/bm2015812. URL http://dx.doi.org/10.1021/bm2015812.

[149] Félix Rico, Calvin Chu, Midhat H. Abdulreda, Yujing Qin, and Vincent T. Moy. Temperature Modulation of Integrin-Mediated Cell Adhesion. *Biophysical Journal*, 99(5):1387–1396, August 2010. ISSN 0006-3495. doi: 10.1016/j.bpj.2010.06.037. URL http://www.cell.com/article/S0006349510007800/abstract.

[150] LinShu Liu, Marshall L. Fishman, Joseph Kost, and Kevin B. Hicks. Pectin-based systems for colon-specific drug delivery via oral route. *Biomaterials*, 24(19):3333–3343, August 2003. ISSN 0142-9612. doi: 10.1016/S0142-9612(03)00213-8. URL http://www.sciencedirect.com/science/article/pii/S0142961203002138.

[151] D. A. Powell, E. R. Morris, M. J. Gidley, and D. A. Rees. Conformations and interactions of pectins: II. Influence of residue sequence on chain association in calcium pectate gels. *Journal of Molecular Biology*, 155(4):517–531, March 1982. ISSN 0022-2836. doi: 10.1016/0022-2836(82)90485-5. URL http://www.sciencedirect.com/science/article/pii/0022283682904855.

[152] Michael Rubinstein and Audrey V. Dobrynin. Associations leading to formation of reversible networks and gels. *Current opinion in colloid & interface science*, 4 (1):83–87, 1999. URL http://www.sciencedirect.com/science/article/pii/S1359029499000138.

[153] Redouane Borsali, Huy Nguyen, and R. Pecora. Small-Angle Neutron Scattering and Dynamic Light Scattering from a Polyelectrolyte Solution: DNA. *Macromolecules*, 31(5):1548–1555, 1998. ISSN 0024-9297. doi: 10.1021/ma970919b. URL http://dx.doi.org/10.1021/ma970919b.

[154] Maurice Drifford and Jean Pierre Dalbiez. Light scattering by dilute solutions of salt-free polyelectrolytes. *The Journal of Physical Chemistry*, 88(22):5368–5375, 1984. ISSN 0022-3654. doi: 10.1021/j150666a052. URL http://dx.doi.org/10.1021/j150666a052.

[155] Stephan Förster, Manfred Schmidt, and Markus Antonietti. Static and dynamic light scattering by aqueous polyelectrolyte solutions: effect of molecular weight, charge density and added salt. *Polymer*, 31(5):781–792, May 1990. ISSN 0032-3861. doi: 10.1016/0032-3861(90)90036-X. URL http://www.sciencedirect.com/science/article/pii/003238619090036X.

[156] D.-G. Liu, C.-H. Chang, C.-Y. Liu, S.-H. Chang, J.-M. Juang, Y.-F. Song, K.-L. Yu, K.-F. Liao, C.-S. Hwang, H.-S. Fung, and others. A dedicated small-angle X-ray scattering beamline with a superconducting wiggler source at the NSRRC. *Journal of synchrotron radiation*, 16(1):97–104, 2008. URL http://scripts.iucr.org/cgi-bin/paper?s0909049508034134.

[157] Nigel M. Kirby, Stephen T. Mudie, Adrian M. Hawley, David J. Cookson, Haydyn D. T. Mertens, Nathan Cowieson, and Vesna Samardzic-Boban. A low-background-intensity focusing small-angle X-ray scattering undulator beamline. *Journal of Applied Crystallography*, 46(6):1670–1680, December 2013. ISSN 0021-8898. doi: 10.1107/S002188981302774X. URL http://scripts.iucr.org/cgi-bin/paper?S002188981302774X.

[158] Yen-Cheng Li, Kuei-Bai Chen, Hsin-Lung Chen, Chain-Shu Hsu, Cheng-Si Tsao, Jean-Hong Chen, and Show-An Chen. Fractal Aggregates of Conjugated Polymer in Solution State. *Langmuir*, 22(26):11009–11015, December 2006. ISSN 0743-7463. doi: 10.1021/la0612769. URL http://dx.doi.org/10.1021/la0612769.

[159] G. Beaucage. Small-Angle Scattering from Polymeric Mass Fractals of Arbitrary Mass-Fractal Dimension. *Journal of Applied Crystallography*, 29(2):134–146, April 1996. ISSN 00218898. doi: 10.1107/S0021889895011605. URL http://scripts.iucr.org/cgi-bin/paper?S0021889895011605.

[160] G. Beaucage. Approximations Leading to a Unified Exponential/Power-Law Approach to Small-Angle Scattering. *Journal of Applied Crystallography*, 28(6):717–728, December 1995. ISSN 0021-8898. doi: 10.1107/S0021889895005292. URL http://scripts.iucr.org/cgi-bin/paper?S0021889895005292.

[161] Boualem Hammouda. Analysis of the Beaucage model. *Journal of Applied Crystallography*, 43(6):1474–1478, 2010. URL http://scripts.iucr.org/cgi-bin/paper?S0021889810033856.

[162] M. A. F. Davis, M. J. Gidley, E. R. Morris, D. A. Powell, and D. A. Rees. Intermolecular association in pectin solutions. *International Journal of Biological Macromolecules*, 2(5):330–332, October 1980. ISSN 0141-8130. doi: 10.1016/0141-8130(80)90059-8. URL http://www.sciencedirect.com/science/article/pii/0141813080900598.

[163] V. D. Sorochan, A. K. Dzizenko, N. S. Bodin, and Yu. S. Ovodov. Light-scattering studies of pectic substances in aqueous solution. *Carbohydrate Research*, 20(2):243–249, December 1971. ISSN 0008-6215. doi: 10.1016/S0008-6215(00)81377-4. URL http://www.sciencedirect.com/science/article/pii/S0008621500813774.

[164] J. R. Blundell and E. M. Terentjev. Stretching Semiflexible Filaments and Their Networks. *Macromolecules*, 42(14):5388–5394, July 2009. ISSN 0024-9297, 1520-5835. doi: 10.1021/ma9004633. URL http://pubs.acs.org/doi/abs/10.1021/ma9004633.

[165] Jan-Michael Y. Carrillo, Fred C. MacKintosh, and Andrey V. Dobrynin. Nonlinear Elasticity: From Single Chain to Networks and Gels. *Macromolecules*, 46(9):3679–3692, May 2013. ISSN 0024-9297, 1520-5835. doi: 10.1021/ma400478f. URL http://pubs.acs.org/doi/abs/10.1021/ma400478f.

[166] Erich Schuster, Leif Lundin, and Martin A. K. Williams. Investigating the Relationship between Network Mechanics and Single-Chain Extension Using Biomimetic Polysaccharide Gels. *Macromolecules*, 45(11):4863–4869, June 2012. ISSN 0024-9297. doi: 10.1021/ma300724n. URL http://dx.doi.org/10.1021/ma300724n.

[167] Jan Skov Pedersen and Peter Schurtenberger. Scattering Functions of Semiflexible Polymers with and without Excluded Volume Effects. *Macromolecules*, 29(23):7602–7612, January 1996. ISSN 0024-9297. doi: 10.1021/ma9607630. URL http://dx.doi.org/10.1021/ma9607630.

[168] Wei-Ren Chen, Paul D. Butler, and Linda J. Magid. Incorporating Intermicellar Interactions in the Fitting of SANS Data from Cationic Wormlike Micelles. *Langmuir*, 22(15):6539–6548, July 2006. ISSN 0743-7463. doi: 10.1021/la0530440. URL http://dx.doi.org/10.1021/la0530440.

[169] Steven R. Kline. Reduction and analysis of SANS and USANS data using IGOR Pro. *Journal of Applied Crystallography*, 39(6):895–900, December 2006. ISSN 0021-8898. doi: 10.1107/S0021889806035059. URL http://scripts.iucr.org/cgi-bin/paper?S0021889806035059.

[170] T. Sajjaanantakul, J. P. Van Buren, and D. L. Downing. Effect of Methyl Ester Content on Heat Degradation of Chelator-Soluble Carrot Pectin. *Journal of Food Science*, 54(5):1272–1277, 1989. ISSN 1750-3841. doi: 10.1111/j.1365-2621.1989.tb05972.x. URL http://onlinelibrary.wiley.com.ezproxy.massey.ac.nz/doi/10.1111/j.1365-2621.1989.tb05972.x/abstract.

[171] Eric R. Weeks, J. C. Crocker, Andrew C. Levitt, Andrew Schofield, and D. A. Weitz. Three-Dimensional Direct Imaging of Structural Relaxation Near the Colloidal Glass Transition. *Science*, 287(5453):627–631, January 2000. doi: 10.1126/science.287.5453.627. URL http://www.sciencemag.org/content/287/5453/627.abstract.

[172] Wolfgang Götze. Recent tests of the mode-coupling theory for glassy dynamics. *Journal of Physics: Condensed Matter*, 11(10A):A1–A45, March 1999. ISSN 0953-8984, 1361-648X. doi: 10.1088/0953-8984/11/10A/002. URL http://stacks.iop.org/0953-8984/11/i=10A/a=002?key=crossref.4af40e9123b46a493bb50bb8d1ada888.

[173] Walter Kob and Hans C. Andersen. Testing mode-coupling theory for a supercooled binary Lennard-Jones mixture. *Transport Theory and Statistical Physics*, 24(6-8):1179–1198, July 1995. ISSN 0041-1450, 1532-2424. doi: 10.1080/00411459508203949. URL http://www.tandfonline.com/doi/abs/10.1080/00411459508203949.

[174] M. Kunitz. Syneresis and Swelling of Gelatin. *The Journal of General Physiology*, 12(2):289–312, November 1928. ISSN 0022-1295, 1540-7748. doi: 10.1085/jgp.12.2.289. URL http://jgp.rupress.org/content/12/2/289.

[175] Piet J.H. Daas, Karin Meyer-Hansen, Henk A. Schols, Gerhard A. De Ruiter, and Alphons G.J. Voragen. Investigation of the non-esterified galacturonic acid distribution in pectin with endopolygalacturonase. *Carbohydrate Research*, 318

(1-4):135–145, May 1999. ISSN 00086215. doi: 10.1016/S0008-6215(99)00093-2. URL http://linkinghub.elsevier.com/retrieve/pii/S0008621599000932.

[176] Rachel E Courtland and Eric R Weeks. Direct visualization of ageing in colloidal glasses. *Journal of Physics: Condensed Matter*, 15(1): S359–S365, January 2003. ISSN 0953-8984. doi: 10.1088/0953-8984/15/1/349. URL http://stacks.iop.org/0953-8984/15/i=1/a=349?key=crossref.9667273516fd3669cfc82366c0dae64f.

[177] Carolina Brito and Matthieu Wyart. Heterogeneous dynamics, marginal stability and soft modes in hard sphere glasses. *Journal of Statistical Mechanics: Theory and Experiment*, 2007(08):L08003–L08003, August 2007. ISSN 1742-5468. doi: 10.1088/1742-5468/2007/08/L08003. URL http://stacks.iop.org/1742-5468/2007/i=08/a=L08003?key=crossref.2f1894695ec1406bb95f5d989c903275.

[178] Luca Cipelletti, Hugo Bissig, Veronique Trappe, Pierre Ballesta, and Sylvain Mazoyer. Time-resolved correlation: a new tool for studying temporally heterogeneous dynamics. *Journal of Physics: Condensed Matter*, 15(1):S257, 2003. URL http://iopscience.iop.org/0953-8984/15/1/334.

[179] V. M. Dronnet, C. M. G. C. Renard, M. A. V. Axelos, and J. F. Thibault. Characterisation and selectivity of divalent metal ions binding by citrus and sugar-beet pectins. *Carbohydrate Polymers*, 30(4):253–263, August 1996. ISSN 0144-8617. doi: 10.1016/S0144-8617(96)00107-5. URL http://www.sciencedirect.com/science/article/pii/S0144861796001075.

[180] Anna Strom. *Characterisation of pectin fine-structure and its effect on supramolecular properties*. PhD, University College Cork, Cork, Ireland, March 2006.

[181] M. A. K. Williams, A. T. Marshall, P. Anjukandi, and R. G. Haverkamp. Investigation of the effects of fine structure on the nanomechanical properties of pectin. *Physical Review E*, 76(2):021927, August 2007. doi: 10.1103/PhysRevE.76.021927. URL http://link.aps.org/doi/10.1103/PhysRevE.76.021927.

[182] Jan-Michael Y. Carrillo and Andrey V. Dobrynin. Polyelectrolytes in Salt Solutions: Molecular Dynamics Simulations. *Macromolecules*, 44(14):5798–5816, July 2011. ISSN 0024-9297. doi: 10.1021/ma2007943. URL http://pubs.acs.org/doi/abs/10.1021/ma2007943.

[183] Andrey V. Dobrynin. Electrostatic Persistence Length of Semiflexible and Flexible Polyelectrolytes. *Macromolecules*, 38(22):9304–9314, November 2005. ISSN 0024-9297. doi: 10.1021/ma051353r. URL http://dx.doi.org/10.1021/ma051353r.

[184] Andrey V. Dobrynin. Effect of Counterion Condensation on Rigidity of Semiflexible Polyelectrolytes. *Macromolecules*, 39(26):9519–9527, December 2006. ISSN 0024-9297. doi: 10.1021/ma061030a. URL http://dx.doi.org/10.1021/ma061030a.

[185] J. Combet, P. Lorchat, and M. Rawiso. Salt-free aqueous solutions of polyelectrolytes: Small angle X-ray and neutron scattering characterization. *The European Physical Journal Special Topics*, 213(1):243–265, December 2012. ISSN 1951-6355, 1951-6401. doi: 10.1140/epjst/e2012-01674-3. URL http://link.springer.com.ezproxy.massey.ac.nz/article/10.1140/epjst/e2012-01674-3.

[186] B. Guilleaume, J. Blaul, M. Ballauff, M. Wittemann, M. Rehahn, and G. Goerigk. The distribution of counterions around synthetic rod-like polyelectrolytes in solution. *The European Physical Journal E*, 8(3):299–309, June 2002. ISSN 1292-8941. doi: 10.1140/epje/i2001-10105-8. URL http://link.springer.com/article/10.1140/epje/i2001-10105-8.

[187] Marián Sedlák. Real-time monitoring of the origination of multimacroion domains in a polyelectrolyte solution. *The Journal of Chemical Physics*, 122(15):151102, April 2005. ISSN 0021-9606. doi: 10.1063/1.1900086.

[188] Norbert Stribeck. *X-ray scattering of soft matter*. Springer Science & Business Media, 2007. URL http://books.google.com/books?hl=en&lr=&id=oe5DAAAAQBAJ&oi=fnd&pg=PA1&dq=%22the+concept+is+restricting+the+presentation+of+the+mathematical+background%22+%22of+the+fundamental+ideas+and+their+repetitive+use+in+different+subareas+of%22+%22in+the+soft-condensed+matter+review-committee+of+the+European%22+&ots=MZC247ADjW&sig=5WyeZoMoB2dN-HEL_X3Ni9HnS9U.

[189] Ferenc Horkay, Peter J. Basser, Anne-Marie Hecht, and Erik Geissler. Chondroitin Sulfate in Solution: Effects of Mono- and Divalent Salts. *Macromolecules*, 45 (6):2882–2890, March 2012. ISSN 0024-9297. doi: 10.1021/ma202693s. URL http://dx.doi.org/10.1021/ma202693s.

[190] K. Salamon, D. Aumiler, G. Pabst, and T. Vuleti. Probing the Mesh Formed by the Semirigid Polyelectrolytes. *Macromolecules*, 46(3):1107–1118, February 2013. ISSN 0024-9297. doi: 10.1021/ma3021486. URL http://dx.doi.org/10.1021/ma3021486.

[191] Jessie Owen and M A K Williams. Biophysical Approaches to Elucidating Structure-Function Relationships in Polysaccharide Co-polymer Systems, August 2015. URL http://www.amn-7.com.